

4-6-2016

# Microfluidically Reconfigurable Frequency-Agile RF Filters with Wide Frequency Tuning Range and High Power Handling Capability

Timothy Joseph Palomo

Follow this and additional works at: <http://scholarcommons.usf.edu/etd>

 Part of the [Electromagnetics and Photonics Commons](#)

## Scholar Commons Citation

Palomo, Timothy Joseph, "Microfluidically Reconfigurable Frequency-Agile RF Filters with Wide Frequency Tuning Range and High Power Handling Capability" (2016). *Graduate Theses and Dissertations*.  
<http://scholarcommons.usf.edu/etd/6124>

This Dissertation is brought to you for free and open access by the Graduate School at Scholar Commons. It has been accepted for inclusion in Graduate Theses and Dissertations by an authorized administrator of Scholar Commons. For more information, please contact [scholarcommons@usf.edu](mailto:scholarcommons@usf.edu).

Microfluidically Reconfigurable Frequency-Agile RF Filters  
with Wide Frequency Tuning Range and High Power Handling Capability

by

Timothy Palomo

A dissertation submitted in partial fulfillment  
of the requirements for the of  
Doctor of Philosophy  
Department of Electrical Engineering  
College of Engineering  
University of South Florida

Major Professor: Gokhan Mumcu, Ph.D.  
Thomas Weller, Ph.D.  
Jing Wang, Ph.D.  
Nathan Crane, Ph.D.  
Paul Herzig, B.S.E.E.

Date of Approval:  
March 25, 2016

Keywords: Tunable, Resonator, X-band,  
Microstrip, High-power

Copyright © 2016, Timothy Palomo

## DEDICATION

First of all, I would like to dedicate this dissertation to my mother, Ailen Delgado, and my father, Eusebio Palomo. They have been role models since I was a kid, and they have motivated me to follow my dreams and work hard to accomplish them. Thanks to them, I started pre-school at the age of two years old, and they have always taught me the importance of education. However, the most important principle I have learned from my parents is to never give up. My mother's kindness have taught me to love what I do, and to treat everyone the same, while my father's character has taught me to fight for everything I want. Second, I would like to dedicate this dissertation to my grandparents, Nelia Baez and Jose Delgado, they have set an example my entire life, and next to my parents they have been the first, and most important, teachers in my life. To me, my grandparents have been more than just my family, they have been my friends, my teachers, my guardians, my role models, among other things. I have always looked up to my grandfather since he is the person that I admire the most for his character, his correctness, his intelligence, and his physical condition.

Then, I would like to say thanks to the rest of my family, since they have all been an important part in my life, both in my personal and professional growth. Specially, my grandmother Maria Mesones, my siblings Ruben and Simone Palomo, my uncle Jose Delgado Baez, my aunt Josmar Morales, my cousins Kevin and Johan Delgado and many others. Also, to my girlfriend Jennyfer Sanchez who has loved me unconditionally and has supported me in every step I have made to get to this point.

I would like to thank my advisor Gokhan Mumcu, who has taught me as much as he could in the field of RF and microwave area since I was still at the undergraduate level, and he has motivated me every day of my young career to be better. Last, but not least, I would like to dedicate this dissertation to my home country Venezuela, to its beautiful beaches and mountains, to its desert and jungles, and to everyone who is currently struggling and fighting to save the country from its terrible social situation, and to bring back the country that helped me grow and forged my character.

## ACKNOWLEDGEMENTS

I first would like to acknowledge all the members of my committee, Dr. Thomas Weller, Dr. Jing Wang, Dr. Nathan Crane, and Mr. Paul Herzig for their invaluable collaboration with my dissertation defense, and for sharing their knowledge with me in this very important chapter of my life. I can just say thanks for accommodating my defense in such a short notice. I would like to acknowledge all the employees at the Nanotechnology Research and Education Center (NREC) because they made possible for me to accomplish the fabrication of the devices developed under this dissertation. I would also like to acknowledge Rogers Corp. for providing me with plenty of material that was utilized throughout my doctoral studies. Last, but not least, I would like to acknowledge the entire WAMI group at the University of South Florida because they have shared this journey with me closer than nobody else, with some special mentions to Abhishek Dey and Eduardo Rojas for all their collaborations through these years.

## TABLE OF CONTENTS

LIST OF TABLES .....	iii
LIST OF FIGURES .....	iv
ABSTRACT .....	vii
CHAPTER 1: INTRODUCTION .....	1
1.1 Semiconductor Varactors .....	2
1.2 Ferroelectric Varactors .....	3
1.3 RF Micro-ElectroMechanical Systems (MEMS) Varactors and Switches .....	5
1.4 Evanescent Cavity Resonator Filters .....	7
1.5 Microfluidically Reconfigurable Devices .....	8
CHAPTER 2: WIDEBAND BAND-STOP X-BAND FILTER USING ELECTRICALLY SMALL TIGHTLY COUPLED RESONATORS .....	19
2.1 Filter Design .....	19
2.2 Experimental Verification .....	22
2.3 Concluding Remarks of Chapter 2 .....	24
CHAPTER 3: FREQUENCY-AGILE BANDPASS FILTER USING LIQUID METAL TUNABLE BROADSIDE COUPLED SPLIT RING RESONATORS .....	26
3.1 Filter Design .....	26
3.2 Experimental Verification .....	30
3.3 Concluding Remarks of Chapter 3 .....	31
CHAPTER 4: HIGHLY RECONFIGURABLE BANDPASS FILTER USING MICROFLUIDICALLY CONTROLLED METALLIZED GLASS PLATES .....	33
4.1 Filter Design .....	33
4.2 Fabrication .....	38
4.3 Experimental Verification .....	39
4.4 Concluding Remarks of Chapter 4 .....	39
CHAPTER 5: MICROFLUIDICALLY RECONFIGURABLE METALLIZED PLATE LOADED FREQUENCY-AGILE RF BANDPASS FILTERS .....	41
5.1 Filter Design .....	41
5.1.1 Resonator Model .....	41
5.1.2 External $Q_e$ and Coupling Coefficient .....	45
5.1.3 4 <sup>th</sup> Order Filter with Linear Resonator Arrangement .....	47

5.1.4 4 <sup>th</sup> Order Filter with Diagonal Resonator Arrangement .....	48
5.2 Microfluidic Channel Design .....	49
5.3 Fabrication .....	52
5.4 Experimental Verification .....	54
5.4.1 4 <sup>th</sup> Order Filter with Linear Resonator Arrangement .....	54
5.4.2 4 <sup>th</sup> Order Filter with Diagonal Resonator Arrangement .....	56
5.5 Concluding Remarks of Chapter 5 .....	56
CHAPTER 6: WIDELY TUNABLE, LOW LOSS FILTERS USING MICROFLUIDICALLY CONTROLLED VARIABLE LENGTH RESONATORS .....	58
6.1 Resonator Design .....	58
6.2 Filter Design .....	62
6.3 Fabrication .....	67
6.4 Experimental Verification .....	70
6.5 Power Handling Characterization .....	72
6.6 Concluding Remarks of Chapter 6 .....	75
CHAPTER 7: FUTURE WORK .....	77
REFERENCES .....	81
APPENDIX A: MICROFLUIDIC CHANNEL FABRICATION .....	88
A.1 Microfluidic Channel Design.....	88
A.2 Micromold Fabrication .....	89
A.3 Polydimethylsiloxane (PDMS) Preparation .....	92
A.4 Sealing the Channel (Bonding) .....	92
A.5 Selectively Metallized Plate Fabrication .....	94
APPENDIX B: COPYRIGHT PERMISSIONS .....	95
ABOUT THE AUTHOR .....	END PAGE

## LIST OF TABLES

Table 1	Thermal properties of the materials utilized .....	75
Table 2	Summary of filters realized through this dissertation .....	76



## LIST OF FIGURES

Figure 1	Varactor based tunable bandpass filter .....	2
Figure 2	Ferroelectric varactor based tunable bandpass filter .....	4
Figure 3	Continuously tunable MEMS based filter .....	5
Figure 4	Discretely tunable RF MEMS based filter .....	6
Figure 5	MEMS loaded evanescent-mode cavity resonator based filter .....	8
Figure 6	Microfluidically reconfigurable devices .....	9
Figure 7	Microfluidically reconfigurable bandstop filter .....	10
Figure 8	Liquid metal electromagnetic band-gap .....	11
Figure 9	Liquid metal CPW bandpass filter .....	12
Figure 10	Stopband filter .....	20
Figure 11	Normalized reactance slope ( $X/Z_0$ ) as a function BCB film thickness and signal line separation .....	20
Figure 12	Experimental verification of stopband filter .....	23
Figure 13	The tube based coupled line geometry and its equivalent multilayered strip model .....	26
Figure 14	Liquid metal $Q_e$ and $K$ extraction .....	27
Figure 15	Liquid metal filter .....	30
Figure 16	Two-pole filter .....	34
Figure 17	External quality factor ( $Q_e$ ) extraction .....	35
Figure 18	Variation of coupling coefficient ( $K$ ) .....	36

Figure 19	Fabricated two-pole filter .....	38
Figure 20	Reconfigurable capacitive loaded microfluidically based resonator .....	42
Figure 21	External quality factor extraction and coupling coefficient for different resonator arrangements .....	43
Figure 22	Designed 4 <sup>th</sup> order filters with linear resonator arrangement .....	46
Figure 23	Designed 4 <sup>th</sup> order filters with diagonal resonator arrangement .....	48
Figure 24	Metallized plate and channel shapes investigated for the linear and diagonal resonator arrangement .....	50
Figure 25	Experimental characterization of the 4 <sup>th</sup> order bandpass filter with linear resonator arrangement .....	53
Figure 26	Experimental characterization of the 4 <sup>th</sup> order bandpass filter with diagonal resonator arrangement .....	55
Figure 27	Microfluidically reconfigurable half wavelength resonator .....	59
Figure 28	External $Q_e$ extraction with tapping approach .....	61
Figure 29	External $Q_e$ extraction for capacitive coupling approach .....	63
Figure 30	External $Q_e$ extraction for capacitive coupling approach with added tuning stub .....	64
Figure 31	External $Q_e$ performance for three different approaches .....	65
Figure 32	Coupling coefficient for different S values .....	65
Figure 33	Microfluidically reconfigurable half wavelength resonator filter .....	66
Figure 34	Microfluidic channel fabrication .....	68
Figure 35	Separated layers .....	69
Figure 36	Experimental verification .....	71
Figure 37	Thermal simulations of the 4 <sup>th</sup> order bandpass filter with half wavelength resonators for different input power levels at 2.5 GHz .....	73

Figure 38	Power handling characterization of the 4 <sup>th</sup> order bandpass filter utilizing half-wavelength resonators at the lowest resonator's $Q_u$ frequency of 2.5 GHz .....	74
Figure 39	Piezo electric disk actuation proposed for future work .....	79

## ABSTRACT

Radio Frequency (RF) filters are among the key components of today's multifunctional devices and test equipment. However, the multifunctionality need significantly drives the required filter number and causes large areas to be allocated for filters. To alleviate this issue, over the recent years, reconfigurable filters have been proposed as an attractive alternative. Nevertheless, existing reconfigurable filter technologies demonstrate degraded performances in terms of loss, frequency tunability bandwidth, and power handling capability. This work investigates, for the first time, microfluidic based reconfiguration techniques for implementation of RF bandpass filters. Specifically, microfluidics is shown to provide mechanisms for achieving compact RF bandpass filters that can exhibit low loss, high power handling, and high frequency tunability. First, we present the utilization of liquid metals for realization of a frequency-agile microstrip bandpass filters consisting of broadside coupled split ring resonator (BC-SRR). In this design approach, one of the loops of the BC-SRR is realized from liquid metal to be able to microfluidically change the resonator shape and associated resonance frequency. The filter exhibits a 29% frequency tunable range from 870 MHz to 650 MHz, with insertion loss  $<3$  dB, over the entire frequency tuning range, for a fractional bandwidth (FBW) of 5%. To the best of our knowledge, this filter design is the first in available literature that shows a continuously frequency reconfigurable microfluidic RF band-pass filter. To overcome the oxidization and lower conductivity issues associated with liquid metals and enhance the frequency tuning range further, subsequently, we introduce a filter design technique in which microfluidically

repositionable metallized plates are utilized within microfluidic channels with ultra-thin insulator walls. Specifically, this technique is employed to design a two pole microstrip bandpass filter where microfluidically repositionable metallized plates are used to capacitively load printed open loop resonators. To operate the filter (and control movement of multiple metallized plates) with a single bi-directional micropump unit, a strategically designed meandered microfluidic channel is implemented. The filter exhibits a 50% tuning range (from 1.5 GHz to 0.9 GHz), with an insertion loss  $<1.7$  dB for a fractional bandwidth (FBW) of  $\sim 5\%$ . Following this success, the concept of microfluidic based reconfigurability is generalized to the implementation of higher order filters, for the first time in available literature, by designing two different fourth order bandpass filters. These filters exhibit linear and diagonal layout arrangements to demonstrate that microfluidic based reconfigurable RF filters can meet different footprint requirements as well. Selectively metallized plates are also employed for the first time to alleviate synchronized movement issues. The filters operate with 60% frequency tuning range, 5% ( $\pm 1\%$ ) FBW, and  $<4.5$  dB of insertion loss. Finally, we demonstrate that microfluidically repositionable selectively metallized plates can also be used to dynamically redefine the lengths of the microstrip line half wavelength resonators when resorted to ultra-thin microfluidic channel walls. By using this approach, a microstrip line combline filter is designed to realize a low loss and highly tunable ( $\sim 2.7:1$ ) RF bandpass filter that can also operate with near constant insertion loss performance. The fabricated prototype exhibits a 90% ( $2.7:1$ , 4 GHz to 1.5 GHz) frequency tuning range with 5% ( $\pm 1\%$ ) FBW and insertion loss below 3 dB. Since microfluidics presents an opportunity for high power RF applications, power handling capabilities of these novel combline filters are computationally and experimentally demonstrated. The filters can handle above  $>15$  W input power without the need of thick ground planes and/or heat sinks.

## CHAPTER 1: INTRODUCTION

In the recent years, the demand for compact multifunctional devices has increased significantly. This has placed stringent restrictions in the size of RF front-ends, where filters tend to represent a significant portion of the RF front-end, occupying large areas [1]. Also, with the introduction of LTE bands, the amount of filters utilized in RF transmitter and receiver systems has increased more than double and it is expected to continue on this trend [2]. Therefore, reconfigurable filters have recently been presented as a promising alternative to replace the large filter banks within RF front-ends [3]-[4]. Filters capable of handling high power level have become of great interest due to increasing demand for base station and satellite communications [5]. In addition, RF systems, like test equipment, require high-frequency and widely tunable bandpass filters [6]. With reconfigurable filters the footprint needed could be reduced, and the power consumption could be significantly improved. The existing literature on reconfigurable filter technologies can be classified as “ferromagnetic resonances in yttrium iron garnet (YIG) spheres” [7]-[9], “semiconductor varactors” [10]-[13], “ferroelectric varactors” [13]-[15], “RF micro-electromechanical systems (MEMS) varactors and switches” [17]-[20], and “evanescent mode cavity resonators” [21]-[23]. However, this literature also shows that achieving reconfigurable filters that can simultaneously provide high frequency tuning range (i.e. 50%), low loss, small footprint, and high power handling capability is still very challenging. To address these issues, “microfluidically reconfigurable devices” has also recently attracted interest in electromagnetics community. Therefore, to emphasize the novelty and importance of this

dissertation work, the following sub-sections present a detailed literature review of these existing reconfigurable RF filter technologies:

### 1.1 Semiconductor Varactors

Semiconductor varactors are popular in designing compact and fast tuning filters [10]-[13]. For example in [10], a varactor diode based filter is presented. The filter is designed utilizing suspended line resonator with an interdigital topology. Except for the first and last resonator, all the resonators are loaded with commercially available semiconductor varactors. The filter layout, and fabricated prototype, can be seen in Fig. 1(a) and Fig.1(b), respectively. A challenge for semiconductor varactor technology is to achieve a wide frequency tuning range with stable insertion loss performance. In addition, insertion loss significantly increases at higher

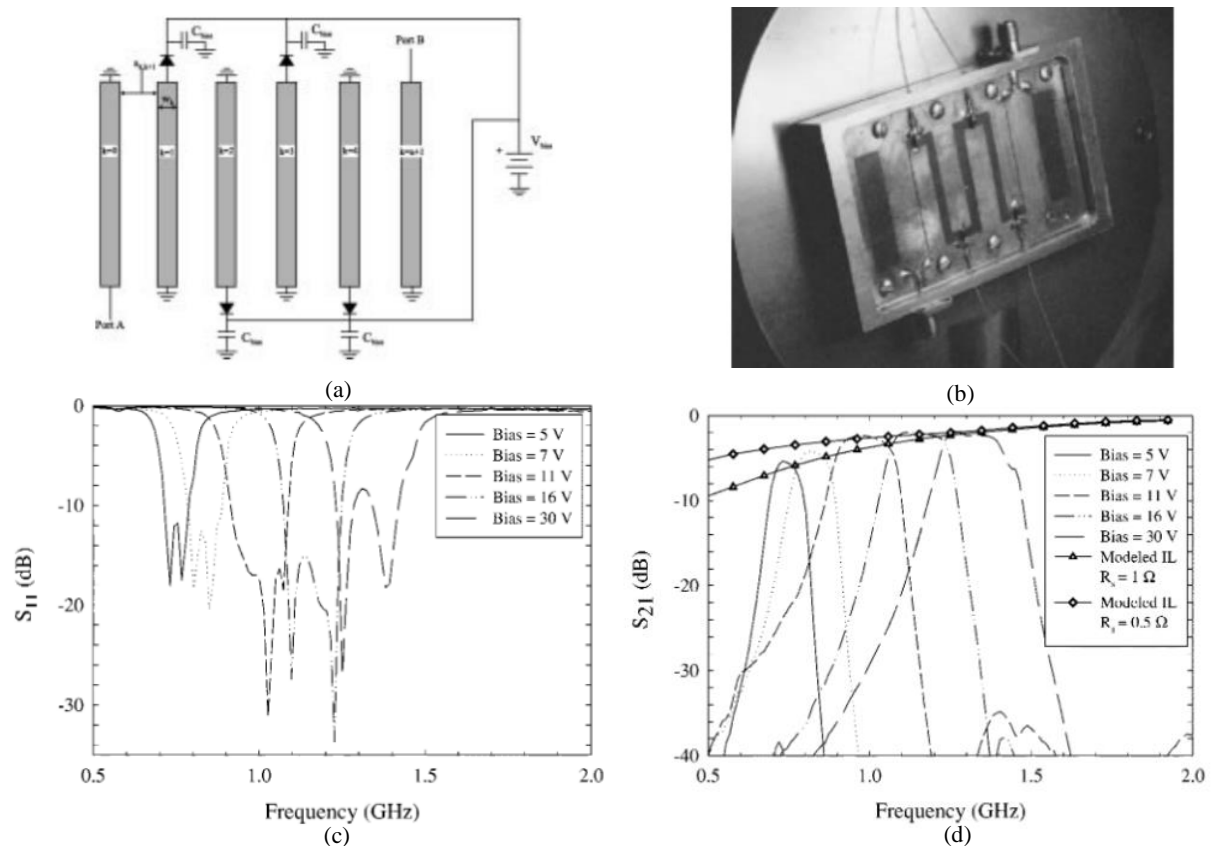


Figure 1: Varactor based tunable bandpass filter. a) Filter layout; b) Fabricated prototype; c)  $S_{11}$  measurements; d)  $S_{21}$  measurements and predicted loss. Images were taken from [10]

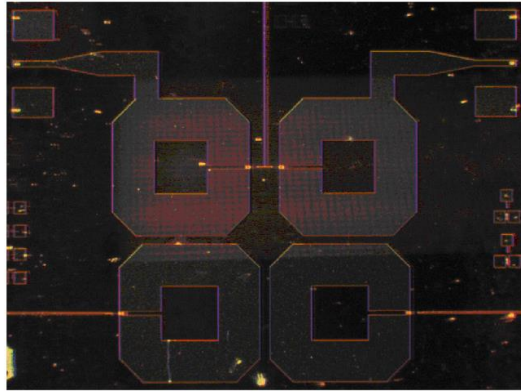
frequency implementations due to the equivalent series resistances of varactors. For example the shown filter presents a frequency tunable range of 60% (1.3 GHz to 0.7 GHz), however, the fractional bandwidth and insertion loss remains relatively constant as 16% and  $<3$  dB, respectively, only within a small frequency tuning range of 30% (1.3 GHz to 1 GHz). In addition, 3dB insertion loss from a 16% wide fractional bandwidth implies a low resonator quality factor and this is associated with the large series resistance ( $\sim 1\Omega$ ) of the semiconductor varactors (see Fig. 1(c) and (d)).

In general, filters loaded with semiconductor varactors exhibit a frequency tuning range that is proportional to the capacitance variation range of the varactors. By using diodes with higher capacitance variation (1.6 pF to 10 pF), reference [13] shows a 60% (2:1) tunable filter. However, such varactors are not available at high frequencies ( $>1\text{GHz}$ ) or exhibit high series resistance. Consequently, the filter in reference [13] was designed at a lower frequency of 0.6 GHz. Hence, achieving low loss performance over a wide frequency tuning range ( $>50\%$ ) at higher operational frequencies ( $>1\text{GHz}$ ) remains a challenge in this technology.

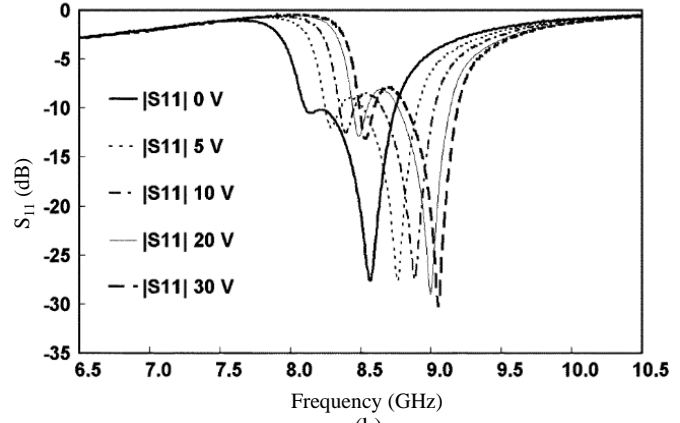
## 1.2 Ferroelectric Varactors

Ferroelectric materials are attractive for obtaining RF reconfigurable devices as applied external voltage across a ferroelectric material can reduce the value of its relative dielectric constant. Hence, ferroelectric materials can be utilized to form capacitors that can change their capacitance with applied bias voltage (i.e. ferroelectric varactors). Specifically, ferroelectric varactors are found attractive for realizing reconfigurable filters at higher frequency bands (e.g. X-band) since they exhibit better insertion loss and high power handling performances as compared to semiconductor varactors. Nevertheless, existing filter examples in literature demonstrate high level of insertion loss as a major limitation. In addition, frequency tuning

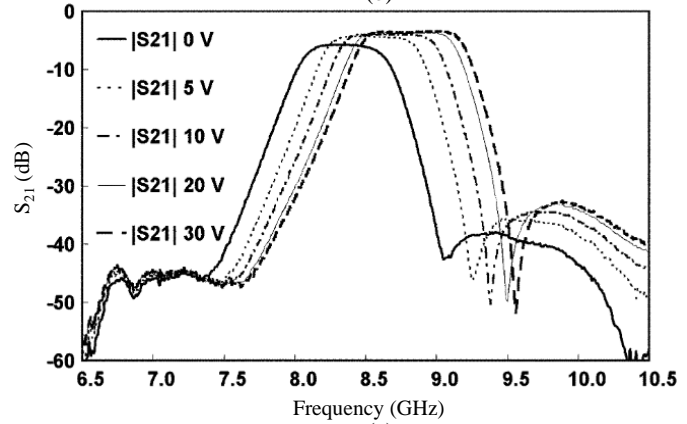




(a)



(b)



(c)

Figure 2: Ferroelectric varactor based tunable bandpass filter. a) Fabricated prototype; b)  $S_{11}$  measurements; c)  $S_{21}$  measurements and predicted loss. Images were taken from [15]

ranges are generally below 50%. As a typical example, we consider reference [15] that presents the design of a quasi-elliptic ferroelectric tunable filter. The filter is enabled by open-loop resonators loaded with high-Q ferroelectric barium strontium titanate (BST) varactors (Fig. 2(a)). This 4<sup>th</sup> order filter provides a 6% frequency tunable range centered at 8.35 GHz with an insertion loss (IL) and return loss (RL) performances varying between 5.7 – 3.5 dB and 10.2 – 7.9 dB, respectively (Fig. 2(b)). The correspondent 1 dB FBW varies from 5.5% to 7.3%. The overall footprint of the filter was measured as 5.7 x 5.5 mm<sup>2</sup>. As can be seen, ferroelectric varactors allow for realization of this compact tunable filter. However, the insertion loss is significantly high and frequency tuning range is very small due to the limited capacitance variation in ferroelectric varactors.

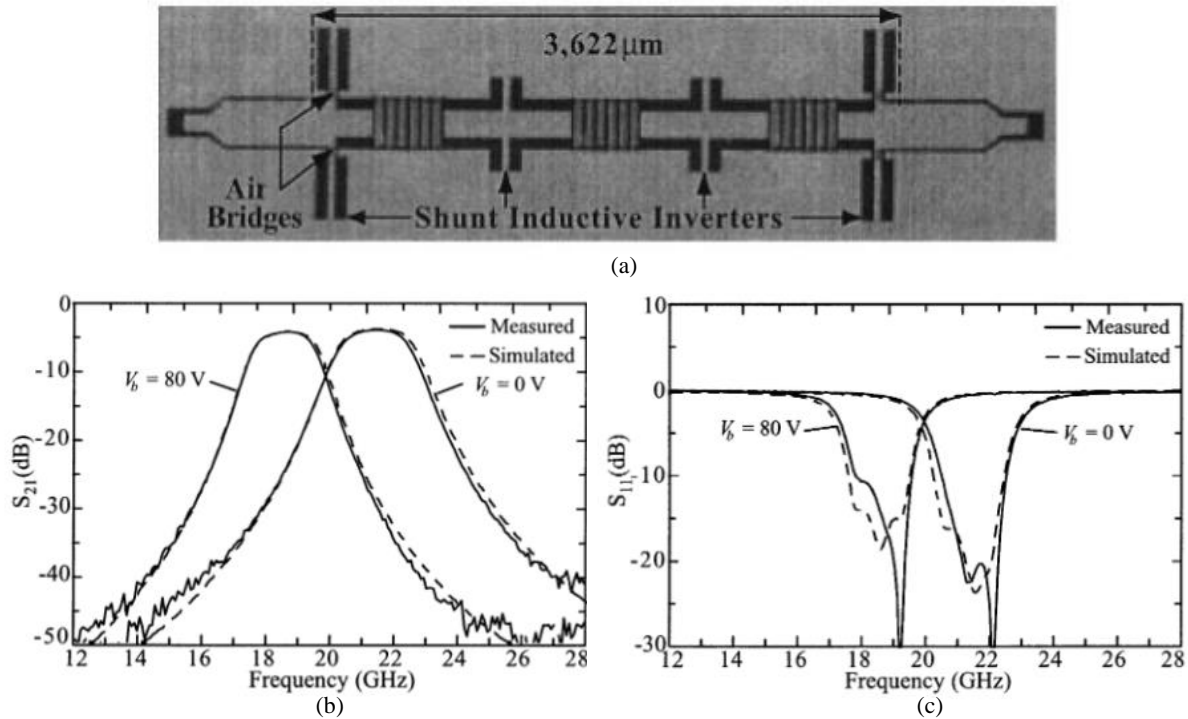


Figure 3: Continuously tunable MEMS based filter. a) Fabricated prototype; b)  $S_{21}$  measurements; c)  $S_{11}$  measurements and predicted loss. Images were taken from [17]

### 1.3 RF Micro-ElectroMechanical Systems (MEMS) Varactors and Switches

In order to further reduce the losses obtained from ferroelectric varactors, MEMS technology has been utilized to obtain miniaturized low-loss frequency tunable filters at high operational frequencies. As an example for the performance of MEMS technologies, we consider reference [17] that presents a coplanar waveguide (CPW) MEMS based tunable filter. The filter is formed by resorting to three CPW short-ended half-wavelength resonators loaded with high- $Q$  MEMS bridge capacitors. The capacitance obtained with MEMS technology is very small (in the femto scale). Therefore, as shown in Fig. 3(a), to obtain the required capacitance value, to load each resonator with 70fF, six bridges needed. As can be seen in Fig. 3(b), the filter was capable of providing a frequency reconfigurable filter at 20 GHz with a low IL <4.15 dB with a constant FBW of 7.5%. The tuning speed of the filter was characterized as 150 MHz per  $\mu$ s. However,

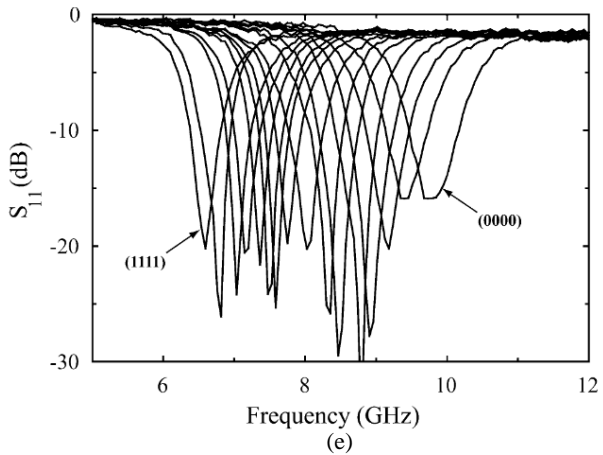
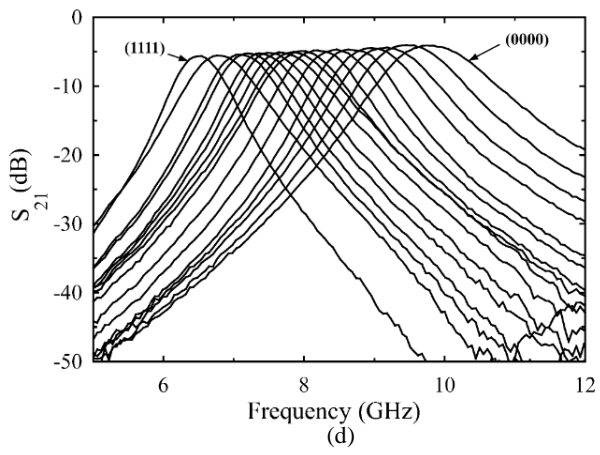
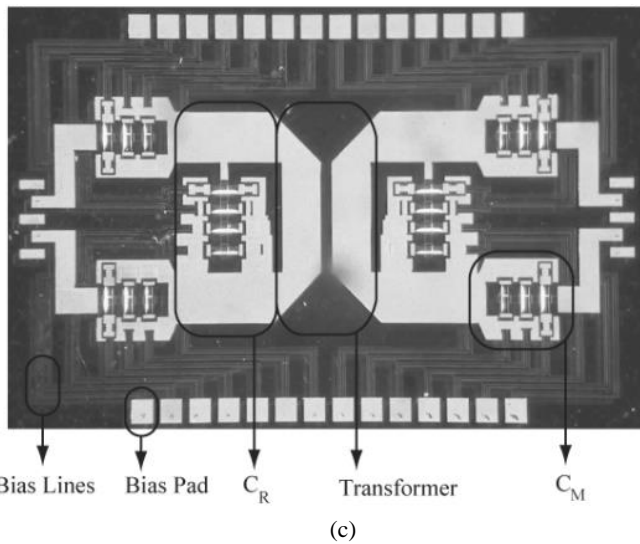
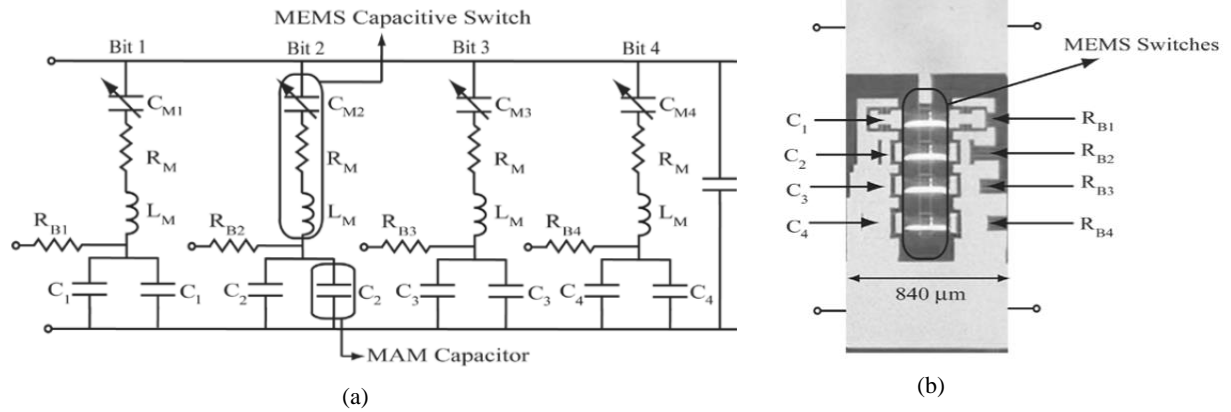


Figure 4: Discretely tunable RF MEMS based filter. a) 4-bit capacitor unit cell circuit model; b) Fabricated 4-bit capacitor unit cell; c) Fabricated Filter; d)  $S_{21}$  measurements; e)  $S_{11}$  measurements. Images were taken from [20]

due to the limitations in capacitance variation of MEMS capacitors, a small frequency tuning range (14%) was obtained. The continuous frequency tuning range of MEMS based filters is generally small, therefore, filters employing discrete MEMS switches have also been proposed to enlarge the frequency tuning range. As an example, we consider reference [20], where a capacitor bank with four unit cells (see Fig. 4(a) for circuit model and Fig. 4(b) for fabricated) is used as the digital tuning mechanism. In Fig. 4(a),  $C_M$ ,  $R_M$  and  $L_M$  represent the MEMS capacitor, while  $R_B$  represents the bias resistor. More specifically, this 4-bit differential filter (Fig. 4(c)) is capable of tuning 44% (from 6.5 GHz to 10 GHz) in 16 different discrete states. The insertion loss performance of the filter was measured to be  $<5.6$  dB at the smallest frequency of operation (Fig. 4(d)) with better than 16 dB return loss over the entire frequency range (Fig. 4(e)).

MEMS technology still presents several limitations in terms of continuous frequency tuning range and poor power handling capabilities ( $\sim 100$  mW). In addition, MEMS capacitors present a degraded performance in time. This makes their operational lifetime significantly shorter than semiconductor and ferroelectric varactor technologies.

#### **1.4 Evanescent Cavity Resonator Filters**

Evanescent cavity resonators have been known for providing very high unloaded  $Q$  ( $\sim 650$ ). Thanks to their high- $Q$  performance, evanescent cavity resonators can be combined with MEMS to achieve high tuning range, with very low insertion loss performance. For example, reference [22] utilized a MEMS membrane to change the capacitive loading on the post of an evanescent cavity resonator. This resonator topology is shown in Fig. 5(a). The resonance frequency can be varied from 1.9 GHz to 0.5 GHz while keeping a high- $Q$  value ( $>300$ ). Utilizing the resonator shown in Fig. 5(a), a two pole filter bandpass filter was designed (Fig.

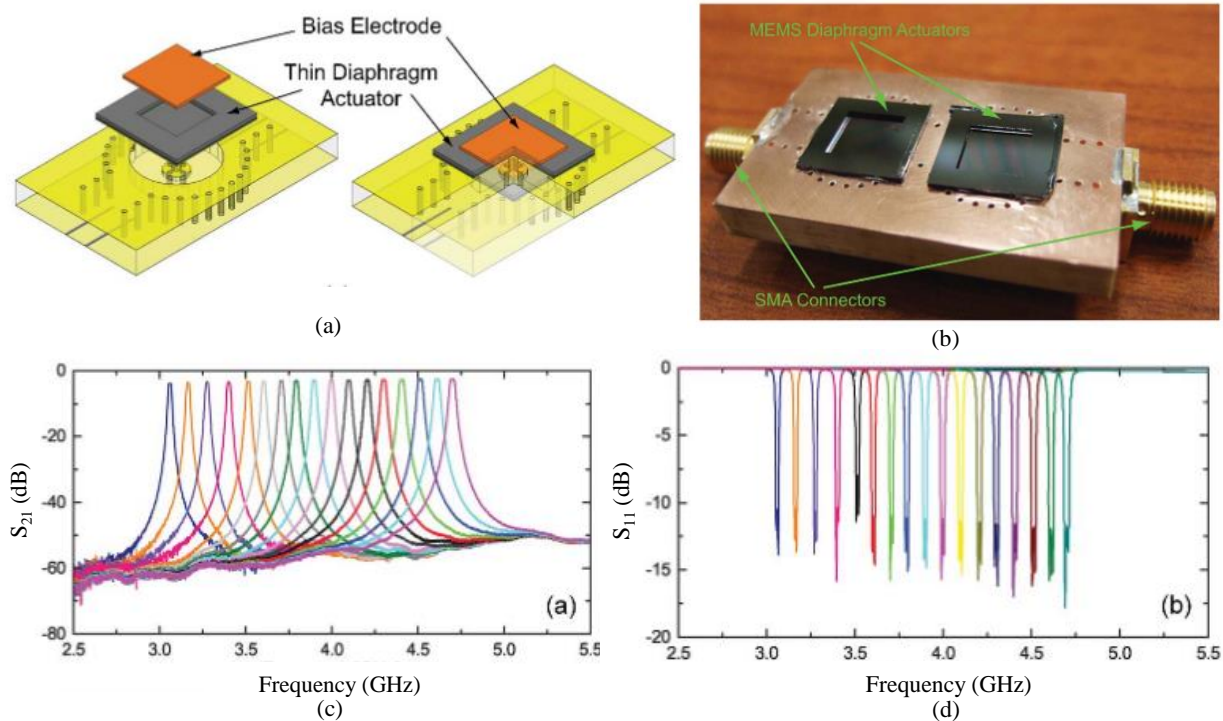


Figure 5: MEMS loaded evanescent-mode cavity resonator based filter. a) Tunable resonator; b) Fabricated two-pole tunable filter; c)  $S_{21}$  measurements; d)  $S_{11}$  measurements. Images were taken from [22]

5(b)). The filter performance, as shown in Fig. 5(c) and (d), is less than 3.5 dB of insertion loss for a 0.7% FBW over 40% (4.71 GHz to 3.04 GHz) frequency tuning range. However, as compared to printed microstrip line filters, the size of the filter is significantly large for a 4.5GHz filter by being  $42 \times 18 \text{ mm}^2$ . Also, since the tuning mechanism is based on MEMS, the operational lifetime and mechanical stability remains an issue.

### 1.5 Microfluidically Reconfigurable Devices

Since the end of the 20<sup>th</sup> century, and the beginning of the 21<sup>st</sup> century, microfluidics have been utilized in a variety of areas such as medical research [24]-[30], cooling systems [31], and optical devices/sensors [32]-[34], among others. It did not take long before microfluidics

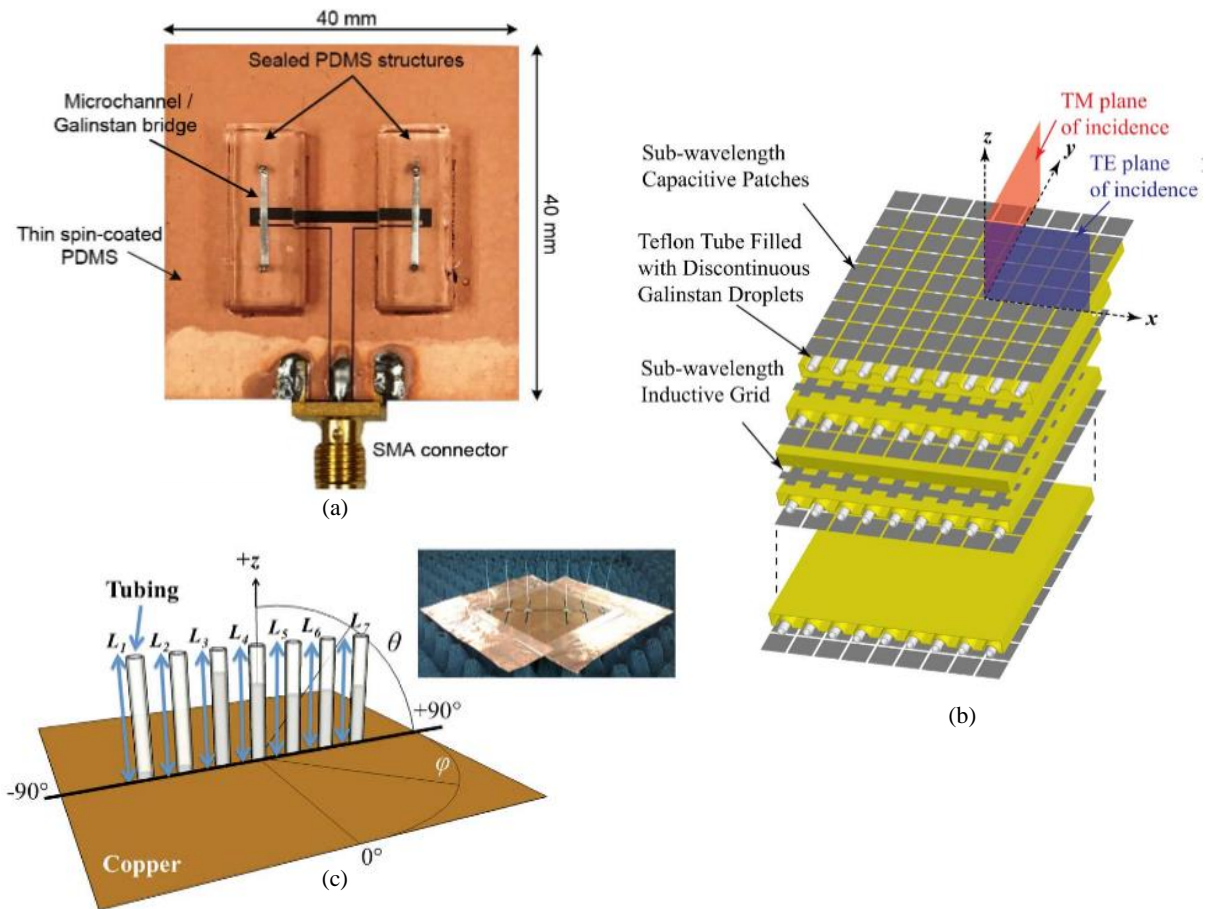


Figure 6: Microfluidically reconfigurable devices. a) CPW folded slot antenna; b) Frequency selective surface; c) Monopole array with beam-steering. Images (a), (b), and (c) were taken from [37], [42], and [44] respectively.

caught the interest of RF and microwave researchers [35]-[36]. More specifically, microfluidics have been used to obtain a variety of RF devices such as antennas [37]-[40], frequency selective surfaces [41]-[43], and beam steering [44]. Fig. 6 shows some of the fabricated devices. More recent studies have shown that microfluidics can be utilized to accomplish reconfigurability in RF filters [45]. Use of microfluidics in reconfigurable RF filters is especially attractive for obtaining low-cost, low loss, and highly reconfigurable filters capable

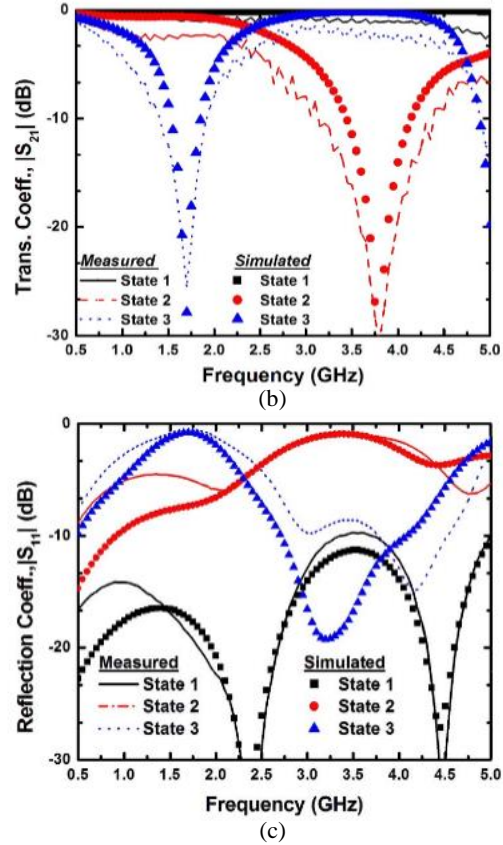
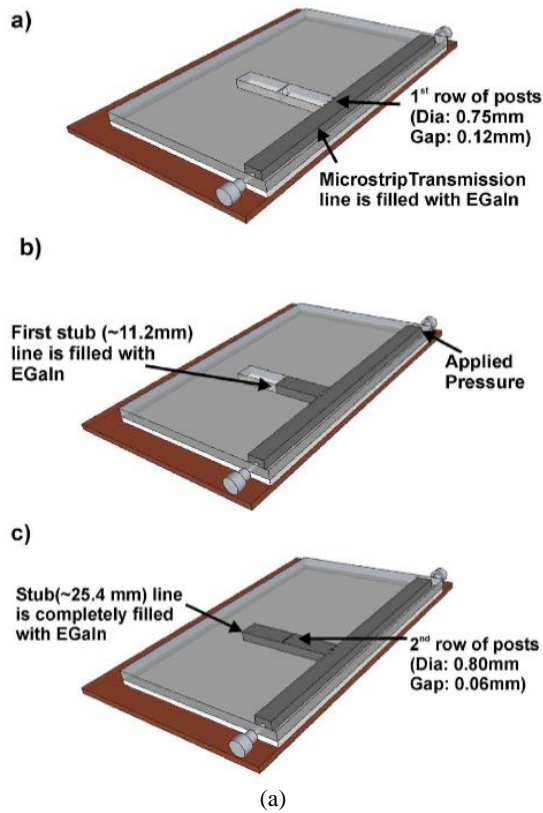


Figure 7: Microfluidically reconfigurable bandstop filter. a) 3-D representation of the filter; b) Measured and simulated  $S_{21}$ ; c) Measured and simulated  $S_{11}$ . Images were taken from [46]

of handling high RF powers. So far, the most common microfluidic based reconfiguration approach has been the utilization of liquid metals to reshape, load, or change dielectric properties of RF devices. The earliest work demonstrated the potential of microfluidics in realizing reconfigurable RF filters, but these filters were only one-time reconfigurable. For example, in [46] a microstrip bandstop filter is shown to be capable of operating at three different frequencies. The filter consists on a transmission line made out of liquid metal with an open stub. In the first state, the open stub is empty, and therefore, not seen by the signal. To prevent the liquid metal from flowing into the open stub, a row of post is utilized to work as a Laplace barrier Fig. 7(a). As a certain pressure is applied, the liquid metal will break the Laplace barrier and will flow into the open stub generating the stopband respond as seen in Fig. 7 (a). The same

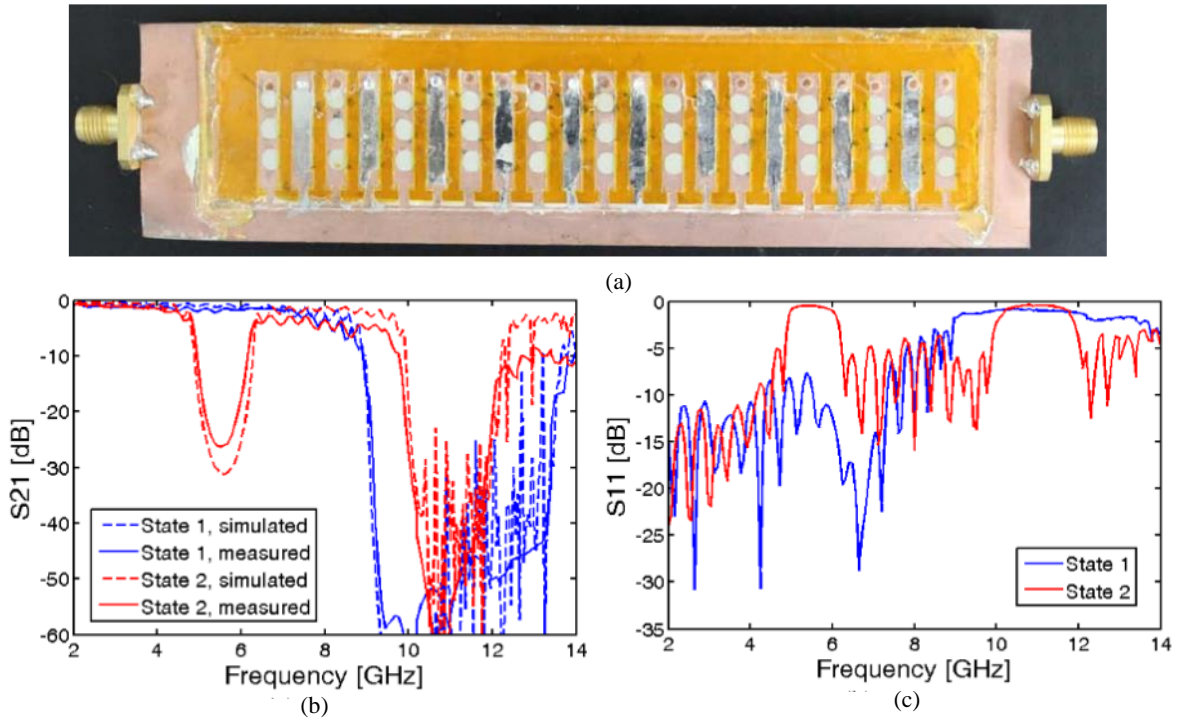


Figure 8: Liquid metal electromagnetic band-gap. a) Fabricated prototype; b) Measured and simulated  $S_{21}$ , c) Measured and simulated  $S_{11}$ . Images were taken from [47]

principle is utilized to divide the open stub in two regions (state 2 and state 3). Fig. 7 (b) and (c) show the simulated and measured  $S_{21}$  and  $S_{11}$  responses, respectively. However, once the liquid metal is flown to fill a channel it cannot be taken back to reverse the frequency reconfiguration due to sticking of the liquid metal to the channel. A different approach to obtain a one-time tunable bandstop filter was presented in [47]. The filter operated by filling out different reservoirs with liquid metals (see Fig. 8(a)) to reconfigure an electromagnetic band-gap structure coupled to a microstrip line. The filter was designed to operate at 10.1 GHz, and results showed good agreement between measurements and simulations at the initial state (state 1) and at state 2 (~5.5 GHz) (see Fig. 8(b) and (c)). More recently, a reconfigurable filter was presented in [48] by parasitically loading coplanar waveguide (CPW) resonators with liquid metals flown in microfluidic channels that are in close proximity of the resonators (Fig. 9). Due to the physical



separation between liquid metal and the resonator metallization, the filter is capable of reconfiguration by changing the liquid metal configuration. When the channel is filled with liquid metal, a capacitive loading effect is generated. Different states would represent different capacitive values. Therefore, in this filter, the tuning was accomplished in discrete steps by loading each resonator with the four variable liquid metal bridges. By filling, and emptying, the

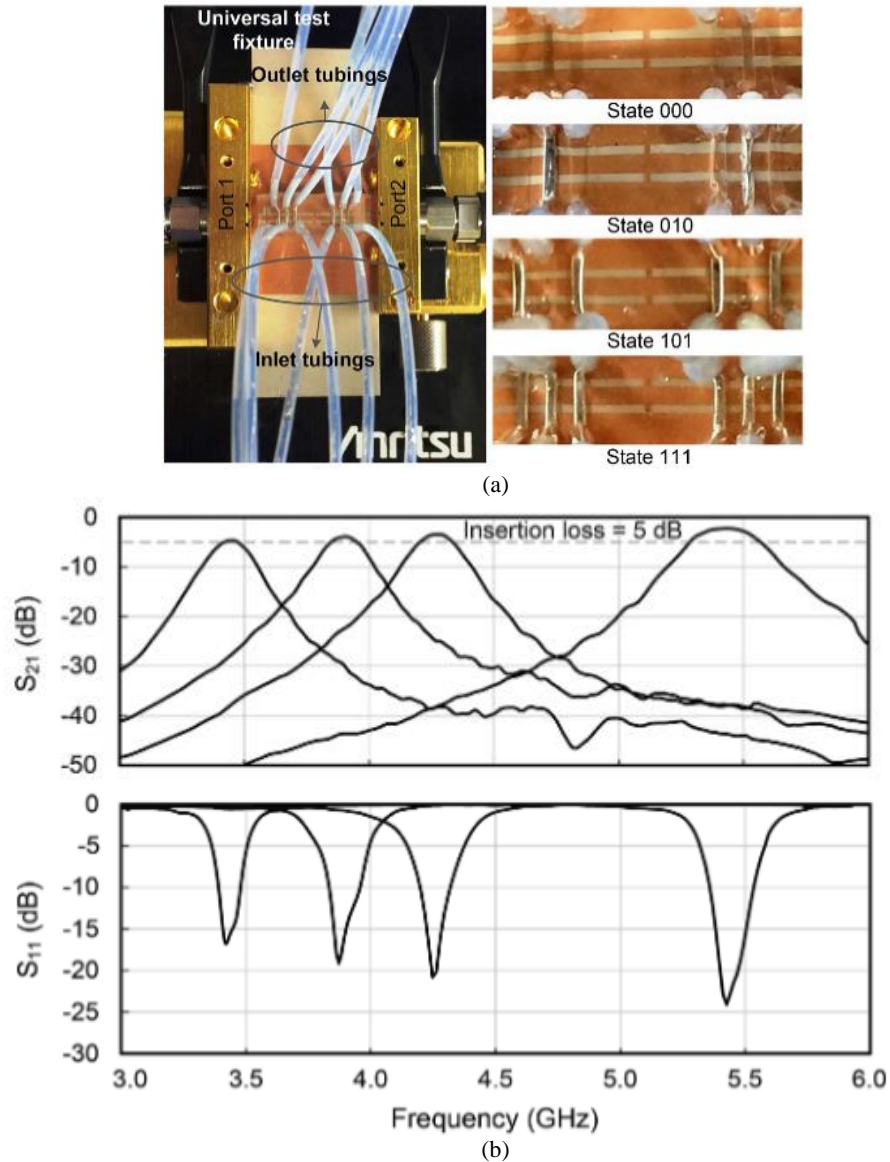


Figure 9: Liquid metal CPW bandpass filter. a) Fabricated prototype with 4 different states; b) Measured and simulated  $S_{21}$  and  $S_{11}$ . Images were taken from [48]

bridges, the filter in [48], was capable of providing a 47% discrete frequency tunable range through four different states. The insertion loss performance was  $<5$  dB with a relatively constant FBW of 5% as can be seen in Fig. 9(b). It is also important to note that reliable actuation of liquid metals is an on-going research effort and there is currently not a well-established solution. Rapid oxidization of liquid metals (significantly severe for non-toxic liquid metal Galinstan) causes them to stick to the channel walls irreversibly. Hence, life time of such filters are quite limited unless the liquid metal volume in use periodically gets replenished with new liquid metal volume free of oxidization [49].

Our research group has been a major contributor in the emerging area of microfluidically reconfigurable RF filters. When this dissertation work started, microfluidic based reconfigurable filters were at infancy with significant limitations, but with high promise for addressing the limitation of the previously mentioned technologies. More specifically, microfluidic reconfiguration was promising for obtaining widely tunable, low loss, and high power handling RF filters. The following sections of this dissertation will detail our contributions in this area and the evolution of our work throughout the last 4 years. Our initial work in [50] focused on implementation and miniaturization of band-stop microstrip filters by utilizing thin film fabrication procedures (such as benzocyclobutene (BCB)). It was found that thin-films can be used to achieve significant capacitance enhancement. The initial work in [50] utilized this capacitance enhancement to achieve a *compact* X-band filter with a *wideband* band-stop response. From this work, it became obvious that if thin-film fabrication techniques are applied for reconfigurable filters, a high frequency tuning range can be accomplished if a mechanism can be utilized to alter this capacitance during the device operation. This motivated us to investigate microfluidics potentially with thin film fabrication aspects. Our early work in microfluidically

reconfigurable RF filters dates back to 2013 [51] when one-time reconfigurable liquid metal based RF filters were being introduced. In contrast, we have (to the best of our knowledge) demonstrated for the first time the possibility of using microfluidics to realize frequency reconfigurable RF filters. This demonstration was carried out by designing and implementing a two-pole frequency-agile bandpass filter based on microfluidically reconfigurable broadside coupled split ring resonators (BC-SRRs). In these resonators, the top loop was constructed from liquid metal that can be flown inside Teflon microtubes. Hence, the resonance frequency of the filter could be changed repetitively by redefining the shape of the top loop of the resonator. A meandered microfluidic channel was also designed to be able to operate the filter with a single bi-directional micropump unit. The filter was shown to provide a continuous frequency tuning range from 650 to 870 MHz with a constant fractional bandwidth (FBW) of 5% and  $<3$  dB of insertion loss. The frequency tuning range of the filter was shown to be limited by the wall thicknesses of the tubes as the wall thickness affects the capacitive coupling between the two loops of a BC-SRR (i.e. capacitive loading of the resonator). In addition, the liquid metal based construction (Galinstan or Mercury) caused a reliability issue due to the aforementioned issues. For example, oxidization issue can be reduced by using mercury but its toxicity rules the technology out from commercial applications. A non-toxic liquid metal is Galinstan, however it oxidizes very fast and cause sticking within the tubes, potentially resulting in breakdowns in the liquid metal volume. Although several techniques have been presented to prevent the oxidization of Galinstan, such as covering the inside of the microfluidic channel with liquid Teflon solution [52], none of the techniques had proven success to completely remove the oxidization problem for a long device life time.

To overcome the limitations found with liquid metals, in [53] we took a major step by replacing liquid metal volumes within microfluidic channels with metalized plates that can still be moved within the channels. We demonstrated this novel technique by realizing a two pole reconfigurable bandpass filter with open-loop resonators where the open ends were loaded with microfluidically movable metalized plates. In this approach, the metalized plate acts as a capacitive load at the open ends of the open loop resonator. By microfluidically repositioning the metallized plate, the capacitive loading can be varied. To maximize the capacitance variation, microfluidic channels were constructed by utilizing 25.4  $\mu\text{m}$  thick Liquid Crystal Polymers (LCP) in order to exhibit a very thin wall above the printed filter area. As compared to prior liquid metal and tubed implementation, this novel two-pole bandpass filter exhibited a decrease of  $\sim 1.3$  dB to 1.7 dB improved insertion loss and a 50% frequency tuning range that is 60% more than the previous implementation. The toxicity and oxidization drawbacks associated with liquid metals were successfully addressed with the metalized plate approach.

The microfluidically reconfigurable metalized plate based filters exhibit multiple resonators each having their own metalized plate. In order to use a single bi-directional micropump, a single microfluidic channel was meandered over multiple resonators. This necessitated to have a synchronized motion of multiple plates within the microfluidic channels. Experiments performed with the two-pole filter mentioned above demonstrated that the metalized plate technique can suffer from synchronization issue due to the customized fabrication/placement of metalized plates. The synchronization issue is expected to be much more challenging for higher order filters exhibiting several resonators. Therefore, in [54], we introduced the concept of “microfluidically reconfigurable selectively metalized plates” to solve the synchronization issues and applied this concept to realize higher (4<sup>th</sup>) order bandpass filters.

To the best of knowledge, these were also the first higher order filters demonstrated with any microfluidic reconfiguration technique. Moreover, we also demonstrated that selectively metalized plate approach can be utilized for meeting different footprint requirements. A hybrid (EM + Lumped) circuit model was utilized in design of these filters in contrast to lengthy full-wave simulations employed for our prior filter designs. The filters were also controlled electronically with external micropumps. To the best of our knowledge, all the previous literature on microfluidic filters was done utilizing syringes, and no speed characterization can be found. With this set-up speed characterizations were performed and novel microfluidic channel shapes were introduced for speed improvements. The fabricated prototype was measured to provide a 5% (+/-1%) FBW over a 61% frequency tuning range with a worst case insertion loss of 4.5 dB.

Extending the frequency tuning range of open loop resonators that are loaded with microfluidically repositionable metalized plates beyond 2:1 is possible. However, high level of capacitive loading needed to lower the operational frequency of the resonator significantly reduces the unloaded quality factor of the resonator ( $Q_u$ ) and therefore the filter's insertion loss performance. A traditional approach to solve this issue would be to employ resonators with higher  $Q_u$  factors and perform microfluidic based reconfigurable capacitive loading to tune the resonance frequency. However, resonators employing higher  $Q_u$  factors are volumetric (such as evanescent cavity resonators and suspended microstrip line resonators) and therefore significantly increases filter size. As an alternative solution, in our most recent work, we introduce a novel approach for reconfiguration of conventional printed half wavelength microstrip resonators using microfluidics. Specifically, by placing a microfluidically repositionable selectively metalized plate on top of a conventional half wavelength microstrip resonator, the physical length of the resonator is dynamically redefined. This is accomplished by

utilizing an ultra-thin channel wall between the plate metallization and printed resonator so that an RF short is created. Since resonator is not externally loaded, the resonator exhibits a close to constant  $Q_u$  throughout the entire tuning range. To enlarge the frequency tuning range of the resonator beyond 2:1, a transition between open ended and short ended half wavelength microstrip resonators is also employed. By combining this two tuning approaches (i.e. extend the length of the resonator and transition from open ended to short ended structure), a resonator tunable over a wide frequency tuning range is accomplished. Utilizing this novel resonator, a 4<sup>th</sup> order bandpass filter was designed at 4 GHz. The presented results show that the filter operates with a 90% (2.7:1) tuning range, constant 5% FBW, and insertion loss performance less than <2 dB. To demonstrate that microfluidically reconfigurable filters are promising for high power RF applications, power handling characterization of the filter was also performed. Experimental results showed that this filter is capable of handling >15 W of input RF signal power at the highest operation frequency which also represents the lowest unloaded quality factor within the frequency tuning range. The power handling capability is limited by the highest temperature the materials within its construction can withstand to. The power handling capabilities of the filter can be significantly increased with addition of thicker ground planes, heat sinks, and/or by utilization of ceramic substrates.

In the following chapters, the contributions of this dissertation will be detailed. These contributions can be briefly summarized as:

- First time realization of a microfluidically reconfigurable frequency-agile bandpass filter.
- Introduction of microfluidically controlled metallized plates technique to alleviate reliability and high losses related to liquid metals.

- First time realization of higher order (4<sup>th</sup> order) microfluidically reconfigurable frequency-agile bandpass filters. These filters also show superior frequency tuning (~2:1) and high power handling capability.
- Introduction of a novel technique for synchronously tuning several resonators with a microfluidically repositionable *selectively* metallized plate.
- Introduction of strategically designed microfluidic channel and selectively metalized plate shapes for tuning speed improvement.
- Introduction of a novel half wavelength microfluidically reconfigurable resonator structure performing with close to constant unloaded quality factor across a very wide frequency tuning range (2.7:1, 1.5 GHz to 4.0 GHz).
- Realization of higher order frequency-agile bandpass filters with 90% frequency tuning range exhibiting low and close to constant insertion loss performances.
- Power handling characterization of microfluidically reconfigurable filters showing capability for handling >15 W of power.

## CHAPTER 2: WIDEBAND BAND-STOP X-BAND FILTER USING ELECTRICALLY SMALL TIGHTLY COUPLED RESONATORS<sup>1</sup>

Filter size becomes especially important when the receive/transmit circuits of large antenna arrays need to be tightly integrated. For this work, a critical performance requirement was a very narrow footprint (<2.5 mm) for a bandstop filter in the X-band region with a broad bandwidth of 25%. To address the contending size and bandwidth demand, the presented filter employed electrically small capacitively-loaded open loop resonators over a 7  $\mu\text{m}$  thin Benzocyclobutene (BCB,  $\epsilon_r=2.4$ ,  $\tan\delta=0.0015$ ) layer in order to bring them in close proximity of the microstrip signal line and maximize the coupling. Consequently, a compact wideband band-stop filter with a footprint of  $15.7 \times 2.5 \text{ mm}^2$  (i.e.  $\lambda_0/2 \times \lambda_0/13$  at 9.2 GHz) was realized. The fabricated filter demonstrated >25 dB IL from 8.1 GHz to 9.64 GHz. Moreover, it operated with <1.5 dB measured IL within its passband (i.e. <7.3 GHz and >11.2 GHz) and satisfied the desired selectivity criteria.

### 2.1 Filter Design

A microstrip implementation was utilized to be compatible with the desired installation requirements. To keep the size and passband IL small, the substrate material was selected as 99.9% Alumina ( $\text{Al}_2\text{O}_3$ ,  $\epsilon_r=9.8$ ,  $\tan\delta = 0.0004$ ). The circuit layout of the band-stop filter consisted of  $\lambda_g/4$  separated resonators coupled to a uniform microstrip signal line. As detailed in [55], the adjacent resonators are alternated on each side of the signal line to minimize their mutual coupling (see Fig. 10). Since the selected substrate thickness of 0.508 mm results in a

<sup>1</sup>This chapter was previously published in [50]. Permission is included in Appendix B.



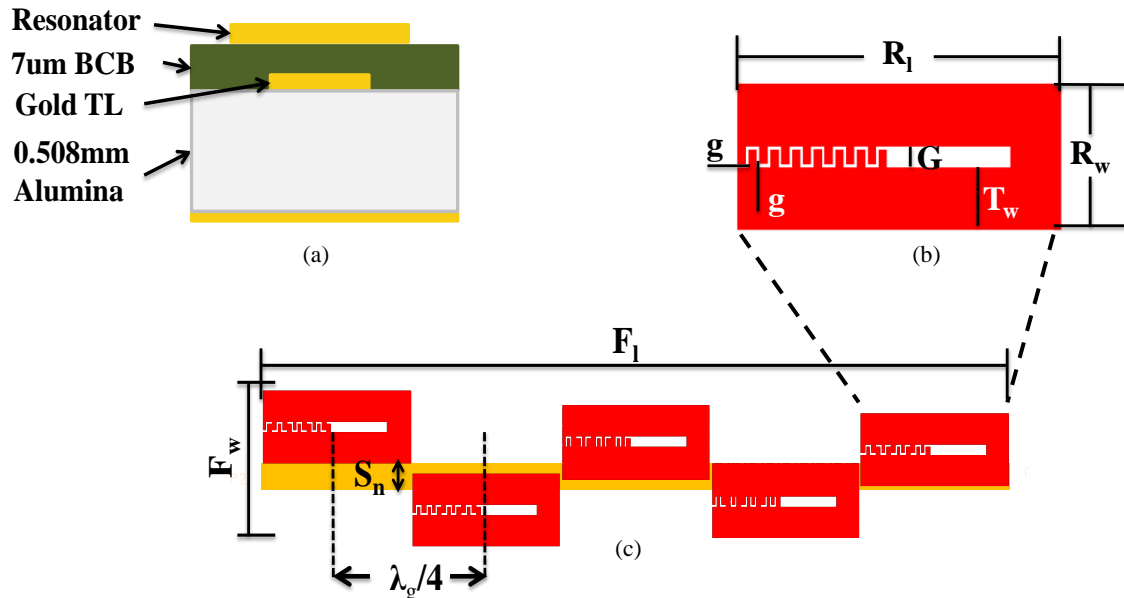


Figure 10: Stopband filter. (a) Substrate stack-up; (b) Capacitively-loaded (14 fingers) open loop resonator; (c) Filter layout. The dimensions (in  $\mu\text{m}$ ) are:  $T_w=406$ ,  $R_w=1100$ ,  $R_1=3000$ ,  $g=24$ ,  $G=167$ ,  $F_w=2400$ ,  $F_1=15700$ ,  $S_1=401$ ,  $S_2=160$ ,  $S_3=165$ ,  $S_4=23$ ,  $S_5=48$ ,  $\lambda_g/4=3100$ . The signal line width is  $406 \mu\text{m}$ .

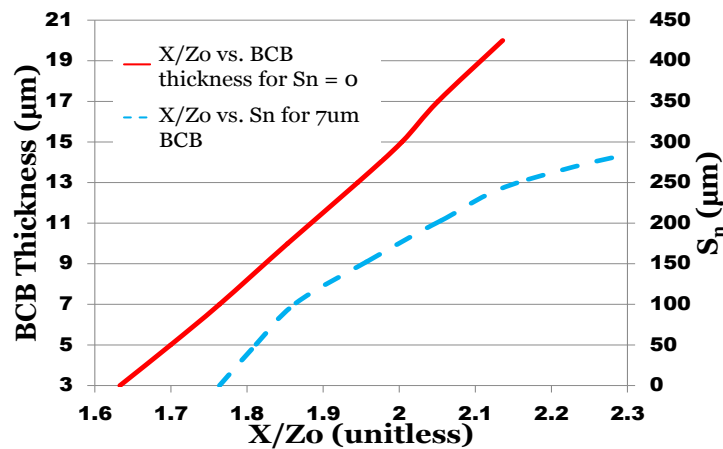


Figure 11: Normalized reactance slope ( $X/Z_0$ ) as a function BCB film thickness and signal line separation.

0.4947 mm wide  $50 \Omega$  signal line, the width of the resonator footprints had to be  $<1$  mm to meet the overall filter width specification of 2.5 mm. In addition, the  $\lambda_g/4$  separation limits the maximum resonator length to 3.1 mm. To address this size limitation, we considered the spiral (SR), split-ring (SRR), and capacitively-loaded open-loop resonators in an elongated rectangular shape (see Fig. 10(b)) as potential choices of electrically small designs. The coupling coefficient

studies with the conventional single layer realizations revealed that the desired 25% FBW was unattainable regardless of which type of resonator was used. For example, a separation of 0.5  $\mu\text{m}$  between any resonator type and the signal line leads to a small coupling coefficient that can only provide about 12% FBW. Consequently, a low loss thin film BCB layer was introduced between the signal line and the resonators to increase the coupling by overlapping the resonators and the signal line as shown in Fig. 10(c).

The performance evaluation of the resonators was carried out over a 20  $\mu\text{m}$ -thick BCB layer. For all resonators, it was found that the coupling was maximized as the line width of the overlapping trace of the resonators ( $T_w$ ) gets closer to that of the signal line. The layouts of the resonators were modified to fit into the specified area of  $3.1 \times 1.5 \text{ mm}^2$  and the one that provides the highest amount of coupling with the signal line was selected for the implementation. The normalized reactance slope ( $X/Z_0 = f_0/2\Delta f_{3\text{dB}}$ ,  $f_0$ : resonance frequency and  $\Delta f_{3\text{dB}}$ : 3dB IL bandwidth of a loosely coupled resonator) was extracted using the Momentum suite of the Agilent's Advanced Design System (ADS). SR and SRR resonators were able to fit into the given footprint area when smaller trace widths were utilized, however, this also resulted in larger  $X/Z_0$  values implying a smaller coupling level. The area of the open-loop resonator was miniaturized with the capacitive loading and by employing a trace width ( $T_w$ ) that is slightly narrower (i.e. 406  $\mu\text{m}$ ) than the signal line. With this configuration, the capacitively-loaded open loop resonator was found to provide the smallest  $X/Z_0$  value.

Having decided on the resonator type, the thickness of the insulator was investigated to realize the desired  $X/Z_0$  values. Fig. 11 presents the  $X/Z_0$  as a function of the insulator thickness when the resonator is positioned directly above the signal line ( $S_n=0$ ) for maximum coupling. Since  $X/Z_0$  must be smaller than 1.8 for the desired 25% BW, it is observed that the BCB layer

thickness should be kept below 8  $\mu\text{m}$ . Therefore, to accommodate fabrication tolerances of up to 10% while still remaining below the maximum 8  $\mu\text{m}$  thickness, and to reduce the impact of the resonators on the passband IL performance, a 7  $\mu\text{m}$  BCB layer thickness was chosen for the filter implementation. With this choice of BCB thickness the resonator dimensions representing the capacitive loading was first modified to tune the resonance frequency to 9.2 GHz. The desired  $X/Z_0$  values were realized by adjusting the position of the resonators relative to the signal line (i.e.  $S_n$  as indicated in Fig. 10(c)). As shown in Fig. 11,  $X/Z_0$  increases almost linearly with a rate of 0.0453 per  $\mu\text{m}$  as the resonator is moved away from the signal line. It is important to mention that since the desired selectivity values were not identical for the upper and lower passband edges, the final step in the design was to optimize the location of the resonators relative to the signal line to meet these specifications. This resulted in asymmetric resonator spacing within the filter layout as seen in Fig. 10(c). Additionally, optimizing the width of the signal line beneath the resonators was found to improve the passband IL. This is likely due to the variation in the characteristic impedance of the signal line due to the close proximity of the resonators. Specifically, the signal line width optimization resulted in a line width of 0.406 mm and improved the computed IL performance from 3 to 1.5 dB by improving the impedance matching within the filter, resulting in a better return loss. The finalized layout dimensions of the filter are given in Fig. 10(c). The filter implementation was carried out with 3  $\mu\text{m}$  thick gold to minimize the skin-effect loss.

## 2.2 Experimental Verification

The first conductor layer representing the feed-line was electroplated using 15 nm and 20 nm thick seed layers of chrome and gold, respectively. The BCB layer (Dow Cyclotene 3022-35 dry etch resin) was deposited using a spinner at the appropriate rate to achieve a 7  $\mu\text{m}$  thickness

and subsequently cured in a vacuum oven for 2.5 hours at 250° C. A slow temperature ramp (100° C per hour) was used to obtain a planar film. To form the second conductor layer representing the resonators a sputtering system was used to deposit 3 μm of gold and lift-off was performed subsequently with 3000py negative photo resist. Finally, the BCB was removed from the ends of the filter using O<sub>2</sub> and SF<sub>6</sub> plasma in a ratio of 5:1. As the BCB is etched at the same rate of the photoresist mask, a thick (17 μm) 4620 positive photoresist was used to protect the filter during the plasma etching process. Aluminum and gold were evaporated onto the backside of the wafer to obtain a good conductive ground. For RF measurements, the filter wafer and

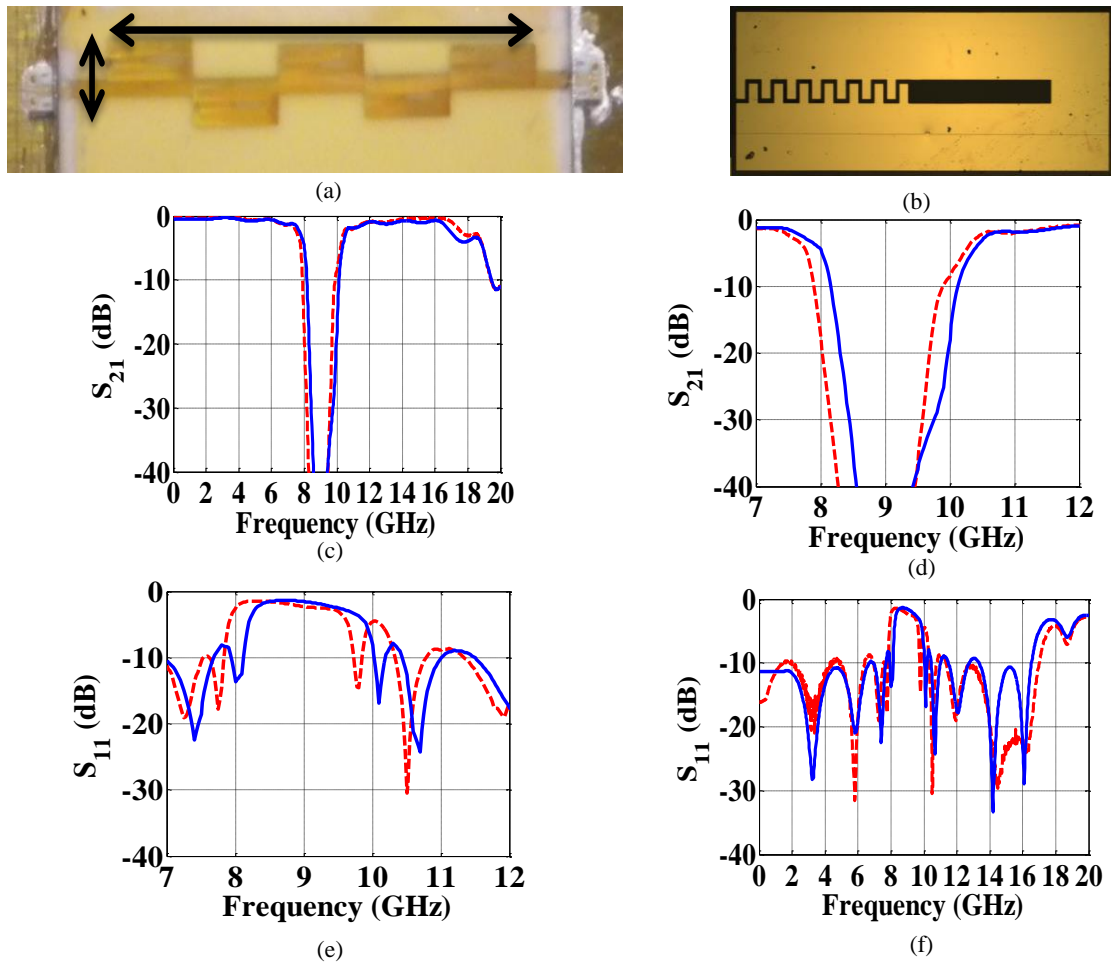


Figure 12: Experimental verification of stopband filter. (a) Fabricated filter and testing assembly with J-micro-probes; (b) Close-up snapshot of the resonator. Measured (—) and simulated (x-x-x) S-parameters: (c) & (d)  $S_{21}$ ; (e) & (f)  $S_{11}$ .

Jmicro Technology probe points were attached to a brass carrier using silver epoxy and interconnected using gold wire bonds. Fig. 12 (a) and (b) shows fabricated filter assembly and close-up view of the resonator on top of the BCB layer.

As a consequence of using an insulator layer with a thickness comparable to that of the conductor layer, a bulge was found to be formed along the length of the filter in the BCB layer even though a slow temperature ramp was used for the curing. Profilometer measurements revealed the height of this bulge to be  $\sim 3.5 \mu\text{m}$  higher than the nominal  $7 \mu\text{m}$  BCB height on top of the TL, with a width of  $\sim 0.5 \mu\text{m}$ . In order to accurately simulate this feature, the filter was modeled using the full-wave electromagnetic solver Ansys HFSSv14 by approximating the BCB surface and the overlaid resonators with small sections of rectangular planes. It was found that the bulge in the BCB accounted for a 300 MHz shift in the frequency response. Accordingly, future designs in need of wider bandwidths should consider an extra polishing step to planarize the BCB layer prior to the resonator metallization.

As shown in Fig. 12(c), (d), (e), and (f), the simulated and measured data are in good agreement. The measurements were performed using an Anritsu Lighting VNA and ground signal ground Picoprobes by GGB Industries, Inc. The measured passband IL was  $<1.5 \text{ dB}$  below 7.3 GHz and above 11.2 GHz. The 3 dB IL bandwidth extended from 7.62 GHz to 10.37 GHz, with more than 25 dB rejection between 8.1 GHz and 9.64 GHz and a selectivity of  $>40\text{dB}$  at both stop-band edges. Hence, the prototype successfully met the desired IL and selectivity criteria by providing 25% FBW.

### **2.3 Concluding Remarks of Chapter 2**

An electrically small coupled resonator X-band filter capable of exhibiting a 25% fractional bandwidth band-stop response was presented. Different than the existing designs, a 7

$\mu\text{m}$  thin BCB layer was utilized to bring the resonators within the close proximity of a microstrip feed line to achieve the desired wideband response. The resonator shape was specifically modified to minimize the width of the filter to 2.5 mm (i.e.  $\lambda_0/13$ ) at the center frequency of 9.2 GHz. The coupling level between the resonators and the signal line was presented as a function of BCB thickness and resonator position. Layout analysis and optimizations have demonstrated that the very thin BCB layer thickness results in variation in the optimum signal line width. In addition, the planarization of the insulator surface is important for the accuracy of the measured results. With this study it was found that high capacitance value can be obtained with a multilayer approach by resorting to thin-film insulators. In the following chapters the realization of multilayer filters, and the utilization of thin-film insulators, will be further extended to reconfigurable RF filters.

## CHAPTER 3: FREQUENCY-AGILE BANDPASS FILTER USING LIQUID METAL TUNABLE BROADSIDE COUPLED SPLIT RING RESONATORS<sup>2</sup>

Frequency-agile filters are among the key components for fulfilling the stringent requirements of emerging wideband and multifunctional RF front-ends. Due to the interest in liquid metals for achieving reconfigurable devices with lower loss and higher power handling capability, this work has introduced a continuously tunable liquid metal filter for the first time. The proposed two pole filter consists on a microstrip line broadsided coupled split ring resonator (BC-SRR) in which the top loop is made out of liquid metal. The frequency tuning is accomplished by gradually moving liquid metal out of the resonator region by displacing it with a low loss dielectric liquid.

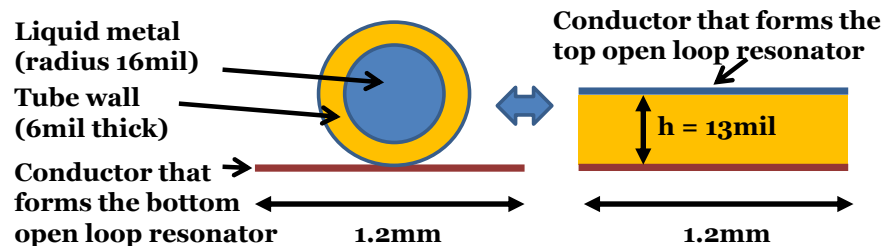
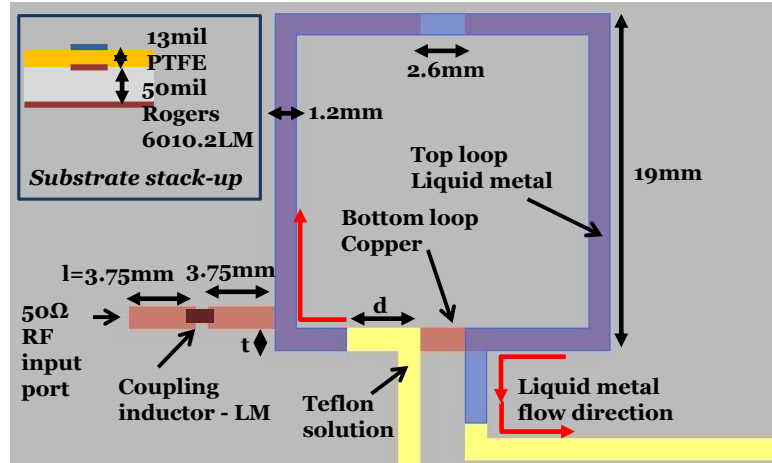


Figure 13: The tube based coupled line geometry and its equivalent multilayered strip model

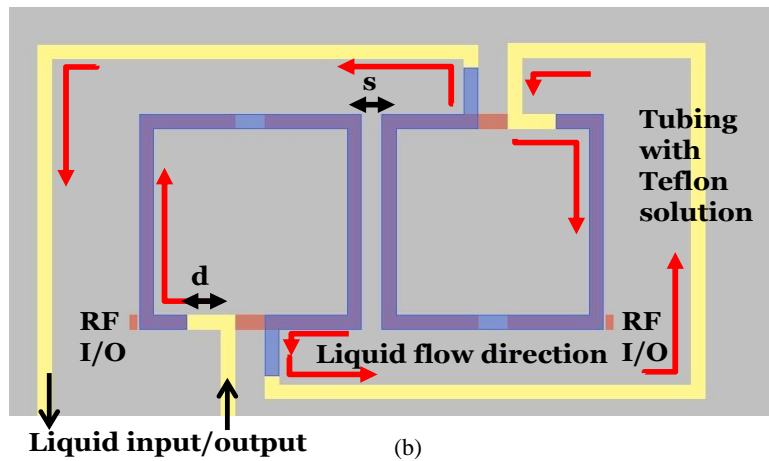
### 3.1 Filter Design

To verify the proposed concept without resorting to microchannel fabrication, the BC-SRRs of the presented filter are realized by making use of PTFE tubing. As shown in Fig. 13, the top open loop resonators of the BC-SRRs are constructed from overlaid liquid metal filled PTFE tubes having 16 mil (0.4064 mm) inner radius and 6mil (0.1524 mm) wall thickness. The

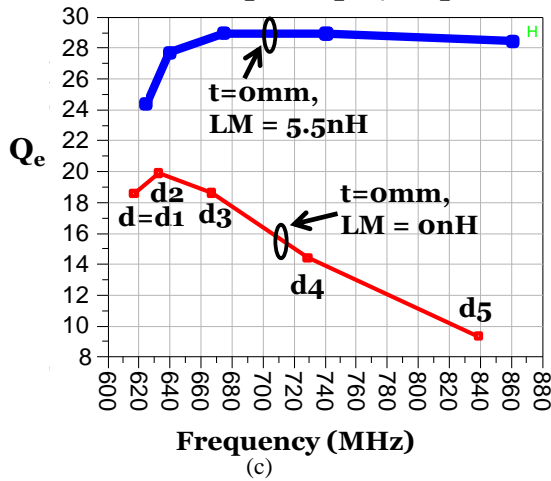
<sup>2</sup> This chapter was previously published in [51]. Permission is included in Appendix B.



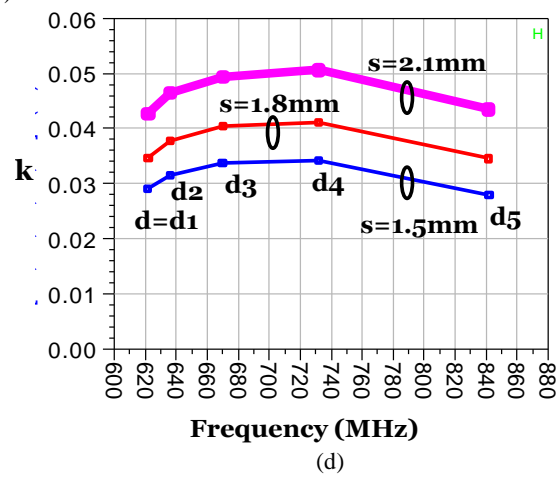
(a)



(b)



(c)



(d)

Figure 14: Liquid metal  $Q_e$  and  $K$  extraction. (a) The geometrical details of the liquid metal tunable BC-SRR; (b) Stabilization of the variation in  $Q_e$  over the frequency using coupling inductor as the filter is tuned by moving liquid metal to different positions ( $d=d_1=0$ ,  $d_2=7$ ,  $d_3=16.5$ ,  $d_4=26$ ,  $d_5=35.5$  mm); (c) Coupling alignment of adjacent resonators; (d) Coupling coefficient –  $k$  vs. frequency as the filter is tuned by moving liquid metal to different positions ( $d=d_1=0$ ,  $d_2=7$ ,  $d_3=16.5$ ,  $d_4=26$ ,  $d_5=35.5$  mm).



bottom loop of the resonator is formed by a  $50 \Omega$  microstrip line with 1.2 mm width. The design and parametric optimizations of this geometry through full wave electromagnetic simulation software is computationally expensive and quite time consuming. In order to utilize the fast planar circuit simulation tools (i.e. circuit schematics and Momentum) of Agilent Advanced Design System (ADS), an equivalent multilayered strip model was employed by considering the capacitance per unit length between the two conductor lines of the BC-SRR. Ignoring the fringing fields, equating the capacitance per unit length of the two structures shown in Fig. 13 results in an equivalent thickness of  $h=11.5$  mil for the multilayered strips. The resonance frequency comparison between the full wave (Ansys HFSSv14) and the ADS model of a BC-SRR resonator demonstrated that  $h=13$  mil is more accurate for representing the resonance frequency. Hence, the filter design was carried out by the equivalent model that represents the liquid metal with a 1.2 mm wide line printed on a 13 mil (0.3302 mm) thick PTFE substrate ( $\epsilon_r=2.2$ ,  $\tan\delta=0.0001$ ).

Fig. 14 depicts the computational model of the BC-SRR with its substrate stack-up and physical dimensions. The BC-SRR is square and its dimensions are adjusted such that its bottom open loop resonates at about 850 MHz without the presence of the top loop. When the top loop is completely filled up with liquid metal (i.e.  $d=0$  mm), the proposed BC-SRR configuration resonates at its lowest frequency of 630 MHz. This frequency is determined by the physical separation between the loops of the BC-SRR and can be further reduced if tubes with thinner walls or microfabrication techniques are utilized. Moving the liquid metal out of the resonator area by displacing it with Teflon solution ( $\epsilon_r=2.2$ ) gradually shifts the resonance frequency to that of the single loop resonator for  $d=35.5$  mm.

The required external quality factor ( $Q_e$ ) and coupling coefficient ( $K$ ) of a second order Butterworth coupled resonator filter can be calculated from its lowpass lumped circuit prototype ( $g_0=g_3=1$ ,  $g_1=g_2=1.4142$ ) as  $Q_e = g_0 \cdot g_1 / \text{FBW} = 28$  and  $K = \text{FBW} / \sqrt{(g_1 \cdot g_2)} = 0.0354$  for a FBW of 5% [55]. Such a filter can exhibit a well-matched constant FBW performance only if  $Q_e$  and  $K$  are maintained relatively constant over the tuning range of its resonators. As depicted in Fig. 14(c), the  $Q_e$  of the liquid metal based BC-SRR significantly decreases as it is tuned to higher frequencies. This behavior is independent of the tapping location  $t$ . To stabilize the variation in  $Q_e$  over the tuning range, a lumped coupling inductor (LM) was introduced to the feed line as shown in Fig. 14(c). The reactance of the inductor is proportional to the frequency and counteracts the reduction in  $Q_e$  at higher frequencies. Parametric studies were carried out in ADS and a tapping location of  $t=0$  mm with  $\text{LM}=5.5$  nH was determined to provide a relatively constant  $Q_e$  over the operational band. These studies were carried out by simultaneously considering five different liquid metal locations ( $d=d_1=0$ ,  $d_2=7$ ,  $d_3=16.5$ ,  $d_4=26$ ,  $d_5=35.5$  mm) and these are identified as data points in the design curves presented in Figures 14(c) and (d).

To achieve a relatively constant  $k$  over the frequency range, different resonator alignments were initially considered. Among these, the  $180^\circ$  rotated alignment shown in Fig. 14(b) was found to satisfy the desired need. As depicted in Fig. 14(b), the separation between the resonators was selected to be 1.8 mm to ensure that the minimum filter bandwidth was at least 5% over the tuning range. Specifically, the  $k$  is 0.035 at the edges and 0.04 at the middle of the operation band. It should be noted that non-square resonator shapes can be potentially employed possibly with lumped coupling capacitors to realize different tunable bandwidth characteristics such as increasing/decreasing or constant absolute bandwidth. Such shape modifications may also provide better  $Q_e$  and  $K$  stability over frequency and they are currently being investigated.

Fig. 14(b) also demonstrates the proposed tubing layout of the filter. As seen, the frequency tuning of the resonators can be simultaneously controlled using a single syringe pump or micropump unit. This requires an accurately adjusted Teflon solution spacing between the liquid metal volumes.

### 3.2 Experimental Verification

Fig. 15(a) shows the fabricated filter prototype. The PTFE tubing was accurately aligned and positioned over the printed open loop resonators by milling cut outs through low loss 1.575 mm thick Rogers 5880 substrate ( $\epsilon_r=2.2$ ,  $\tan\delta=0.0009$ ). The tubes were stabilized in their locations by using Scotch™ tape. Mercury and Galinstan are the two types of liquid metals that can be employed for the proposed filter. Galinstan is known to be sticky due to oxidation, but it

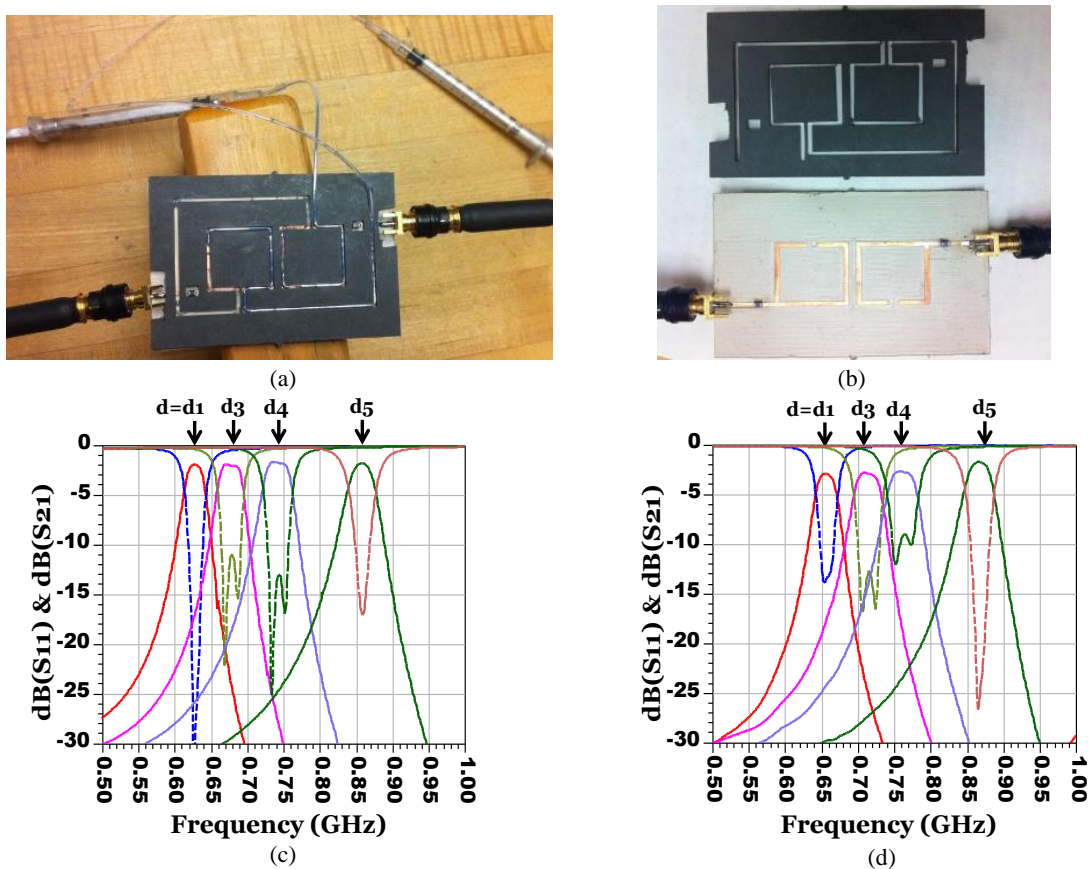


Figure 15: Liquid metal filter. a) Fabricated filter board; b) Microfluidic channels loaded with metalized glass plate; c) Simulated and d) Measured insertion and return loss performances

can still be moved within the PTFE tubing with the aid of Teflon solution (AF 400S2-100-1, 1% Teflon™ powdered resin dissolved in 3M FC-40, acquired from Dupont). Due to its non-toxicity, Galinstan ( $\sigma=3.46 \times 10^6$ ) was selected for the experimental verifications. The liquid metal and Teflon solution was controlled by two syringes as depicted in Fig. 15(a). The ADS simulations of the overall filter for various  $d$  values using the  $LM=5.5$  nH coupling inductors resulted in a return loss that is not well matched ( $<8$  dB). To alleviate the issue, a parametric sweep was carried out over the complete filter models. For  $t=0$  mm, increasing the coupling inductors to  $LM=12$  nH was found to provide a return loss performance  $>10$  dB over the whole frequency range as shown in Fig. 15(c). The inductors were acquired from the Coilcraft 0805CS series and were modeled to exhibit a  $Q$  of 50 at 850 MHz. The simulated insertion loss is about 2 dB throughout the operation band. Fig. 15(d) presents the measured performance of the filter. For the filter prototype,  $LM=10$  nH was experimentally determined to provide the best  $>10$  dB return loss performance. The measured filter responses are about 20 MHz higher than the simulated data. The measured insertion loss is 3 dB at the lowest frequency. These slight deviations in measurements can be associated with the imperfections in fabrication, unaccounted loss of the PTFE tubing and the overlaid substrate used for guiding the tubing. The filter exhibits a measured tunability from 650 to 870 MHz with near constant 5%, -3 dB, FBW. The footprint of the resonators is about  $20 \times 40$  mm<sup>2</sup>.

### 3.3 Concluding Remarks of Chapter 3

Frequency-agile filters based on liquid metal tunable BC-SRRs were presented. The concept is demonstrated through a second order Butterworth filter prototype realized by using PTFE tubing filled with Galinstan and Teflon solution. Specifically, a constant 5% FBW bandpass filter tunable from 650 to 870 MHz was demonstrated to operate with  $<3$  dB insertion

loss. The tunability range of these filters can be significantly extended using microfabrication techniques to bring the liquid metal physically closer to the bottom open-loop resonator of the BC-SRR. By using ultra-thin micro-channels, the tuning speeds can be less than milliseconds. The piezoelectric based micropumps can be utilized for convenient control of the tuning mechanism. The presented design is also suitable to be generalized to higher order tunable filters that are controlled only with a single pump. Realization of these aspects will be presented in the following chapters. However, it is important to mention that its tuning speed will be significantly lower as compared with other type of tunable filters like piezoelectric or ferroelectric based. Also due to its mechanical properties, lifetime of the filter can be compromised; therefore, in the following chapter we demonstrate a filter with metallized plates instead of liquid metal to extend its lifetime. Since the tunability is not based on any non-linear device, in future chapters we demonstrate the high power capabilities of microfluidically based filters.

## CHAPTER 4: HIGHLY RECONFIGURABLE BANDPASS FILTER USING MICROFLUIDICALLY CONTROLLED METALLIZED GLASS PLATES<sup>3</sup>

Even though liquid metal represents a strong alternative to accomplish reconfigurable RF filters, it introduces several issues such as its toxicity, low reliability due to quick oxidization, and high losses. To overcome these limitations, we resorted to a novel resonator arrangement that allows for replacing the liquid metal by metallized glass plates. To enhance the capacitive loading of the metallized glass plates, we also resorted to in-house built microfluidic channels constructed from thin insulator walls. As expected, this channel construction increased the frequency tuning range of the filter considerably as compared to prior liquid metal and tube base approach.

### 4.1 Filter Design

Fig. 16(b) depicts the substrate stack-up used to construct the presented microfluidic based reconfigurable filter. A two pole coupled resonator bandpass filter was realized to operate at 1.5GHz utilizing the approach explained in [55]. The filter consisted of two open loop microstrip resonators printed on a 1.27mm thick Rogers 6010.2LM board ( $\epsilon_r = 10.2$ ,  $\tan\delta = 0.0023$ ). The dimensions of the resonator are shown in Fig. 16(a) and they were finalized by utilizing the Momentum suite of Agilent Advanced Design System (ADS).

The tuning mechanism of the filter relied on moving a metallized glass plate over the open ends of the resonators as illustrated in the layout shown in Fig. 16(c). The metallized glass plate creates a capacitive loading effect across the open ends of the resonator and therefore

---

<sup>3</sup>This chapter was previously published in [53]. Permission is included in Appendix B.

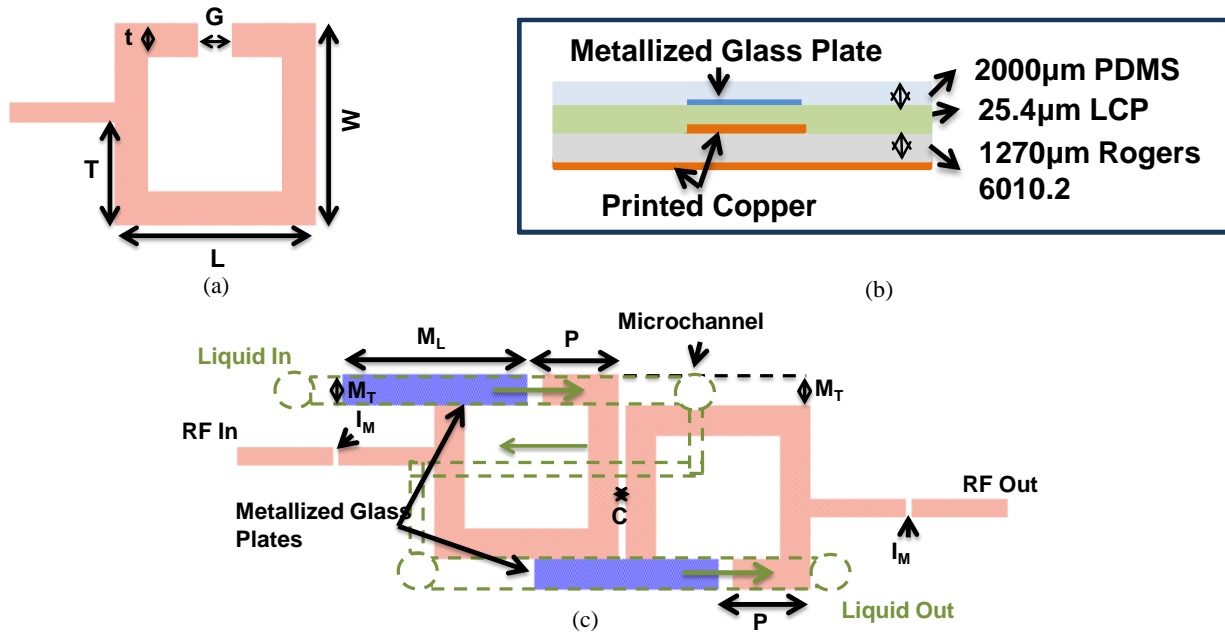


Figure 16: Two-pole filter. a) Printed open-loop resonator ( $G=2\text{mm}$ ,  $T=6.1\text{mm}$ ,  $L=12.4\text{mm}$ ,  $W=12.4\text{mm}$ ,  $t=2\text{mm}$ ); b) substrate stack-up; c) filter layout ( $M_L=10\text{mm}$ ,  $M_T=2\text{mm}$ ,  $I_M$ =matching inductor,  $C=0.4\text{mm}$ ,  $P$ =Position of top plate.)

causes a shift in the resonance frequency. Depending on the position of the metallized plate, the amount of capacitive loading varies and gets maximized (i.e.  $C_{\text{max}}$ ) when the plate is centered over the resonator's arm. Most importantly, this capacitive loading can be completely removed (i.e.  $C_{\text{min}}=0$ ) by retracting the metallized plate completely out of the resonators' gap ( $G$ ). This allows for an extended range of tuning capability as compared to varactors. By resorting to a  $25.4\ \mu\text{m}$  thick readily available LCP insulator between the metallized plate and the printed open loop resonator, the tuning range was pushed down to 0.9 GHz. To obtain a reconfigurable constant FBW response, the glass plates need to be precisely moved on top of the open end of the printed resonators by using microfluidics. Positioning the metallized plate 10mm away from the edge of the resonator (i.e.  $P = 10\text{mm}$  in Fig. 16(c)) causes zero capacitive loading and the filter operates at 1.5 GHz. On the other hand, when  $P = 4\ \text{mm}$ , the capacitive loading increases, and the filter operates at 0.9 GHz, providing 50% frequency tuning range. As expected, the

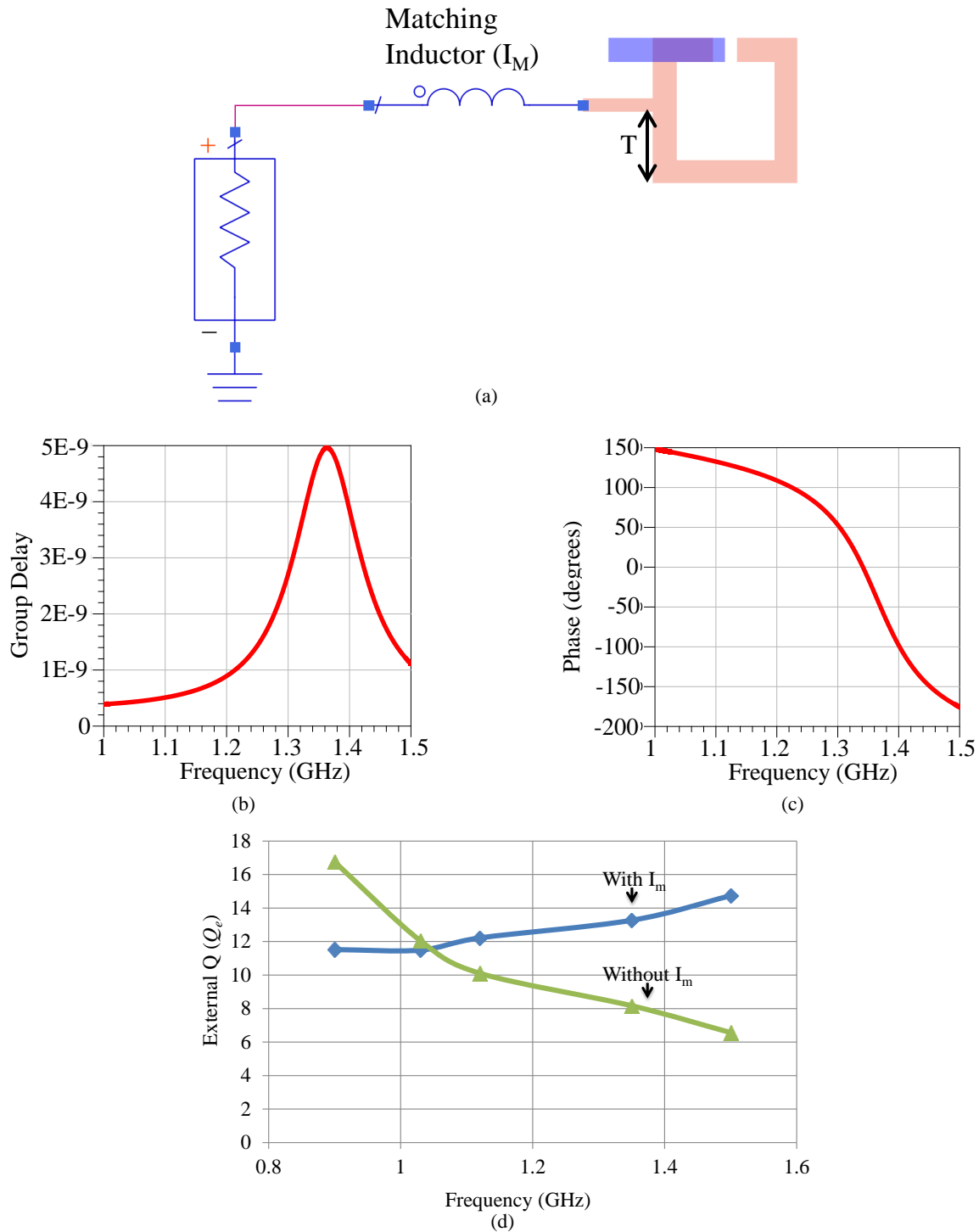


Figure 17: External quality factor ( $Q_e$ ) extraction. a) Hybrid (schematic + Layout) model for extracting  $Q_e$ ; b) Group Delay utilized to determine the center frequency; c) Phase in degrees; d) External  $Q_e$  with and without the matching inductor as a function of frequency for  $I_m = 2.5$  nH (with  $P=P_1=4$ ,  $P_2=4.5$ ,  $P_3=4.7$ ,  $P_4=6$ ,  $P_5=10$ )



insulator layer thickness affects the tuning range of the filter significantly. For example, increasing the insulator thickness from 25  $\mu\text{m}$  to 50  $\mu\text{m}$  decreases the frequency tuning range by more than half.

To design a two pole Chebyshev bandpass filter with 5% FBW, the required external quality factor ( $Q_e$ ) and coupling coefficient ( $K$ ) were calculated from its lowpass lumped circuit

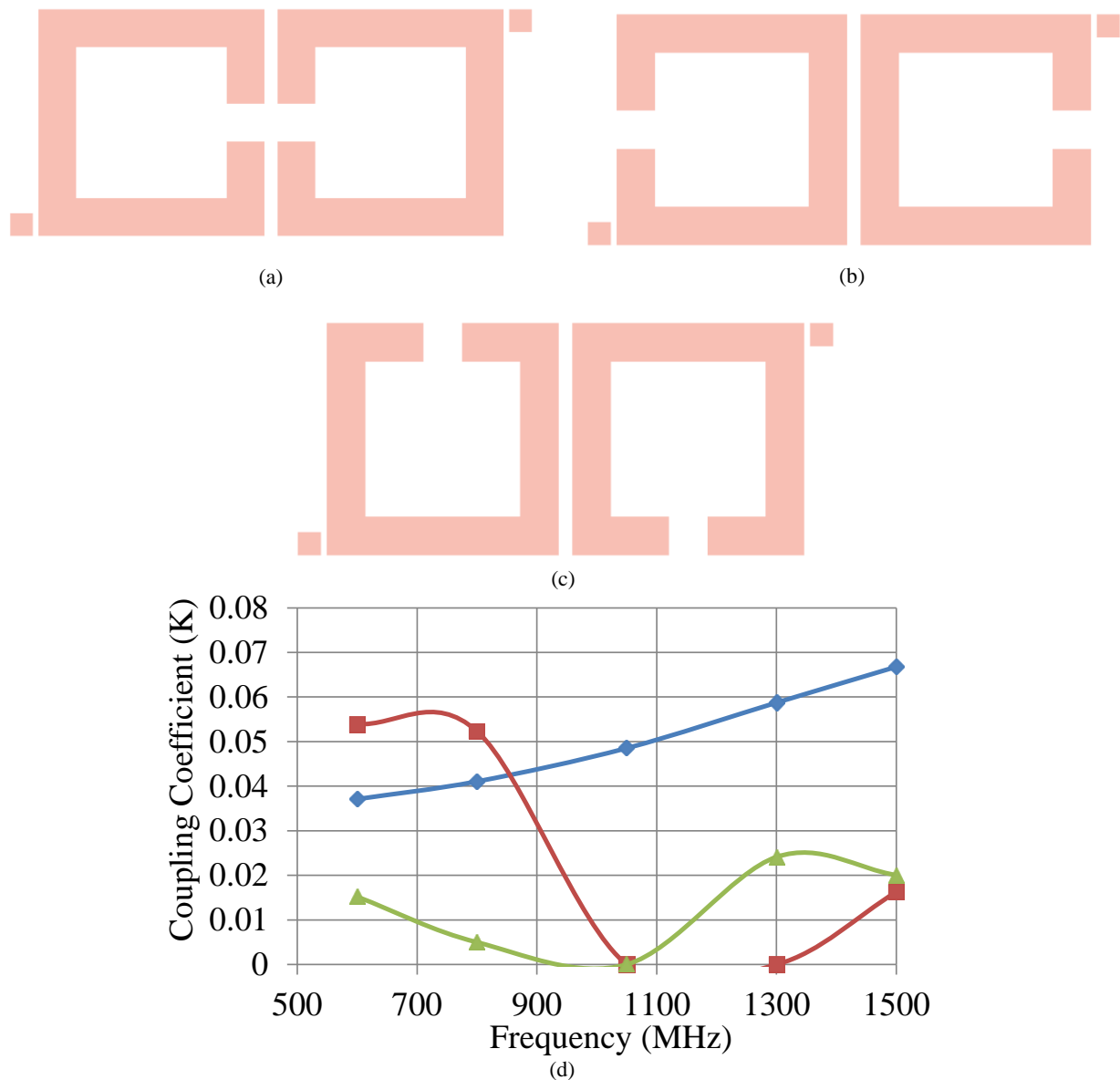


Figure 18: Variation of coupling coefficient ( $K$ ). a) Electric Coupling arrangement; b) Magnetic Coupling Arrangement; c) Mix Coupling Arrangement; d) Calculated coupling coefficient for electric (green), magnetic (red), and mix (blue).

prototype ( $g_0=1$ ,  $g_1=0.6648$ ,  $g_2=0.5445$ ,  $g_3=1.2210$ ) to be 13.296 and 0.0831, respectively. To maintain a constant FBW, it is necessary to keep the  $Q_e$  and  $K$  relatively constant over the frequency tuning range. The ADS studies were carried out by simultaneously considering five different metalized plate locations ( $P1 = 4$ ,  $P2 = 4.5$ ,  $P3 = 4.7$ ,  $P4 = 6$ ,  $P5 = 10$  mm) and these are identified as data points in the design curves presented in Figs. 8 and 9. Using the approach explained in [55], which consist on using the  $S_{11}$  group delay (Fig. 17(b)) to determine the center frequency and using the  $S_{11}$  phase (Fig. 17(c)) to determine the  $Q_e$  with the equation  $Q_e = f_0/f_{\Delta+/-90^\circ}$ , the tapping location that resulted in the required quality factor was found to be  $T=6.1$  mm as shown in Fig. 17(a). To stabilize the variation of  $Q_e$  over the frequency tuning range, a lumped inductor based coupling was utilized. The value of this inductor was determined by utilizing an iterative approach involving ADS schematics and Momentum layouts. The value that provided the nearly required coupling across the entire frequency range was found to be 2.5nH. The ADS simulations of the overall filter for various P values using the 2.5 nH coupling inductors resulted in a return loss that is not well matched (<8 dB). A parametric sweep was carried out over the complete filter model. Increasing the coupling inductors to 7nH was found to provide a return loss performance >10 dB over the whole frequency range. However, this resulted in 8% constant FBW performance. Due to the proof-of-concept nature of the presented work, no further optimizations were pursued to lower the FBW back to 5%. The IL was <1.3 dB over the entire frequency tuning range.

To be able to tune both resonators simultaneously and utilize single pumping unit, a meandered microfluidic channel layout was employed by shifting a resonator slightly down to prevent overlaps (i.e.  $MT = 2$  mm in Fig. 16(c)). The separation (C) that resulted in the required resonator coupling was determined as 0.04 mm. Detailed curves depicting the variation of the

external quality factor and the coupling coefficient as a function of frequency are provided in Fig. 17(d) and Fig. 18(d) respectively.

#### 4.2 Fabrication

The microfluidic channels were fabricated in Polydimethylsiloxane (PDMS) utilizing the micromolding technique explained in [56]-[58]. Metallized glass plates were positioned in a precise way inside the microchannels prior to the bonding of the PDMS with the LCP. The PDMS mold was bonded to the LCP layer using an APTES (3-Aminopropyltriethoxysilane) treatment [59]. The PDMS and LCP bond was then aligned with the PCB board using the alignment holes. Plastic screws and clamps were utilized to hold the PCB and microchannel layers together. Cubic pieces of PDMS were utilized as microfluidic connectors to interface

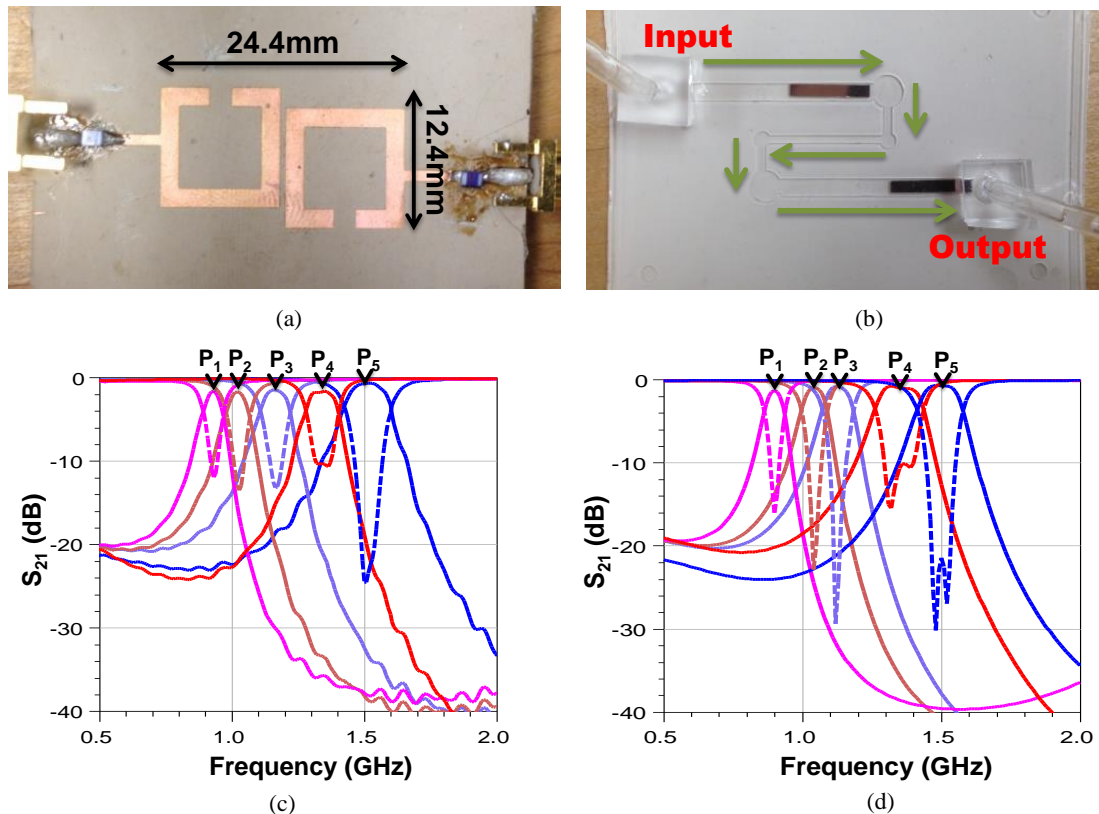


Figure 19: Fabricated two-pole filter. a) Fabricated filter board; b) Microfluidic channels loaded with metallized glass plate; c) Simulated and d) Measured insertion and return loss performances

PTFE tubes with the microchannel. To move the plates inside the microchannels, a two syringe system was implemented to flow Teflon solution inside the channels. The final filter stack-up, as shown in Fig. 16(b), consisted of 1.27 mm thick PCB board, 25.4  $\mu\text{m}$  thick LCP layer, and 2 mm thick PDMS substrate with 250  $\mu\text{m}$  deep and 2.1 mm wide microchannels with 1.9 mm wide metallized glass plates. For a more detail explanation, refer to appendix A.

### 4.3 Experimental Verification

The layers of the fabricated filter assembly are shown in Fig. 19(a) and (b). 6.8 nH Coilcraft inductors from the 0805CS series were utilized at the input and output of the filter. As shown in Fig. 19(c) and (d), the measured insertion and return loss performances are in very good agreement with the simulated results. A frequency tunability range of 50% (1.5 GHz to 0.9 GHz) was accomplished by moving the metallized glass plates a distance of 6mm (i.e. P1 to P5) over the open loop resonators. The worst case insertion loss was found to be 1.7 dB at the lowest frequency, which differs from the simulation results by 0.4 dB. The difference in IL, between simulations and measurements, is due to the lower  $Q$  of the inductors (which was modeled as 50 in ADS simulations). The FBW was measured to vary between 8% and 10% from 0.9 GHz to 1.5 GHz. Increasing the number of poles of the filter will help to stabilize FBW variation as lower coupling and external quality factors will be required. The overall footprint of the filter is  $24.4 \times 12.4 \text{ mm}^2$ , which is  $0.073 \times 0.037 \lambda_0^2$  ( $\lambda_0 =$  free space wavelength) at the lowest frequency.

### 4.4 Concluding Remarks of Chapter 4

A novel approach for realizing a compact, low-loss, and highly tunable bandpass filter was presented by utilizing microfluidically controlled parasitic metalized glass plates. By resorting to metallized glass plates, it provides a more reliable, highly tunable, non-toxic, and low loss performance. Specifically, the bandpass filter provided 50% tuning range with almost

constant 8% FBW. In chapter 5, the microfluidic technique will be extended to higher order bandpass filters. At the same time, integration with micropumps will be introduced for the first time, and speed characterization will be performed.

## CHAPTER 5: MICROFLUIDICALLY RECONFIGURABLE METALLIZED PLATE LOADED FREQUENCY-AGILE RF BANDPASS FILTERS<sup>4</sup>

To extend the utilization of microfluidics to higher order bandpass filters, a 4 pole frequency-agile bandpass filter was designed, fabricated, and tested. Two different filter arrangements were studied to demonstrate that different footprint requirements can be met with the proposed filter approach. To overcome the synchronization issues of multiple metalized plates moving within a single meandered microfluidic channel (in order to use a single pump), a selectively metallized plate implementation was introduced for the first time. In addition, automation of the filters was obtained by introducing a micropump system. The speed of the reconfigurable RF filter was characterized and improved by resorting to strategically designed channel shapes.

### 5.1 Filter Design

#### 5.1.1 Resonator Model

Fig. 20(a) depicts the substrate stack-up used to construct the presented microfluidic based reconfigurable filters. A microfluidically repositionable metalized plate is placed in close proximity to the gap of a traditional open loop resonator to achieve a variable capacitance based frequency tuning mechanism. For a compact filter size, the open loop resonators were placed on a high permittivity 1.27 mm thick Rogers 6010.2LM board ( $\epsilon_r = 10.2$ ,  $\tan\delta = 0.0023$ ). The 0.3 mm thick microfluidic channel is located at the bottom surface of a 2 mm thick Polydimethylsiloxane (PDMS,  $\epsilon_r = 10.2$ ,  $\tan\delta = 0.0023$ ) polymer. The microfluidic channel with

---

<sup>4</sup> This chapter was previously published in [54]. Permission is include in Appendix B.

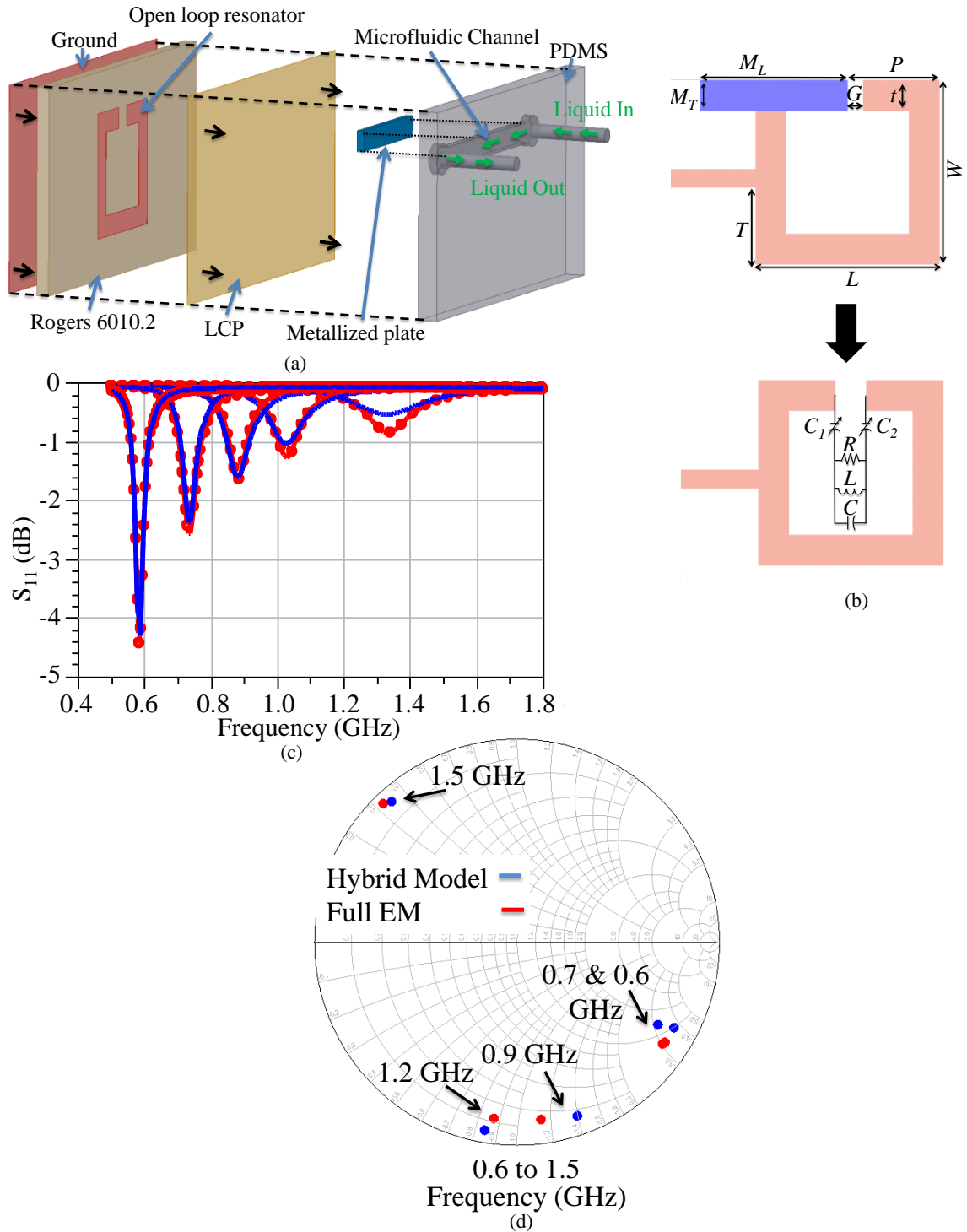


Figure 20: Reconfigurable capacitive loaded microfluidically based resonator. (a) Substrate stack-up; (b) resonator dimensions and its equivalent hybrid (circuit + layout) model ( $G=2\text{mm}$ ,  $T=6.1\text{mm}$ ,  $L=12.4\text{mm}$ ,  $W=12.4\text{mm}$ ,  $t=2\text{mm}$ ); (c)  $S_{11}$  values obtained from simulation of hybrid and full wave models (solid lines represent full wave model) as plate location varies; (d)  $S_{11}$  smith chart representation.

the metalized plate is sealed by bonding a 25.4  $\mu\text{m}$  thick liquid crystal polymer (LCP) based flexible Rogers ULTRALAM 3880 ( $\epsilon_r = 2.4$ ,  $\tan\delta = 0.0025$ ) prepreg with the PDMS layer. The Rogers 6010.2LM board and the microfluidic channel are brought together to form the filter. Depending on the position of the metalized plate, the amount of capacitive loading varies and gets maximized ( $C_{\text{max}}$ ) when the plate is centered over the resonator's arm. Most importantly, this capacitive loading can be completely removed ( $C_{\text{min}} = 0$ ) by retracting the metalized plate half way out of the gap of the open loop resonator. This allows for an extended tuning capability. The dimensions of the unloaded square open loop resonator are shown in Fig. 20(b). The

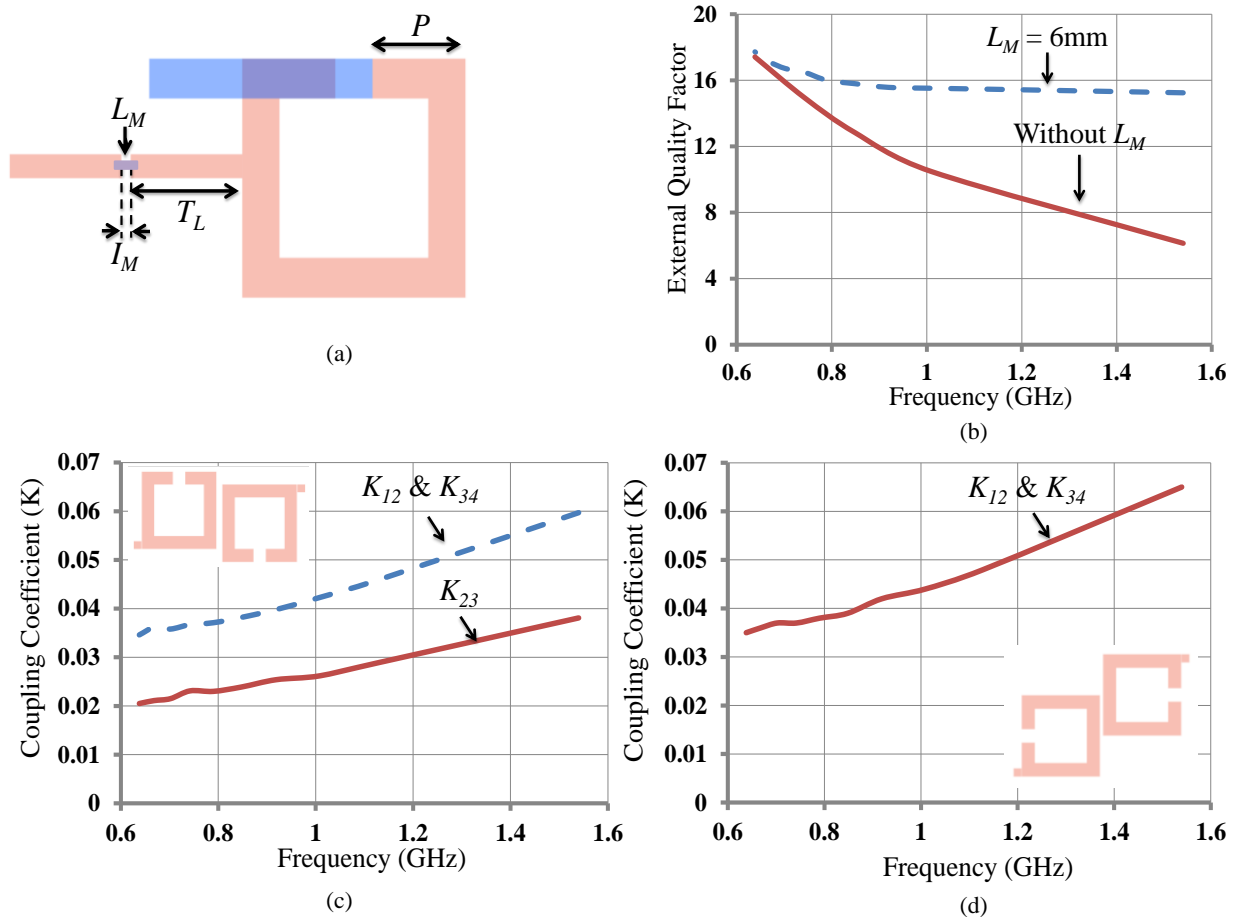


Figure 21: External quality factor extraction and coupling coefficient for different resonator arrangements. (a)  $Q_e$  as a function of frequency; (b) Modified resonator layout for  $Q_e$  stabilization ( $I_M=0.35\text{mm}$ ,  $T_L=6\text{mm}$ ); (c) used both in linear and diagonal footprint filters; (d) used in diagonal footprint filter



resonator is designed to operate at 1.5 GHz by utilizing the Momentum suite of Keysight Advanced Design System (ADS) with the extraction approach outlined in [55]. Assuming that the metalized plate completely fills the microfluidic channel and overlaps with the entire arm of the resonator, the frequency tuning range can be determined to be from 0.61 GHz to 1.5 GHz. Designing the filter across this wide (>2:1) frequency range to exhibit a predefined fractional bandwidth (FBW) performance requires extensive number of full wave simulations to be carried out with changing plate position and results in a time consuming procedure especially for higher order filters. To alleviate this issue, a hybrid model that represents the metalized plate as a lumped circuit network is utilized for design purposes as shown in Fig. 20(b). Since the metalized plate can have a different overlap area on the open arms of the resonator, its interaction with the resonator is represented with two series capacitors (i.e.  $C_1$  and  $C_2$ ). Due to the selected resonator configuration, the metalized plate always completely covers the left arm of the open loop resonator resulting in  $C_1 = \epsilon M_t(L - G)/2h$ , where  $M_t$  is the width of the plate,  $L$  is the side length of the resonator,  $G$  is the width of the gap,  $h$  is the separation between the plate and the resonator, and  $\epsilon$  is the permittivity of the material between the plate and the resonator.  $C_2$  depends on the position of the plate and can be expressed as  $C_2 = \epsilon M_t ((L - G)/2 - P)/h$ , where  $P$  denotes the distance between the plate and the right edge of the resonator. The parallel RLC circuit in series with  $C_1$  and  $C_2$  represents the RF parasitics of the metalized plate located between the open ends of the resonator. The values are initially approximated from the open ended transmission line resonator equations [60]. Subsequently, the values are optimized to match the  $S_{11}$  response of the resonator simulated using full-wave analysis when the metalized plate completely overlaps with the resonator arm. The open loop resonator was full wave simulated without the metalized plate by placing ports to the open ends of the resonator. The

hybrid model was formed in ADS schematic by combining the lumped circuit model with the open end ports of the full wave simulated resonator. Fig. 20(c) and (d) shows that the full wave simulations performed with metalized plate agree well with the equivalent hybrid model. Throughout this paper, to keep the discussion brief, filter performance simulations and experimental verifications are provided at 5 specific plate positions (P1 = 6 mm, P2 = 4.25 mm, P3 = 3.5 mm, P4 = 2 mm and P5 = 0 mm).

### 5.1.2 External $Q_e$ and Coupling Coefficient

To proceed with design of a 4<sup>th</sup> order Chebyshev bandpass filter with 5% FBW, the required external quality factor ( $Q_e$ ) and coupling coefficient ( $K$ ) values were calculated from the corresponding low pass lumped element circuit prototype ( $g_0 = 1$ ,  $g_1 = 0.7654$ ,  $g_2 = 1.8478$ ,  $g_3 = 1.8478$ ,  $g_4 = 0.7654$ ,  $g_5 = 1$ ) as 15.308,  $K_{1,2} = K_{3,4} = 0.04204$  and  $K_{2,3} = 0.02706$ , respectively [55] (where a subscript integer  $i$  represents the resonator number). To maintain an almost constant FBW, it is necessary to keep the  $Q_e$  and  $K$  relatively stable over the tuning range. For the filter implementation, the hybrid resonator model was utilized to extract the  $Q_e$  and  $K$  using the approach explained in [55]. As shown in Fig. 21(b),  $Q_e$  decreases as the resonator is tuned to higher frequency and this behavior is independent of the tapping location ( $T$ ). To stabilize the variation in  $Q_e$  over the tuning range, a lumped coupling inductor  $L_M$  was introduced to the feed line as shown in Fig. 21(a) [51]. Through parametric studies, tapping location and the inductor value were determined as  $T = 6$  mm and  $L_M = 6$  nH, for  $T_L = 6$  mm, for a relatively flat  $Q_e$  response (Fig. 21(b)).

Two different resonator alignment configurations were found to provide stabilized  $K$  variation over the wide tuning range as shown in Fig. 21(c) and (d). To prevent overlapping of the metalized plate with the adjacent resonators, resonators were offset with respect to each other

by  $M_T$ . The configuration in Fig. 21(c) was by itself suitable to implement a 4<sup>th</sup> order Chebyshev filter having its resonators linearly aligned. To accomplish the required  $K_{1,2}$  and  $K_{3,4}$  at 1 GHz, the separation ( $g_{12}$ ) between the resonators was set to 0.98 mm. The gap  $g_{23}$  was 1.58 mm to obtain  $K_{2,3} = 0.027$ . The configuration in Fig. 21(d) was utilized to realize  $K_{12}$  and  $K_{34}$  in a 4<sup>th</sup> order Chebyshev filter with resonators aligned in a diagonal form ( $K_{23}$  was realized again with the configuration in Fig. 21(c)). The separation between the resonators ( $g_{12}$ ) was set to 0.1 mm for achieving the desired coupling at 1 GHz. These resonator configurations exhibit a mixture of electrical and magnetic couplings. It was observed that for the selected configurations,  $K$  still varied as the frequency was tuned across the wide frequency range. The variation of these

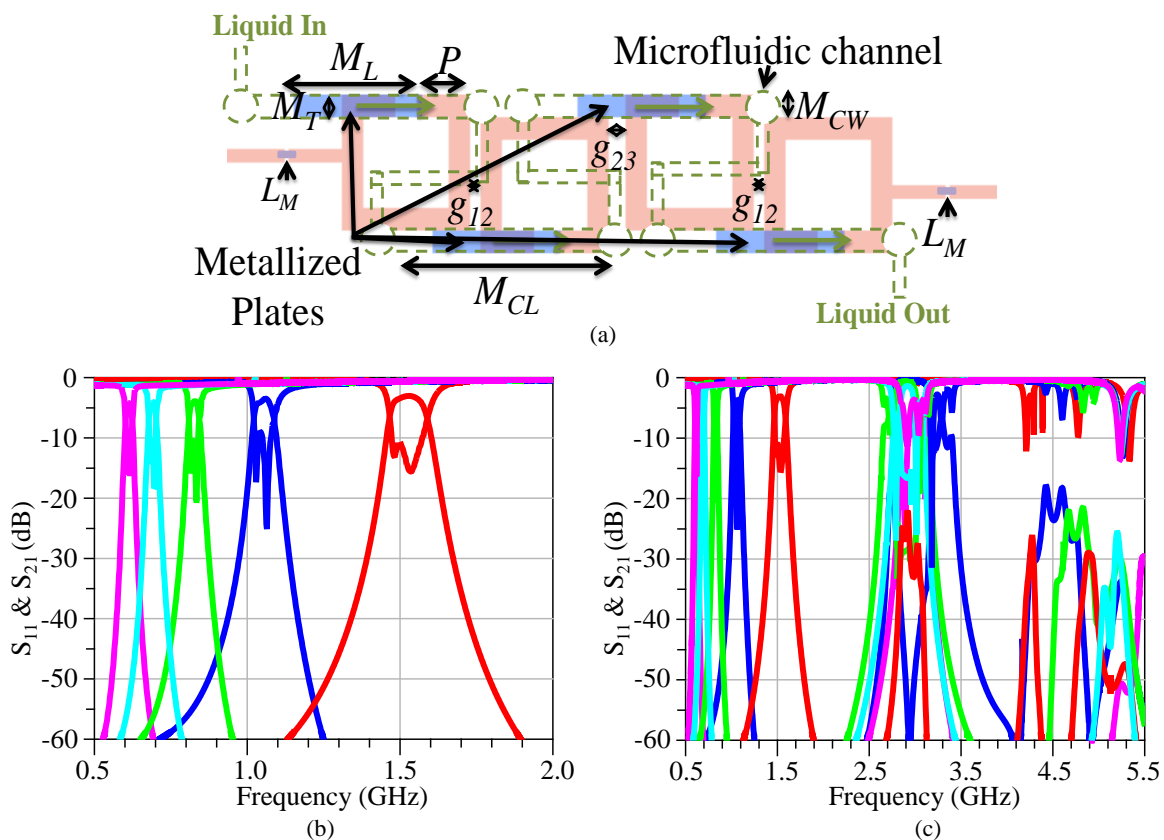


Figure 22: Designed 4<sup>th</sup> order filters with linear resonator arrangement. (a) Layout ( $M_L=12$ ,  $M_T=2$ ,  $M_{CW}=2.05$ ,  $I_M$ =inductor gap,  $C_1=0.98$ ,  $C_2=1.58$ ,  $T_{in}=5$ ,  $P$ =position of top plate) units in mm; (b) Simulated  $S_{21}$  and  $S_{11}$ ; (c) Wideband  $S_{21}$  and  $S_{11}$  performance.

coupling curves could potentially be further stabilized by resorting to non-square resonator shapes. However, since this may potentially complicate the operation of the filters with the proposed selectively metalized microfluidically controllable plates, it was not investigated for the proof-of-concept filters implemented in this paper. The  $K$  variations shown in Fig. 21(c) and (d) were therefore expected to change FBW around the desired 5% goal. According to equation  $K_{i,i+1} = FBW / \sqrt{g_i g_{i+1}}$ , varying  $K_{1,2}$  from 0.04 to 0.07 could generate a FBW variation from 3.36% to 5.8%. It is also important to mention that other resonator configurations that relied extensively on electrical or magnetic coupling were found to exhibit a null coupling coefficient at certain frequency within the desired wide frequency tuning range no matter how the resonators were spaced with respect each other. Consequently, these resonator configurations were not able to exhibit a continuous impedance matching across the tuning range.

### 5.1.3 4<sup>th</sup> Order Filter with Linear Resonator Arrangement

Fig. 22 depicts the 4th order filter with linear resonator arrangement. This filter can be realized with the meandered microfluidic channel approach introduced in our previous work [53] in order to achieve frequency tuning with a single bidirectional micropump unit. However, as will be explained in Section IV, this topology will be further improved with the selectively metalized plate approach to avoid possible movement synchronization issues. Since the simulated unloaded  $Q$  ( $Q_u$ ) of the resonators varies from 190 at 1.5 GHz to 90 at 0.61 GHz, the worst case IL can be estimated as 5.04 dB using the equation  $IL = 4.343 \sum_{i=1}^n g_i / \Delta Q_{ui}$ . As shown in Fig. 22(b), the filter FBW is maintained between 3.5% and 7% across the tuning range. As expected, the IL increases from 3.03 dB to 4.8 dB as the filter is tuned from 1.5 GHz to 0.61 GHz. The overall footprint of the filter is  $51.54 \times 14 \text{ mm}^2$ . Fig. 22(c) shows the performance of the filter across 0.5 GHz to 5.5 GHz. An out of band rejection  $>40$  dB is achieved.

### 5.1.4 4<sup>th</sup> Order Filter with Diagonal Resonator Arrangement

The 4<sup>th</sup> order filter designed with the diagonal resonator arrangement is shown in Fig. 23(a). The design is based on the  $Q_e$  and  $K$  study discussed in Section 5.1.2. Similar to the filter with the linear resonator arrangement, this layout could also be operated with a meandered microfluidic channel to use a single bi-directional pump unit as shown in Fig. 23(a). The filter FBW is maintained between 3.5% and 7.2% across the tuning range. The IL increases from 3.03

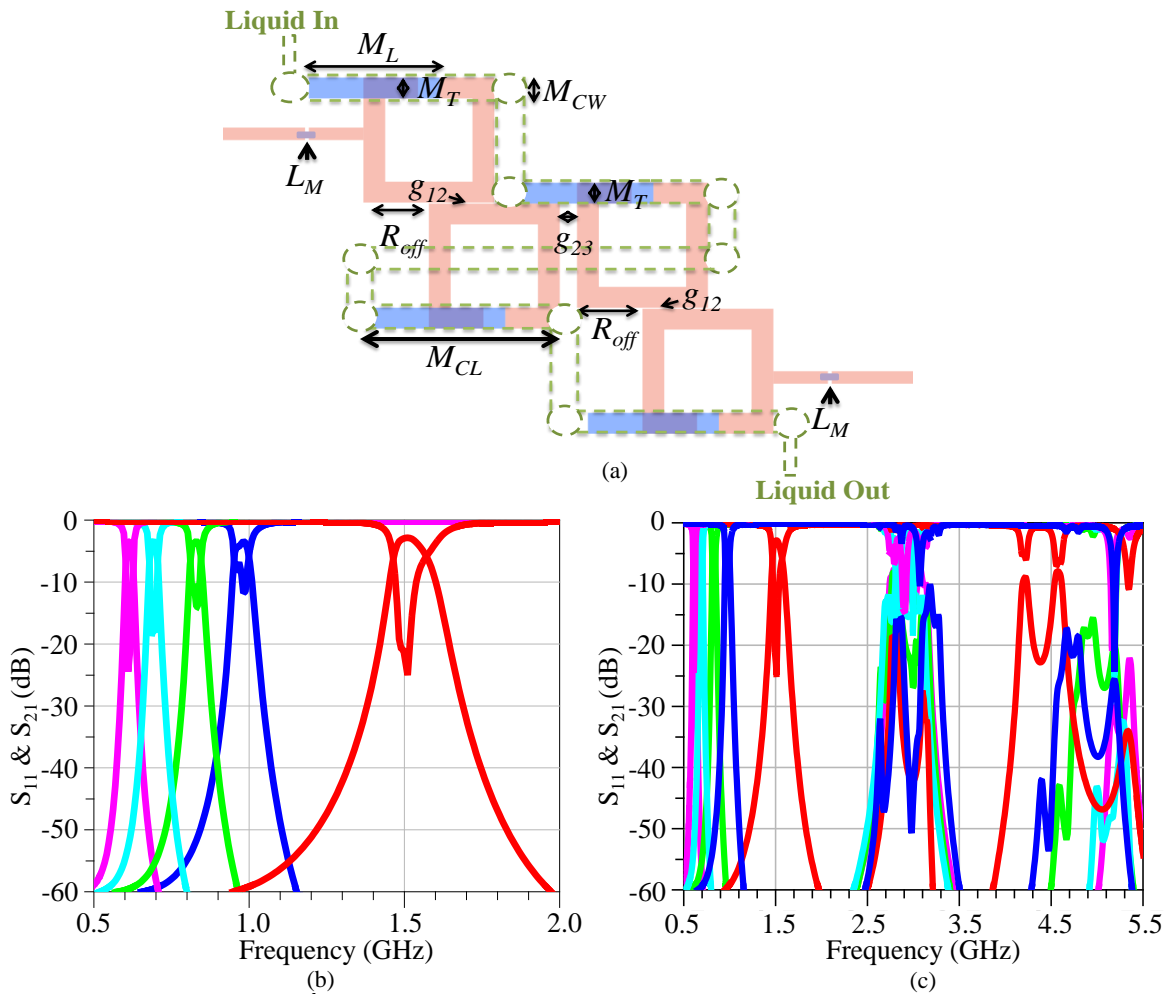


Figure 23: Designed 4<sup>th</sup> order filters with diagonal resonator arrangement. (a) Layout ( $M_L=12$ ,  $M_T=2$ ,  $M_{CW}=2.05$ ,  $R_{off}=6$ ,  $g_{12}=0.1$ ,  $g_{23}=1.58$ ) units in mm; (b) Simulated  $S_{21}$  and  $S_{11}$ ; (c) Wideband  $S_{21}$  and  $S_{11}$  performance.

dB to 4.8 dB as the filter is tuned from 1.5 GHz to 0.61 GHz (Fig. 23(b)). The overall footprint of the filter is  $37.58 \times 34.2 \text{ mm}^2$ . Fig. 23(c) shows the performance of the filter across 0.5 GHz to 5.5 GHz. An out of band rejection  $>40 \text{ dB}$  is achieved.

## 5.2 Microfluidic Channel Design

Although the resonators of the designed filters can be simultaneously tuned with a single pump due to the meandered microfluidic channel layout, utilizing a single meandered channel presents potential reliability issues due to the synchronous movement needed from all the plates. As an alternative, in contrast to our previous work [53], two novel microfluidic channel layouts designed to operate with a selectively metallized plate were pursued for the device implementation as shown in Fig. 24. Specifically, a rectangular wide microfluidic channel was placed over the filter footprint consisting of linearly arranged resonators. The microfluidic channel hosted a single 14 mm wide dielectric plate. This plate was selectively metallized on the areas that will overlap with the resonators. Having the microfluidic channel as the same width of the metallized plate, would not allow a continuous plate movement due to friction generated between the channel walls and the plate walls. Also, as the plate area increase, the separation between the microchannel walls and the selectively metallized plate needs to be increased to reduce the friction. However, if the gap between the selectively metallized plate and the microfluidic channel is too large, the fluid could flow through without moving the plate. To determine the appropriate channel width, microfluidic channels presenting width of 20  $\mu\text{m}$ , 30  $\mu\text{m}$ , 40  $\mu\text{m}$ , 50  $\mu\text{m}$ , and 60  $\mu\text{m}$  wider than the selectively metallized plate were fabricated. It was determined that keeping the channel width 50  $\mu\text{m}$  wider than the metallized plate would minimize the friction generated between the channel walls and selectively metallized plate. Therefore, the dimensions of the wide rectangular microfluidic channel were set to 14.05 x 30.4

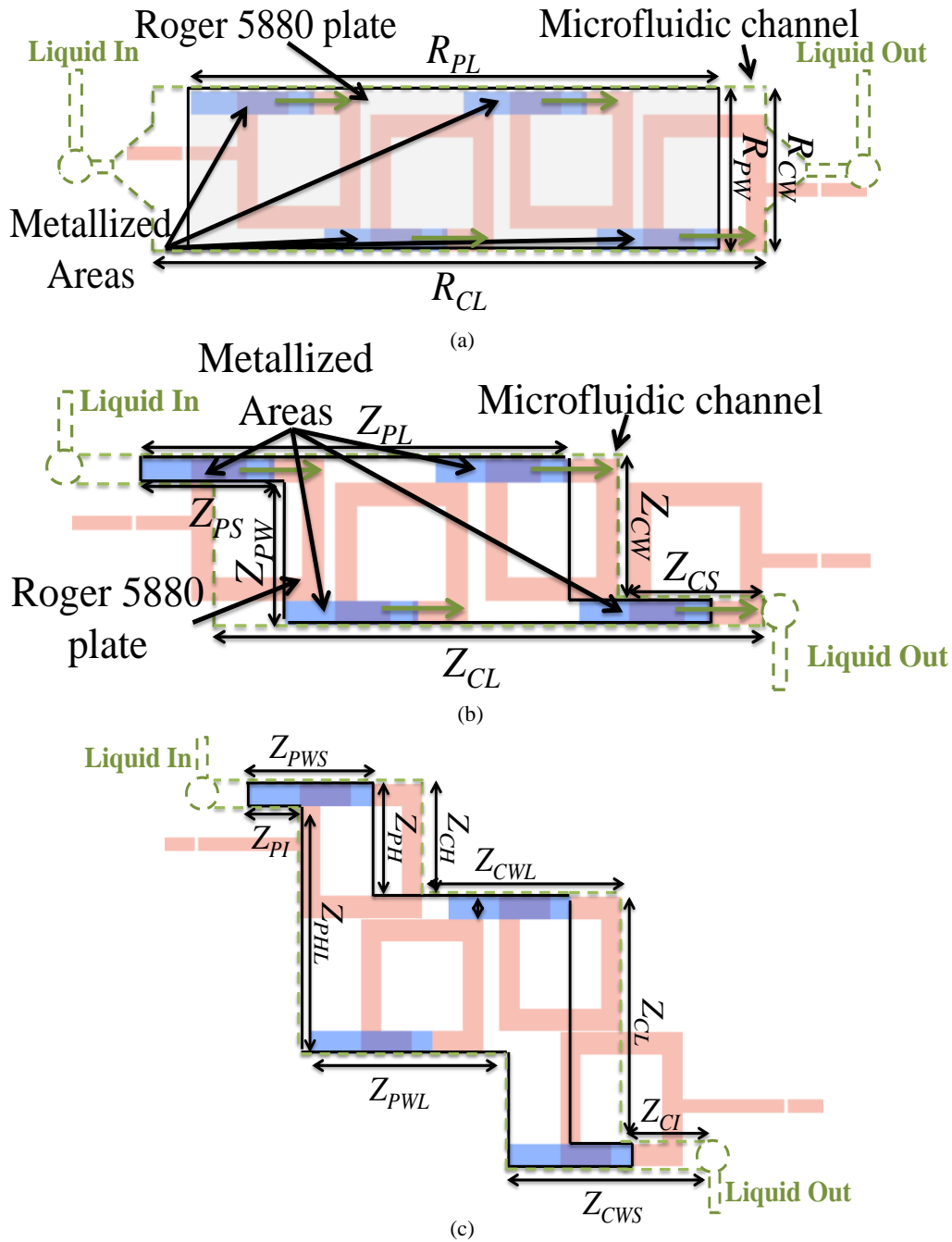


Figure 24: Metallized plate and channel shapes investigated for the linear and diagonal resonator arrangement. (a) Rectangular microfluidic channel:  $R_{CL} = 30.4$  mm,  $R_{CW} = 14.5$  mm,  $R_{PW} = 14.4$  mm, and  $R_{PL} = 24.8$  mm. (b) "Z" shaped microfluidic channel:  $Z_{CL} = 49.6$  mm,  $Z_{CW} = 12.05$  mm,  $Z_{CS} = 12$  mm,  $Z_{PW} = 12$  mm,  $Z_{PL} = 38.56$  mm, and  $Z_{PS} = 12$  mm; (c)  $Z_{CL} = 22.6$  mm,  $Z_{CWL} = 19.68$  mm,  $Z_{CH} = 10$  mm,  $Z_{CI} = 5$  mm,  $Z_{CWS} = 18$  mm,  $Z_{PWS} = 12$  mm and  $Z_{PH} = 10$  mm,  $Z_{PL} = 5$  mm,  $Z_{PHL} = 22.1$  mm,  $Z_{PWL} = 19.58$  mm.

$\mu\text{m}^2$ . The initially selected dielectric fluid was Teflon solution obtained from DuPont (400S2-100-1) which is made out of 1% Teflon dissolved in 3M FC-40 solution (FC-40 density =  $1.855 \text{ g/cm}^3$ ). However, it was found that utilizing only 3M FC-40 solution provided a higher speed due to its lower viscosity. Initial experiments were carried out utilizing glass to implement the metallized plates. However, glass plates required an extra step for the metal deposition and its mobility inside the channel was found to be limited possibly due to its higher density ( $2.33 \text{ g/cm}^3$ ). To ease the plate movement inside the channel, the later plate implementations were carried out with readily available 0.254 mm thick Rogers 5880LZ ( $1.4 \text{ g/cm}^3$ ) substrates exhibiting 17  $\mu\text{m}$  copper cladding. Several microfluidic channels having various heights (0.25 mm, 0.3 mm, and 0.35 mm) were fabricated to determine a height that will enable plate movement. Out of these, 0.3 mm was selected for the microfluidic channel depth.

Since using a larger dielectric plate also required a larger liquid volume displacement, the tuning speed was expected to be lower in the new widened microfluidic channel implementation. To improve the speed, the channel layout and the plate shape was modified as shown in Fig. 24(b) to take a “Z” shape. This way, the pressure point would be the same as with the meandered channel even though the plate is bigger. This allowed for having the metallized areas in one common dielectric plate and required the same volume displacement as the meandered channel implementation. The width of the microfluidic channel was still kept 50  $\mu\text{m}$  wider than the metallized plate. During the experiments, the tuning time of the filter in Fig. 24(a) was measured to be 2.1 s for the required 6 mm full motion range. As expected, the Z shaped channel and plate implementation decreased this time by a factor of 6.4 times to 0.33 s. Due to the success with the Z shaped channel and plate implementation, the filter design with the diagonal resonator



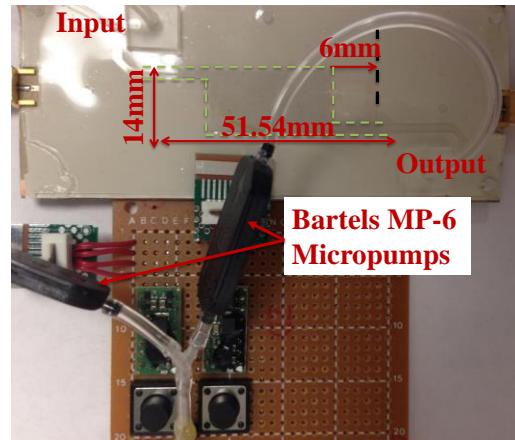
arrangement was pursued only with this technique. Fig. 24(c) depicts the channel and plate dimensions. The measured tuning time was 0.38 s per 6 mm of full range movement.

### 5.3 Fabrication

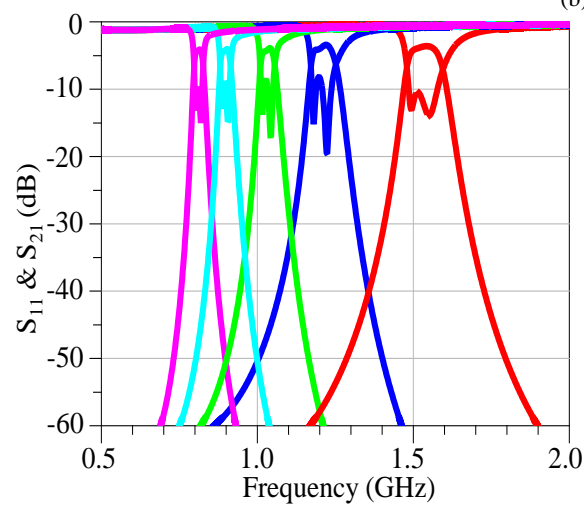
The microfluidic channels were fabricated in PDMS utilizing the micromolding technique explained in [56]-[58]. Metallized plates were manually positioned inside the channels. The PDMS and LCP bond was then aligned with the PCB board using the alignment holes. Plastic screws were utilized to hold the PCB and microchannel layers together. Cubic pieces of PDMS were utilized as microfluidic connectors to interface PTFE tubes with the microchannel. To move the plates inside the microchannels, a two syringe system was implemented to flow 3M FC-40 solution. The fabricated filter exhibiting the Z shape microfluidic channel shape is shown in Fig. 25. It consisted of 1.27 mm thick PCB board, 25.4  $\mu\text{m}$  thick LCP layer, and 2 mm thick PDMS substrate with 0.3 mm deep microchannel carrying the 0.25 mm thick metalized plate. 6.0 nH Coilcraft inductors from the 0302CS series were utilized at the input and output of the filter. To electronically control the filters, the syringes were substituted with two piezo-pumps, with dimensions of 30 x 15 x 3.8 mm<sup>3</sup> from Bartels® (mp-6). These micropumps were chosen due to their piezo actuation mechanism that allows for an accurate control of the liquid displacement via supply voltages. Two of these pumps were connected in series to generate bi-directional flow capability. The pumps were operated with the manufacturer supplied driver circuit that converts 5 V DC current to a 100 MHz 235 V peak to peak sinusoidal wave according to the highest flow rate specifications given for water [61]. The power consumption of the pumps is less than 200 mW.



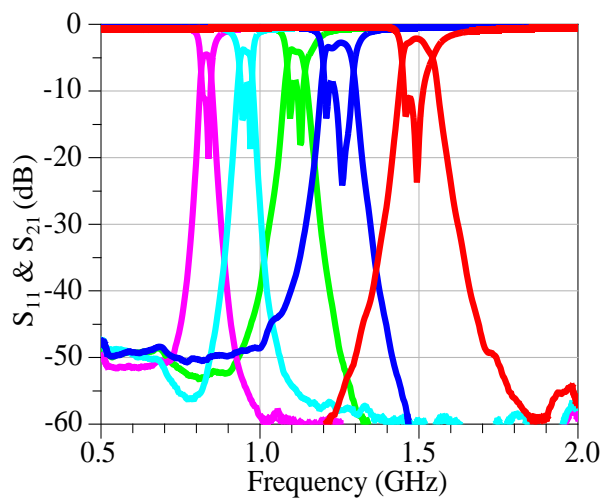
(a)



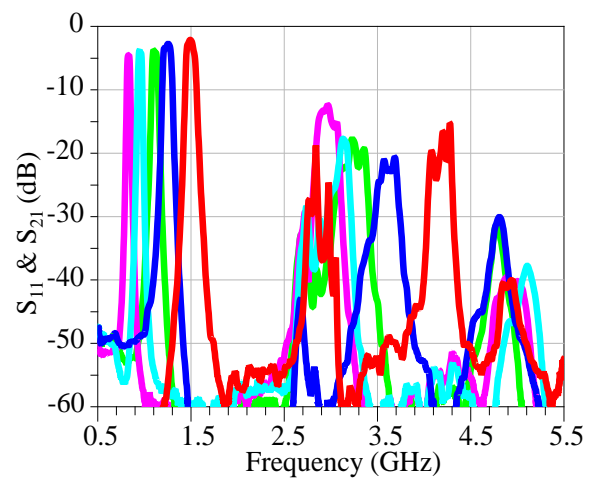
(b)



(c)



(d)



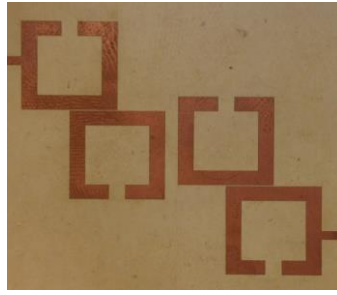
(e)

Figure 25: Experimental characterization of the 4<sup>th</sup> order bandpass filter with linear resonator arrangement. (a) Fabricated filter board; (b) Complete system assembly including pump and control units; (c) Simulated  $S_{21}$  and  $S_{11}$  performance with 58  $\mu\text{m}$  thickness; (d) Measured  $S_{21}$  and  $S_{11}$  performances; (e) Measured frequency response up to third harmonic.

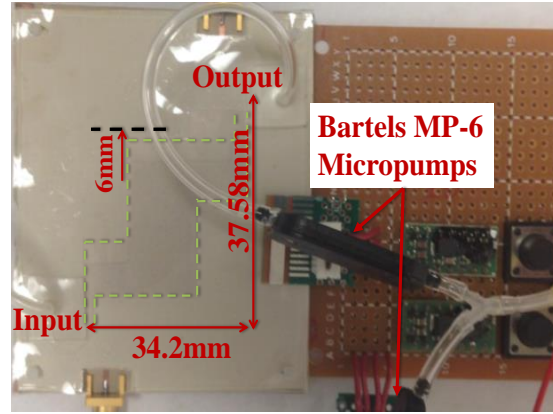
## 5.4 Experimental Verification

### 5.4.1 4<sup>th</sup> Order Filter with Linear Resonator Arrangement

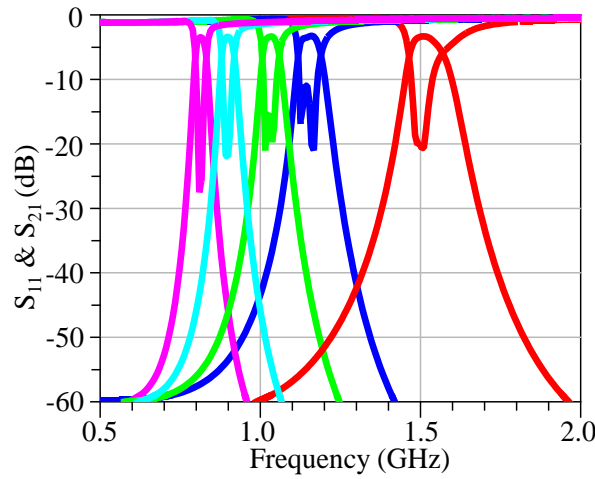
Fig. 25(a) and (b) depict the fabricated filter and the microfluidic control assembly. The measured frequency tuning range was from 0.8 GHz to 1.5 GHz, close to being 2:1. Based on simulation studies, this frequency tuning range was identified to correspond to a physical gap of 54  $\mu\text{m}$  between the plate metallization and the printed loop. Hence, it was concluded that the 0.254 mm thick plate with 17  $\mu\text{m}$  thick metallization floated on the top of the channel due to the density difference of the dielectric fluid and the plate material. Future device fabrications should consider the possible location of the plate within the channel and try to minimize the difference between channel height and plate thickness through more finely sampled channel height characterizations. Optimizing channel height and matching the densities of the plate with the fluid will also minimize the orientation dependent tuning variation due to gravity. Simulated  $S_{21}$  and  $S_{11}$  data with the 54  $\mu\text{m}$  gap is shown in Fig. 25(c) and agrees well with the measured data shown in Fig. 25(d). The worst case IL is 4.5 dB at the lowest frequency. 0.2 dB difference between simulations and measurements can potentially be due to the lower  $Q$  of the inductors (which was modeled as 80 in ADS simulations) and losses added due to dielectric solution. The FBW is measured to vary between 5% and 4% from 1.5 GHz to 0.8 GHz. Less variation in  $Q_e$  and  $K$  due to the smaller frequency tuning range results in a more stable FBW performance. The overall footprint of the filter (excluding the pumps) is  $51.54 \times 14 \text{ mm}^2$ , which is  $0.14259 \times 0.0387 \lambda_0^2$  ( $\lambda_0$  = free space wavelength) at the lowest frequency. Fig. 25(e) shows the wideband frequency response. An out of band rejection  $>40$  dB is realized up to the 2.6 GHz that is within the vicinity of the second harmonic of the unloaded open loop resonator. The frequency tuning time is 0.33 s, for the entire frequency range, with the “Z” shaped microfluidic channel and plate.



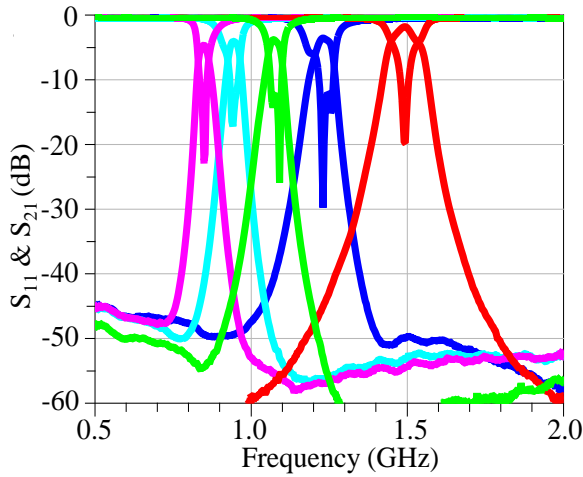
(a)



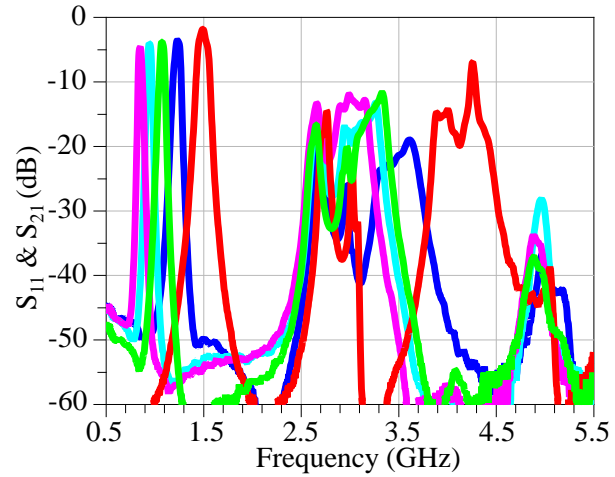
(b)



(c)



(d)



(e)

Figure 26: Experimental characterization of the 4<sup>th</sup> order bandpass filter with diagonal resonator arrangement. (a) Fabricated filter board for the diagonal topology; (b) Complete system assembly including pump and control units; (c) Simulated  $S_{21}$  and  $S_{11}$  performance with 58  $\mu\text{m}$  thickness; (d) Measured  $S_{21}$  and  $S_{11}$  performances; (e) Measured frequency response up to third harmonic.

The measured  $S_{21}$  and  $S_{11}$  performances for different channel implementations are identical and therefore not shown for brevity.

#### 5.4.2 4<sup>th</sup> Order Filter with Diagonal Resonator Arrangement

Fig. 26(a) and (b) show the filter implementation for the diagonal configuration. Simulated (with 54  $\mu\text{m}$  plate and loop metallization separation) and measured results are in very good agreement as can be seen in Fig. 26(c) and (d). The worst case IL is 4.5 dB and identical to the filter with linear resonator arrangement. The tuning range is also identical and from 1.5 GHz down to 0.8 GHz. The measured FBW varies between 5% and 4% over the entire frequency tuning range. The overall footprint of the filter (excluding the pumps) is  $37.58 \times 34.2 \text{ mm}^2$ , which is  $0.10397 \times 0.094612 \lambda_0^2$  at the lowest frequency. Fig. 26(e) shows the wideband frequency response. An out of band rejection  $>40 \text{ dB}$  is realized up to the 2.5 GHz that is within the vicinity of the second harmonic of the unloaded open loop resonator. The tuning time is slightly larger and 0.38 s for entire 6 mm plate motion. This is likely to be due to the implementation with a larger plate mass.

#### 5.5 Concluding Remarks of Chapter 5

A novel approach for realizing a compact, low-loss, and highly tunable high order bandpass filter was presented by utilizing microfluidically controlled metalized plates. A thin film based fabrication technique was employed to increase the capacitive loading and associated frequency tuning range. The shape of the microfluidic channel and resonators are designed to operate the filter with a single micropump unit with near constant fractional bandwidth performance. Specifically, the presented bandpass filter example provided 60% tuning range with almost constant 5% FBW. The tuning range of the filter can be further improved by resorting to thinner insulators. However, this would generate a further decrease in the resonator's

unloaded quality factor and, therefore, increase the insertion loss performance of the filter. As a solution, in chapter 6, a novel resonator will be presented, and utilized to realize a 4<sup>th</sup> order bandpass filter. The resonator explained in chapter 6 will be capable of exhibiting constant unloaded quality factor while providing a 90% (3:1) tuning range. Experimental characterizations showed that the plate location within the depth of the microfluidic channel must be accounted for in accurate modeling of these devices due to the use of thin insulators as microfluidic channel walls. Therefore, in chapter 6, a more detailed fabrication of the microchannel is presented. By utilizing a selectively metalized single plate to simultaneously tune entire resonators of the filter, the issue of synchronization was solved and the reliability of the filters were improved. Electronically controllable micropumps were also successfully added into the system. The filter presented in this chapter provides a low-cost and compact alternative to linear actuator based mechanically tuned filters.

## **CHAPTER 6: WIDELY TUNABLE, LOW LOSS FILTERS USING MICROFLUIDICALLY CONTROLLED VARIABLE LENGTH RESONATORS**

The capacitively loaded open loop resonator based microfluidic reconfigurable filters have been shown to operate with ~2:1 tuning range and unloaded resonator quality factors ( $Q_u$ ) ranging from 150 to 90. This performance is already better than varactor loaded reconfigurable filters and scalable to higher operational frequencies. Extending the frequency tuning range of the open loop resonator based filters is possible by resorting to thinner insulators for higher capacitive loading. However, high level of capacitive loading that lowers the operational frequency of the resonator also significantly reduces the unloaded quality factor ( $Q_u$ ) and therefore the filter's insertion loss performance. In this chapter, we investigate a new technique for designing microfluidically reconfigurable filters that can simultaneously operate over a very wide frequency tuning range and exhibit low insertion loss performance. In order to improve the frequency tuning range and keep the unloaded quality factor of the resonators relatively stable, the microfluidic reconfiguration approach is utilized for redefining the length of half wavelength open ended microstrip resonators. These resonators typically present an unloaded quality factor on the order of 200 and this is also considerably higher than the resonators investigated in the previous chapters.

### **6.1 Resonator Design**

A variable length half wavelength open ended microstrip resonator was designed by resorting to microfluidics as the tuning mechanism. Tunable filters based on this type of

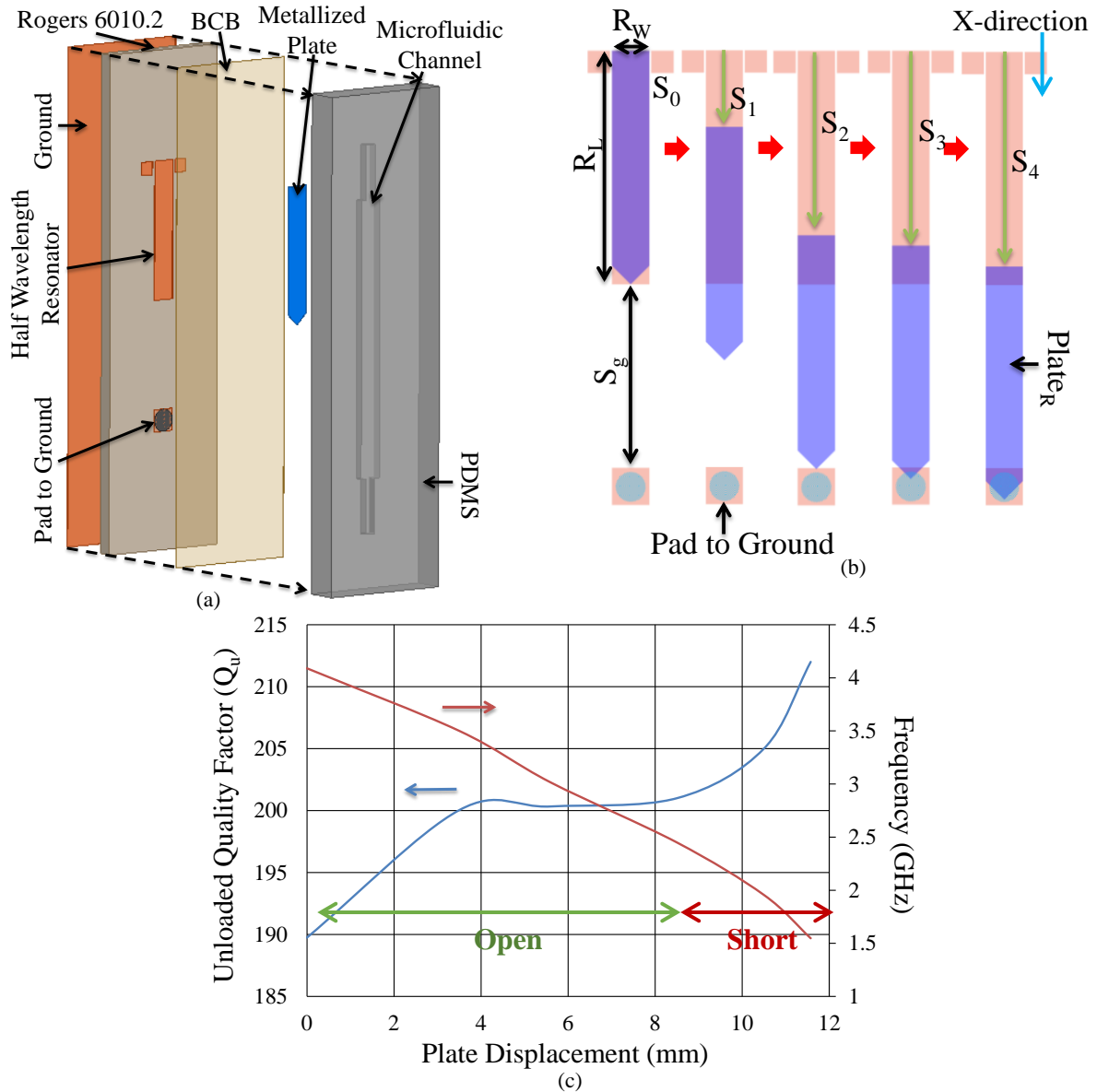


Figure 27: Microfluidically reconfigurable half wavelength resonator. (a) Substrate stack-up: Rogers 6010.2 = 1.27 mm, BCB = 0.006 mm, and PDMS = 2 mm. (b) Different tuning stages of the proposed resonator ( $R_L=12.57$ ,  $R_W=2$ ,  $R_C= 3$ ,  $S_0=0$ ,  $S_1=2.32$ ,  $S_2=4.32$ ,  $S_3=7.83$ ,  $S_4=10.87$ , and  $S_5=11.68$ ). (c) Unloaded quality factor and frequency response as a function of plate movement in mm.

resonators have been previously proposed [62]-[63]. However, in this chapter a novel reconfigurable resonator is proposed as shown in Fig. 27. The proposed resonator consists of two sections: a half wavelength open ended printed resonator (see Fig. 27(a)) and a microfluidically repositionable selectively metalized plate ( $Plate_R$ ). The printed resonator and  $Plate_R$  are separated



by a 6  $\mu\text{m}$  thick insulator. At the highest operational frequency,  $\text{Plate}_R$  completely overlaps with the printed resonator (see Fig. 27(b)). When  $\text{Plate}_R$  is microfluidically moved in the X direction, as shown in Fig. 27(b), the length of the resonator is enlarged and its resonance frequency is decreased. Extending the physical length by a factor of 2 would reduce the resonance frequency by half (2:1 tunability). However, since a small overlap needs to exist between the printed resonator and  $\text{Plate}_R$  to achieve an RF short based connection, extending the physical length of the resonator provides a 1.7:1 frequency tuning range (As shown in Fig. 27 (c)). To further enhance the frequency tuning range, a ground pad is positioned to be 9.875 mm away from the bottom open end of the printed resonator (Fig. 27(a)). The pad to ground has been strategically placed to cause an overlapping area with  $\text{Plate}_R$  as the plate approaches its maximum displacement. Thanks to the strong coupling between  $\text{Plate}_R$  and the printed resonator, the overall resonator transitions from an open ended half wavelength resonator into a short ended resonator. Due to the capacitive nature of the overlapping area, the resonance frequency gets lowered by a factor less than 2 (i.e. 1.6 as in Fig. 27(c)). The unloaded quality factor remains relatively the same. Consequently, this novel reconfigurable resonator presents a frequency tuning range of 2.7:1 with close to constant unloaded quality factor.

Fig. 27(a) and (b) provide substrate stack-up and dimensions of the resonator, respectively. For the filter design, the upper operational frequency is selected to be at 4 GHz. Hence, the printed section of this resonator is a conventional half wavelength open ended microstrip line designed to operate at a frequency of 4 GHz. Using a Rogers 6010.2 ( $\epsilon_r = 10.2$   $\tan\delta = 0.0025$ ) board, at 4 GHz ( $\lambda_g = 23.48$  mm) the length of the resonator should be around 11.74 mm. However, the resonator is also loaded with microfluidic channel and plate. Hence, full wave simulations in Momentum suite of the Agilent's Advanced Design System (ADS) was

utilized to fine tune the length of the resonator to operate at the desired frequency of 4 GHz. The length was determined to be 12.575 mm. The width of the resonator was set to 2 mm which represents a low impedance microstrip line of 37.9 ohms. Using a low impedance line for the resonator helps to keep a high unloaded quality factor of the resonators. Making the resonator wider would increase the capacitance value between the top and bottom layers, however, at high frequencies a wider resonator could radiate. As explained in previous chapters,  $\text{Plate}_R$  is realized on a 0.254 mm Rogers 5880LZ board ( $\epsilon_r = 1.96 \tan\delta = 0.0009$ ). A microfluidic channel was made on the bottom face of a 2 mm thick PDMS layer to host  $\text{Plate}_R$ . To seal the microfluidic channel, once  $\text{Plate}_R$  has been manually positioned inside, a 6  $\mu\text{m}$  thick BCB insulator layer (selected based on readily available materials) is utilized. The BCB layer is also utilized to bond the top layer (Microfluidic channel +  $\text{Plate}_R$ ) to the bottom layer (Rogers 6010.2 board with printed resonator). The BCB thickness defines the separation between the metalized plate and the printed resonator. Fig. 27(b) depicts the plate movement over the resonator. From simulations it

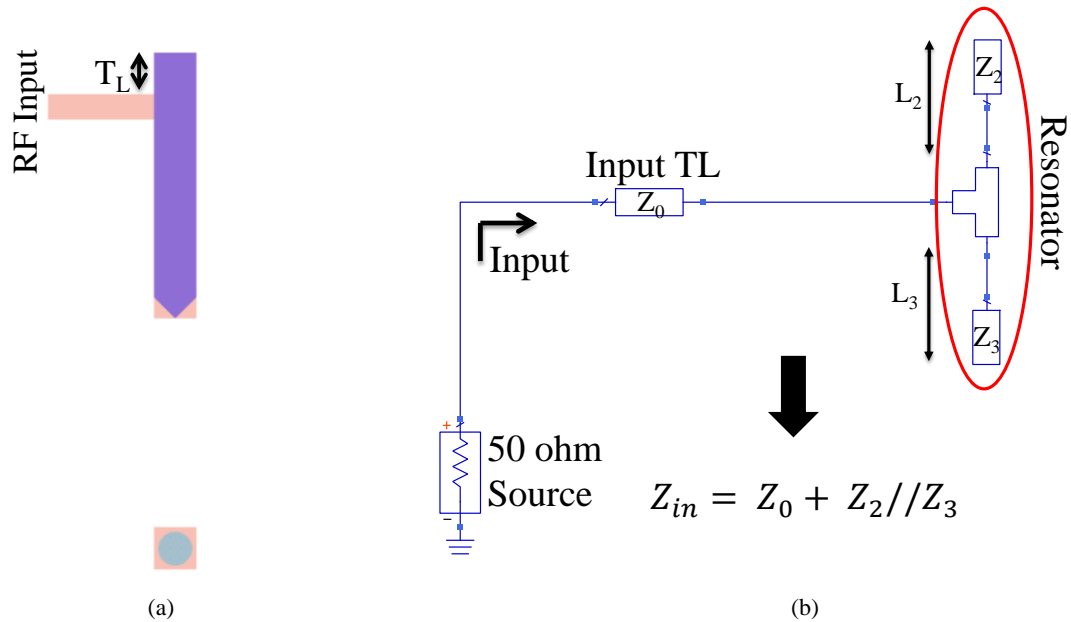


Figure 28: External  $Q_e$  extraction with tapping approach. a) Resonator layout ( $T_L = 3$  mm); b) Resonator circuit (transmission line) model

was determined that for the specified 6  $\mu\text{m}$  BCB thickness the minimum overlap area needed to generate a capacitance value enough to represent an RF short (insertion loss  $< 0.5$  dB) between  $\text{Plater}_R$  and the printed resonator is  $0.8 \times 2 \text{ mm}^2$ . In the design, the minimum overlapping area was kept as  $1 \times 2 \text{ mm}^2$  to have a safety margin for this calculation. As shown in Fig. 27(c), for the specified minimum overlapping area, the frequency tuning range goes from 4 GHz to 1.5 GHz as  $\text{Plater}_R$  is displaced by 11.575 mm. The unloaded quality factor of the resonator is calculated to be 250 at the center frequency of the entire frequency tuning range (e.g. 2.75 GHz) and remains relatively stable ( $\pm 15$ ). Hence, the proposed resonator can be utilized to design highly tunable filters exhibiting constant and low insertion loss performances. Thanks to its narrow footprint, increasing the order of the filter would not generate a significant grow in the overall area of the filter. Therefore, higher order filters can also be implemented.

## 6.2 Filter Design

To be able to compare with the previously presented work in chapter 5, a 4<sup>th</sup> order Chebyshev filter with 5% FBW has been designed. However, due to the higher frequency tuning range and also to demonstrate that microfluidics approach can be applied at higher operational frequencies, the filter's highest frequency of operation was selected as 4 GHz. As in chapter 5, the required external quality factor ( $Q_e$ ) and coupling coefficient ( $K$ ) values were calculated from the corresponding low pass lumped element circuit prototype ( $g_0=1$ ,  $g_1=0.7654$ ,  $g_2=1.8478$ ,  $g_3=1.8478$ ,  $g_4=0.7654$ ,  $g_5=1$ ) as 15.308,  $K_{1,2} = K_{3,4} = 0.04204$  and  $K_{2,3} = 0.02706$ , respectively [55] (where a subscript integer  $i$  represents the resonator number). These two parameters dictate the FBW of the filter. Therefore, to be able to obtain a stable FBW over the wide frequency tuning range, it is necessary to maintain stable external quality factor and coupling coefficients, as explained in Chapter 5. The value of  $Q_e$  can be controlled by keeping the input admittance

seen by the source close to constant. In chapter 5, this was controlled by changing the tapping location of the resonator. However, resorting to the tapping approach utilized in chapters III, IV, and V did not present a viable option for these novel resonators. This can be explained through the circuit models. As seen in Fig. 28(a) and (b), the impedance seen by the source varies with  $L_3$  as operational frequency of the resonator is reduced by increasing  $L_3$ . Consequently,  $Q_e$  is not stable over the frequency range and also tends to be small for the desired filter specifications (see Fig. 31 – red curve). By resorting to a capacitive coupling between the input and the first resonator (see Fig. 29(a) and (b)), the  $Q_e$  value grows and gets stabilized at high frequency band. In this capacitive coupling approach, the input TL is positioned to be parallel with respect to the adjacent resonators and brought in close proximity of the resonator (e.g. 0.05 mm) to achieve a high capacitive coupling. This separation represents a capacitance value of 0.6 pF in the equivalent circuit model. With this configuration, the input impedance seeing by the source can be expressed as  $Z_{in} = Z_0 + Z_g + Z_2$ . The resulting  $Q_e$  obtained with this

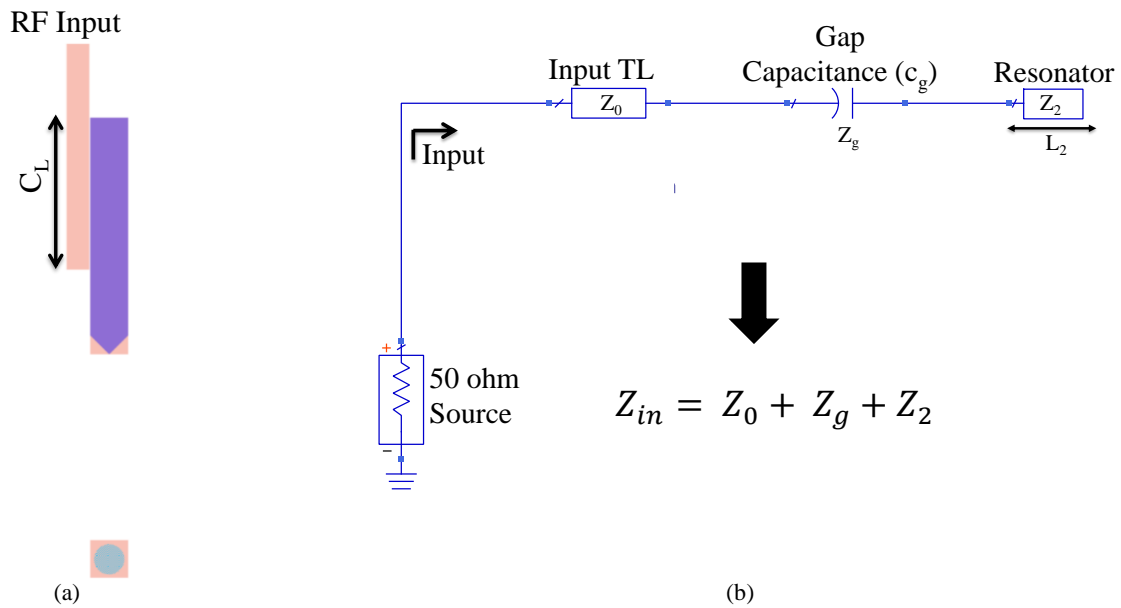


Figure 29: External  $Q_e$  extraction for capacitive coupling approach. a) Resonator layout ( $C_L = 8.75$  mm); b) Resonator circuit (transmission line) model

arrangement can be seen in Fig. 31 (green curve).  $C_L$  was selected as 8.575 mm to obtain the desired  $Q_e$  at 4 GHz. This approach is better than the tapping, but still presents drastic variation in  $Q_e$  at lower frequency range as the series capacitance in the circuit model implies a high series impedance as frequency is lowered. To stabilize the input impedance a high impedance shorted quarter wavelength stub was designed at the highest operational frequency (e.g. 4 GHz) and was added to the input TL as shown in Fig. 30(a) and (b). From Fig. 30(b), the input impedance can be found as  $Z_{in} = Z_0 + (Z_g + Z_2) // Z_3$ . At the designed operational frequency, the stub will act as an RF open, and ideally, it will not affect the  $Q_e$ . While as the frequency is shifted down, it will act as an impedance in parallel with the series C and resonator and effectively reduce the total impedance causing the stabilization of the  $Q_e$  value. The length of the stub was determined as  $S_L = 9$  mm (i.e. quarter wavelength at 4 GHz for the given substrate stack-up). The impedance of the shorted stub section was selected as 108 at 1.5 GHz, which resulted in a line width of 0.6 mm. The shorted stub was placed out of the resonators area. The resulting  $Q_e$  can be seen in Fig.

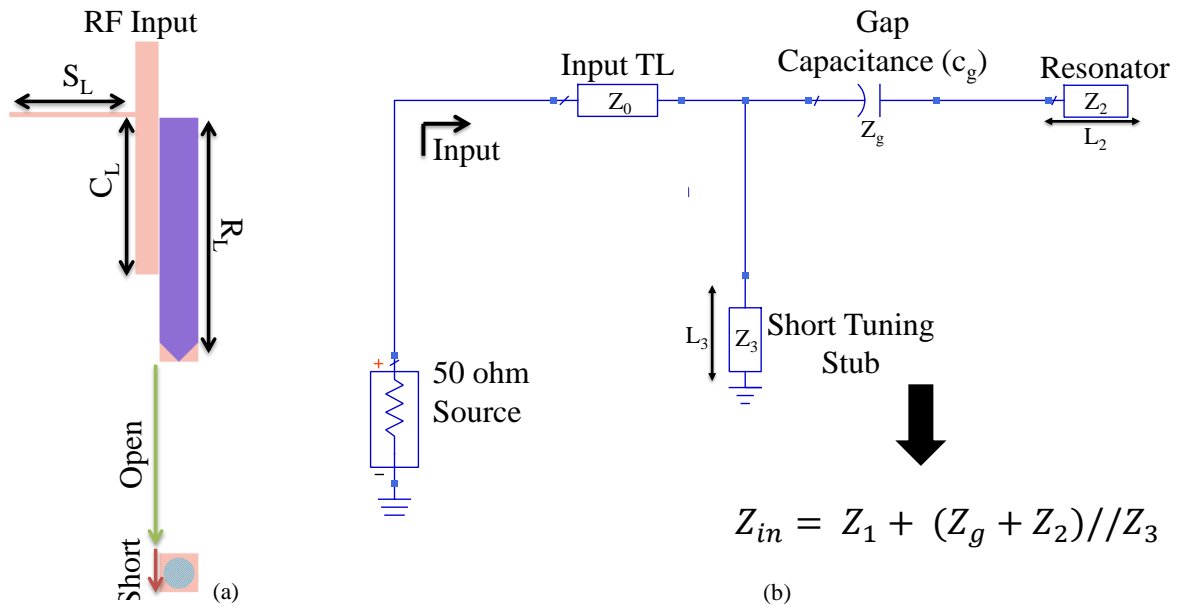


Figure 30: External  $Q_e$  extraction for capacitive coupling approach with added tuning stub. a) Resonator layout ( $C_L = 8.75$  mm,  $S_L = 9$  mm, and  $R_L = 12.575$  mm); b) Resonator circuit (transmission line) model.

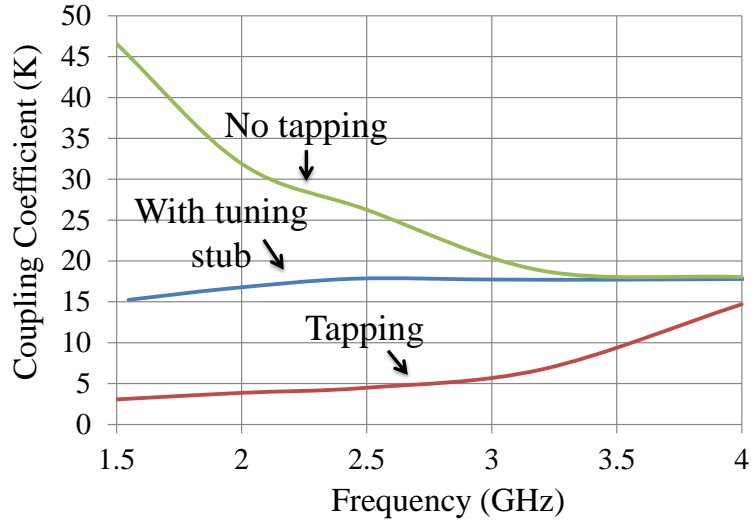


Figure 31: External  $Q_e$  performance for three different approaches. The different curves represent the tapping (red), no tapping (green), and no tapping with tuning stub (blue) approaches.

31 (blue curve) and it is kept constant ( $\pm 1$ ) over the entire frequency tuning range of the resonator. The dimensions of the input network are shown in Fig. 30(a).

As explained in the previous chapters, coupling coefficient ( $K$ ) also needs to be relatively

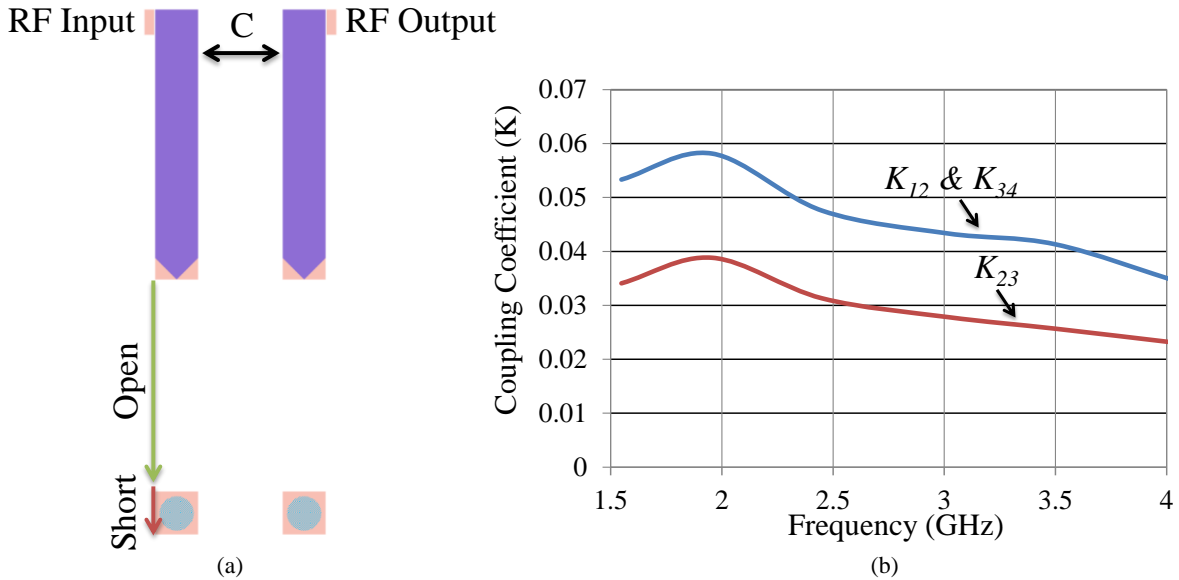


Figure 32: Coupling coefficient for different  $S$  values. (a) Resonator arrangement utilized for  $K$  stabilization (b) Coupling coefficient vs Frequency for two different physical separations:  $K_{12} = K_{34} = 2.75$  mm, and  $K_{23} = 3.95$  mm.

constant over the entire frequency tuning range in order to maintain a constant FBW. Placing the resonators in a parallel manner (Fig. 32(a)) provides a  $K$  relatively stable over the entire frequency tuning range. The lower value for  $K$  was found to occur at the highest operation frequency. Therefore, the required  $K_{12}$ ,  $K_{23}$ , and  $K_{34}$  were determined at the highest frequency to ensure the value of  $K$  will be sufficient at every other frequency to obtain the desired filter response. The separations that resulted in the required  $K_{12} = K_{34} = 0.04204$  and  $K_{23} = 0.02706$ , were found to be 2.75 mm and 3.95 mm respectively. As the operation frequency decreases, the separation between adjacent resonators becomes electrically smaller, which generates an increase in  $K$ . Fig. 32(b) shows the variation of  $K$  as the resonator is tuned down from 4 GHz to 1.5 GHz. From this variation we can expect a 3% change in FBW (from 4% to 7%, at the highest and lowest frequencies, respectively).

Fig. 33(a) shows the 4<sup>th</sup> order reconfigurable bandpass filter layout. As explained in

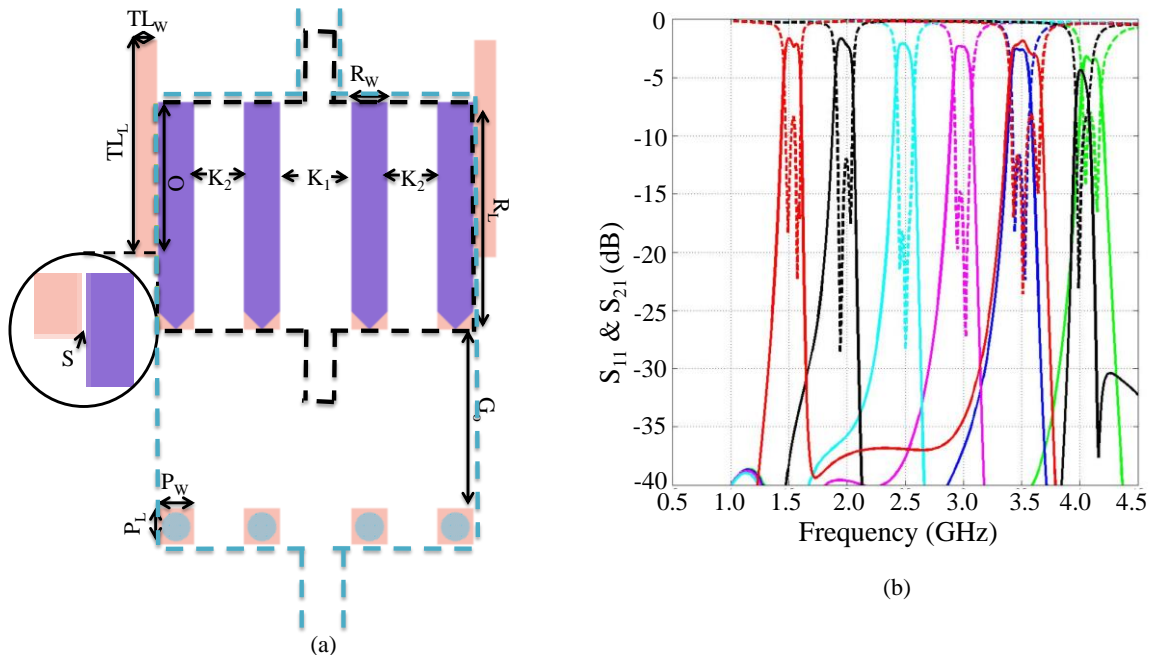


Figure 33: Microfluidically reconfigurable half wavelength resonator filter. (a) Filter layout dimensions:  $TL_L = 12$  mm,  $TL_W = 1.2$  mm,  $O = 8.575$  mm,  $R_L = 12.575$  mm,  $R_W = 2$  mm,  $K_1 = 3.95$  mm,  $K_2 = 2.75$  mm,  $P_W = P_L = 2$  mm,  $S = 0.05$  mm, and  $Go = 9.875$  mm. (b) Simulated  $S_{11}$  &  $S_{21}$  response for five different plate positions.

chapters 4 and 5, all the resonators have to be tuned synchronously for the filter to function properly. Therefore, a selectively metallized plate was utilized to place  $\text{Plate}_R$  of all the resonators. The total footprint of the filter is  $33.95 \times 24.45 \text{ mm}^2$ . The dimensions of the filter can be found in Fig. 33(a). The simulated  $S_{21}$  and  $S_{11}$  performances can be seen in Fig. 33 (b). As expected, the filter presents a tuning range of 90% (from 4 GHz to 1.5 GHz), with 5% (+/- 2%) constant FBW, and  $\text{IL} < 2.7 \text{ dB}$ , and  $\text{RL} > 8.5 \text{ dB}$  for a maximum displacement of 11 mm.

### 6.3 Fabrication

Due to the tight separation between input/output TL and the first/last resonator, and the thin width of the high impedance, shorted stubs, the printed, bottom, layer of the microfluidically reconfigurable resonator was fabricated over a 1.27 mm thick Roger 6010.2 board using conventional photolithography techniques. To accomplish the desired  $6 \text{ }\mu\text{m}$  layer of Benzocyclobutene (BCB) on top of the printed resonators, the spin coating guidelines provided by the manufacturer [64] was utilized. However, due to the thickness of the copper, the BCB was spun at 3500 RPM to obtain a  $7 \text{ }\mu\text{m}$  thick layer, which resulted in a  $\sim 6 \text{ }\mu\text{m}$  layer on top of the resonators (characterized with profilometer measurements). To be able to place SMA connectors at the input and output ports, the end of each was covered with a high temperature resistant tape prior to the BCB spinning and curing. The BCB was cure at a ramping temperature starting at  $0^\circ \text{C}$  and ending at  $250^\circ \text{C}$  for a period of 4 hours.

Using the micromolding technique explained in [56]-[58], the microfluidic channel was fabricated. The detailed steps can be seen in Fig. 34(a). This time, an extra step was added to the molding fabrication to obtain a more accurate thickness. Two layers of photo resist were spun to obtain the desired  $275 \text{ }\mu\text{m}$  thick channel. To maintain the desired synchronization among all the resonators, a 0.25 mm thick selectively metallized plate was utilized as explained in Chapter 5.



1. Clean a silicon wafer
2. Spread coat two layers of SU-8 negative photoresist
3. Using conventional photo lithography techniques, obtain the desired microfluidic channel pattern
4. Poor a, previously mixed, layer of PDMS
5. Let it dry ( $70^{\circ}$  for 1 hour) and peel off the PDMS
6. Place the metallized plate inside the channel
7. Seal the channel with a  $6\ \mu\text{m}$  thick BCB layer through an APTES (3-Aminopropyl-triethoxysilane) process

Silicon



SU-8



Expose and Develop



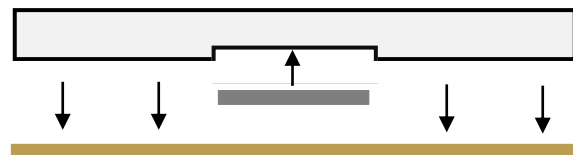
PDMS



Microfluidic Channel



Plate and LCP



(a)

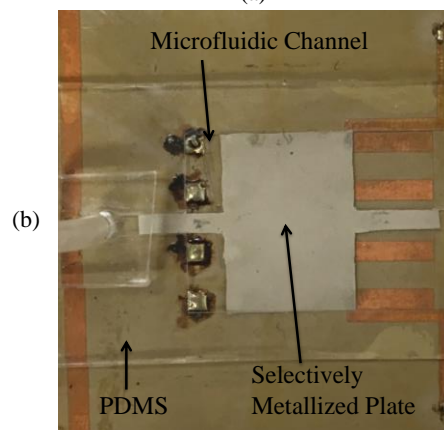


Figure 34: Microfluidic channel fabrication. a) Microchannel fabrication steps; b) Picture of a fabricated microfluidic channel in PDMS

The dimensions of the selectively metallized plate, as well as the microfluidic channel, can be seen in Fig. 35. To keep a relatively fast tuning speed, input and output channels were kept to 2 mm wide, and an extra section of the selectively metallized plate were added in the top and bottom of the plate (Fig. 35(b)). To alleviate the fabrication process, the selectively metallized plate was made in a 0.254 Rogers 5880LZ board ( $\epsilon_r = 1.96$ ,  $\tan\delta = 0.0009$ ) using conventional photolithography techniques, and it was placed inside the microfluidic channel manually prior to sealing it. The microfluidic channel was sealed by bonding it with the BCB layer using an

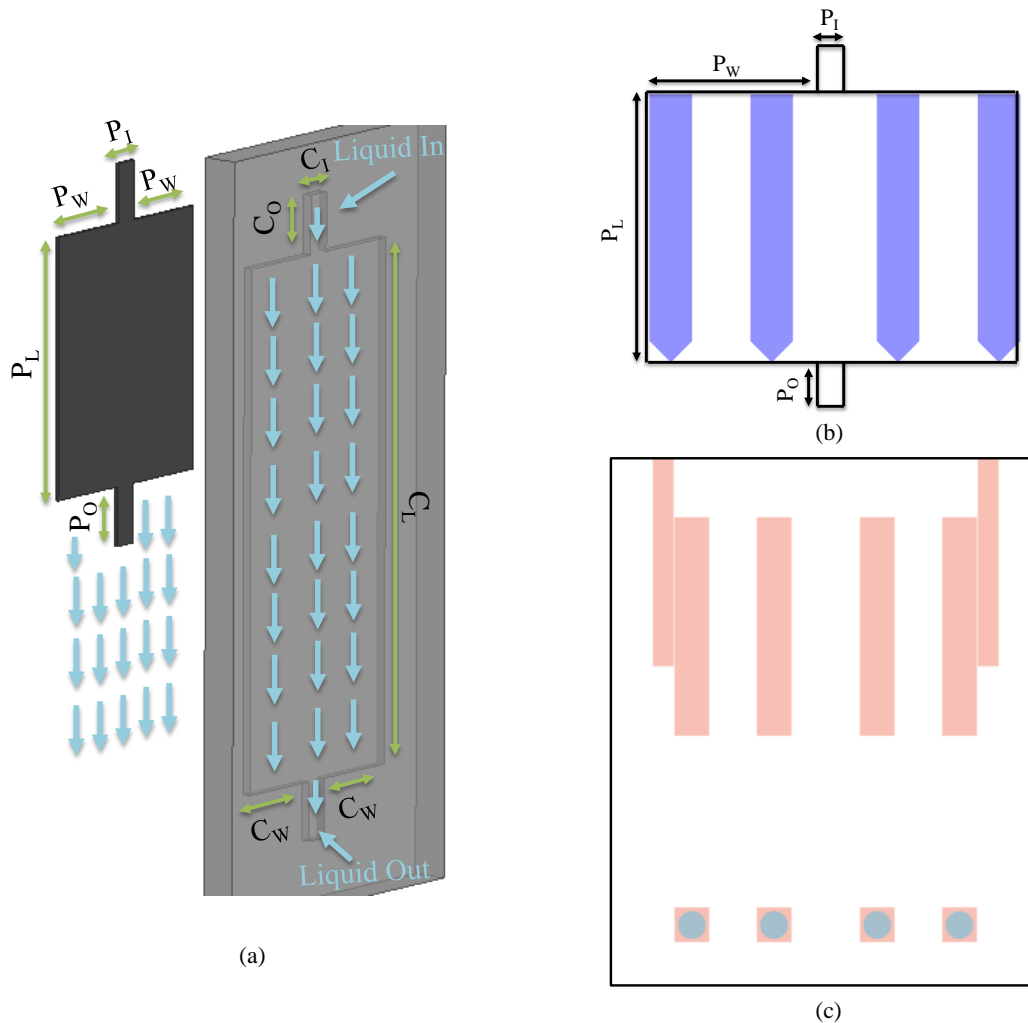


Figure 35: Separated layers. a) Microfluidic channel and selectively metallized plate ( $P_W = 7.25$  mm,  $P_L = 24$  mm,  $P_I = 2$  mm,  $P_O = 5$  mm,  $C_W = 7.3$  mm,  $C_L = 24.1$  mm,  $C_I = 2.1$  mm, and  $C_O = 8$  mm); b) Selectively metallized plate; c) Bottom plate with printed resonators.

APTES (3-Aminopropyltriethoxysilane) treatment [59]. To electronically control the filters, two piezo-pumps, with dimensions of  $30 \times 15 \times 3.8\text{mm}^3$  from Bartels® (mp-6) [61] were utilized. These micropumps were chosen due to their piezo actuation mechanism that allows for an accurate control of the liquid displacement via supply voltages. Two of these pumps were connected in parallel to generate bi-directional flow capability. The pumps were operated with the manufacturer supplied driver circuit that converts 5V DC current to a 100MHz 235V peak to peak sinusoidal wave according to the highest flow rate specifications given for water [61]. The power consumption of the pumps is less than 200 mW.

#### 6.4 Experimental Verification

The fabricated prototype integrated with the pumping system can be seen in Fig. 36(a). As expected, the tuning range of the filter was measured to be 2.7:1 from 4 GHz to 1.5 GHz. Measured  $S_{11}$  and  $S_{21}$  performances can be seen in Fig. 36(b) and (c) and are in good agreement with simulation results. The insertion loss was kept to be less than 3 dB over the entire frequency tuning range with a return loss better than 9.7 dB. This represents an improvement of >1.5 dB in insertion loss with respect to the open loop resonator filter presented in Chapter 5. A constant 5% (+/- 2%) FBW was measured over the entire operational range of the filter. The out of band rejection was >35 dB. However, since the half wavelength structure is kept over the entire frequency range, the second harmonic of the filter is not suppressed, but it is shifted up in frequency due to the shorting effect after a displacement > 9 mm. The overall dimensions of the filter were measured as  $34.975 \times 38.01 \text{ mm}^2$  excluding the pumping mechanism. The input and output TL were extended by 11 mm to alleviate the measurement process. The tuning speed of the filter was found to be, as expected, very close to the filter presented in chapter 5, thanks to the selectively metallized plate approach, and it was measured as 2.5 MHz per ms. The slight

improvement in tuning speed is caused by the smaller size of the plate, which represents less friction from the channel walls.

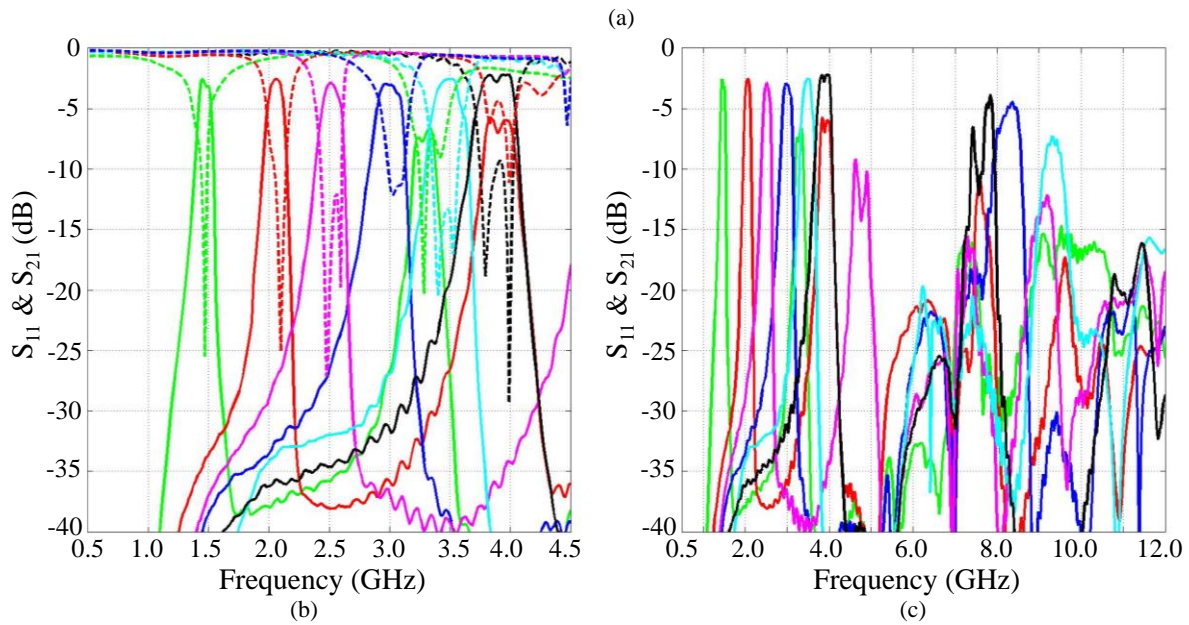
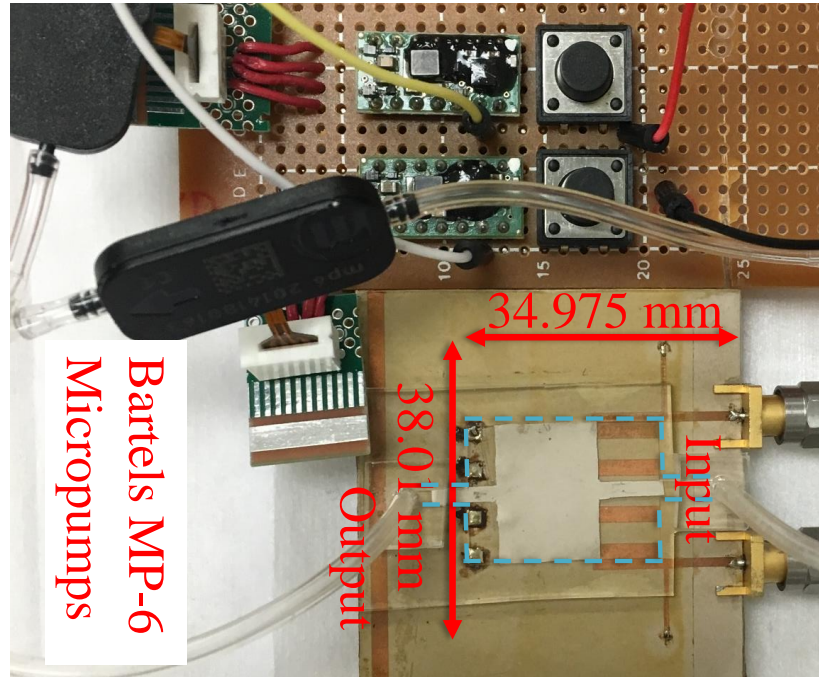


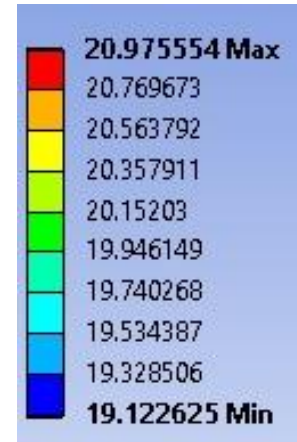
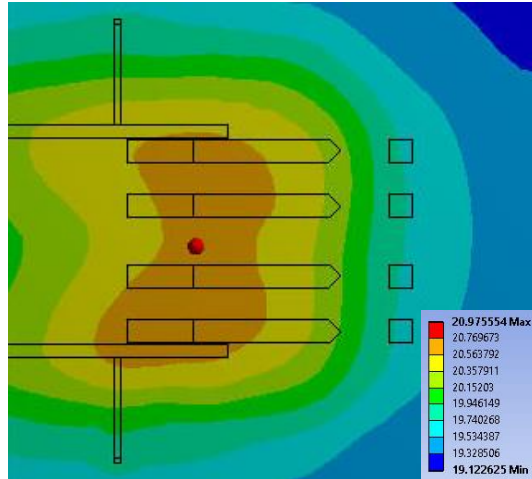
Figure 36: Experimental verification. a) Fabricated filter; b) Measured  $S_{11}$  and  $S_{21}$  performance; c) Wideband responses showing up to the filter's third harmonic.

## 6.5 Power Handling Characterization

In reference [65], it has been demonstrated that half wavelength microstrip resonators are capable of handling power levels above 100 W, making them a great alternative to design filters for high power applications. Microfluidically based reconfigurable filters are suitable for handling high power thanks to absence of nonlinear devices, as shown in [66]. As shown in Reference [48] a microfluidically reconfigurable filter utilizing liquid metal can handle above 10 W of power, and it is only limited by the temperature raising of the materials selected for the substrate stack-up. Therefore, combining half wavelength microstrip resonators with the microfluidically reconfigurable approach presents an interesting solution for high power applications.

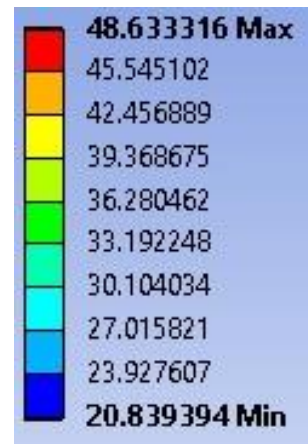
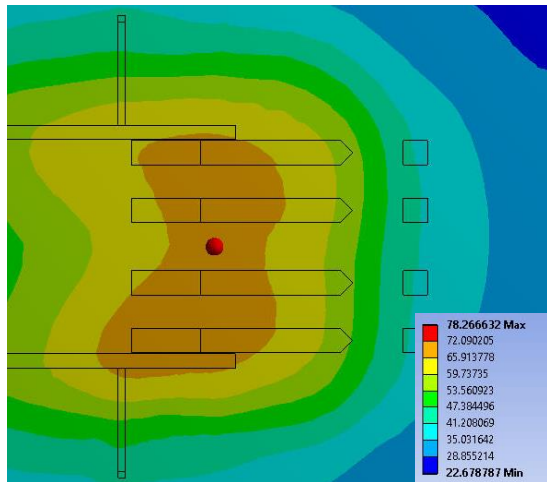
Since no active devices are used in the 4<sup>th</sup> order filter designed in this chapter, and also, as compared with the filter presented in Chapter 5, no lumped components are present in the overall filter, the temperature rising of the substrate stack-up materials would be the limiting factor in terms of power handling capability. Using the Ansys workbench, the filter was tested under high power signal conditions. For an input signal of 1 W of power (Fig. 37(a)), the maximum temperature raise of the filter was found to be 21° C at the center of the microstrip resonators. This represents a small signal condition, and, as expected, the simulated temperature value resides inside the safety range for all the materials utilized (Table 1). Further increasing the input power to 15 W (Fig. 37(b)) raised the steady-state temperature of the filter to a maximum value of 48.6° C, and the maximum temperature is found in among the resonator area. Again, this maximum temperature resides inside the safety operating region for all the materials utilized. To experimentally verify the temperature capabilities of the filter, the setup shown in Fig. 38(a) was utilized. The setup consisted on a high frequency oscillator (e.g. 2.5 GHz), connected to the input

1W Input power



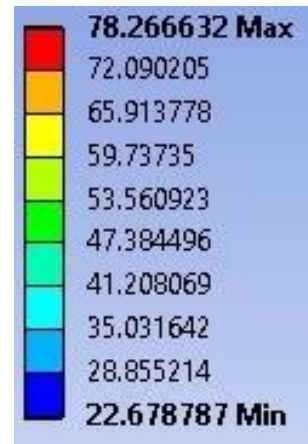
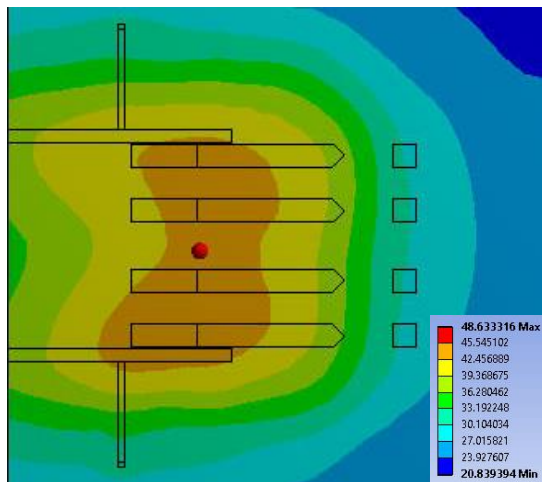
(a)

15 W Input power



(b)

30 W Input power



(c)

Figure 37: Thermal simulations of the 4<sup>th</sup> order bandpass filter with half wavelength resonators for different input power levels at 2.5 GHz. a) 1 W; b) 15 W; c) 30 W.

of a high power amplifier (Mini-Circuits ZHL-16W-43-S+) [67]. The output of the power amplifier is connected to a unidirectional circulator from Trak Microwave Corp. as a safety precaution to protect the high power amplifier. The filter is connected after the isolator and a high power attenuator is placed between the output of the filter and the measurement equipment to protect the ENA. A ENA E5063A was used to measure frequencies up to 4 GHz. It was found that at >15 W of input power, and at 2.5 GHz where the resonators presented their lower  $Q_u$ , the temperature rose up to 46° C (Fig. 38(b)), this is 2° lower than simulated results, and the difference is probably due to unknown ambient temperature of the laboratory. As expected, the entire filter area remained inside the safety range of the materials utilized. Due to the limitation in the power amplifier output power, it was not possible to test for higher input power levels. However, according to simulations with Ansys Workbench, the proposed microfluidically based

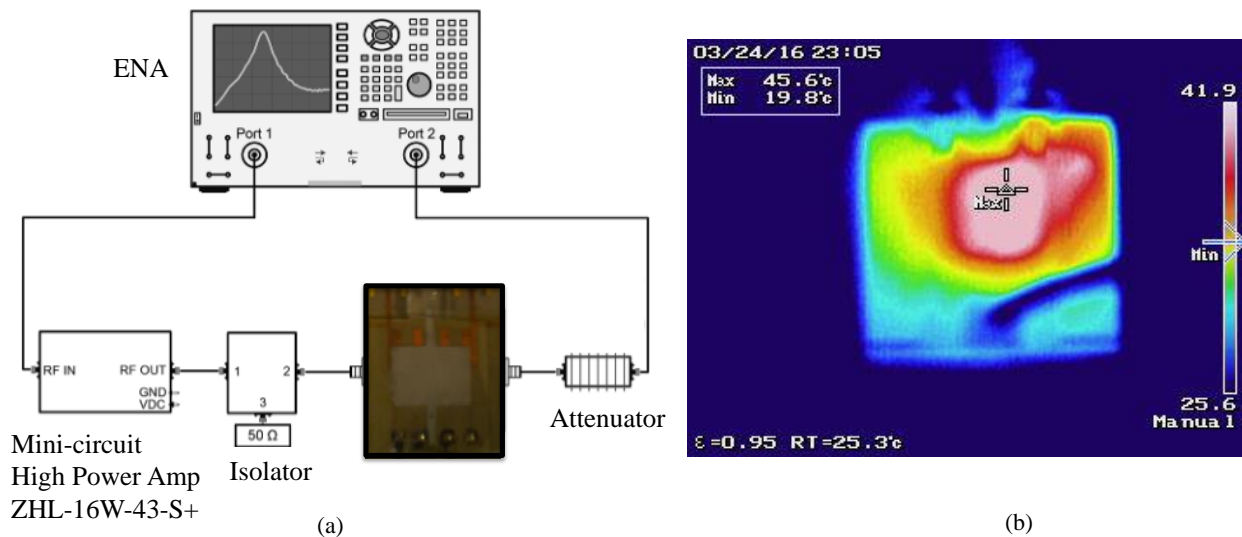


Figure 38: Power handling characterization of the 4<sup>th</sup> order bandpass filter utilizing half-wavelength resonators at the lowest resonator's  $Q_u$  frequency of 2.5 GHz. a) Experimental set up consisting on: ENA E5063A, Trak 60A3001 Isolator, proposed filter prototype, and a high power attenuator; c) Thermal image after steady state condition have been reached (Image taken with Keysight ).

reconfigurable filter is capable of handling  $>30$  W of input power without the addition of external heat sinks. The maximum temperature for 30 W of input power was found to be  $78^{\circ}$  C (Fig. 37(c)).

Table 1: Thermal properties of materials utilized

Material	Thermal Conductivity	Specific Heat	Maximum Temperature
PDMS	0.27 W/mK	1.46 kJ/kgK	200° C
BCB	0.293 W/mC	2.4 kJ/kgK	165° C
FC-40	0.065 W/mC	1.1 kJ/kgC	165° C
Rogers 6010.2	0.86 W/mK	1 kJ/kgK	380° C
LCP	0.2 W/mK	N/A	330° C
Alumina	37 W/mK	0.9 kJ/kgC	1550° C
Glass	1.38 W/mK	0.7 kJ/kgC	1100° C

## 6.6 Concluding Remarks of Chapter 6

It has been demonstrated that microfluidic reconfiguration can be combined with conventional half wavelength open ended microstrip resonators to accomplish a very low loss, highly tunable, and high power handling bandpass filter. The proposed novel filter presents a frequency tuning range of 90%, more specifically, from 4 GHz to 1.5 GHz, which represent an improvement of more than 50% as compared to the capacitively loaded open loop resonator based reconfigurable filter of Chapter 5. To the best of our knowledge, this is the first time that a 2.7:1 continuously tunable filter has been demonstrated. Due to the high unloaded quality factor of the resonators, the filter presents a low, and almost constant, insertion loss of less than 3 dB over the entire frequency tunable range. Power handling characterization was carried out and it



was found that the power handling of the filter is above 15 W. Table 2 provides a summary of all the filters presented in this dissertation.

Table 2: Summary of filters realized through this dissertation

Property	Filter Chapter 3	Filter Chapter 4	Filter Chapter 5	Filter Chapter 6
Resonator type	BC-SRR	Open-Loop	Open-Loop	Half wavelength
Filter Order	2 <sup>nd</sup>	2 <sup>nd</sup>	4 <sup>th</sup>	4 <sup>th</sup>
High-Min Frequencies	870 – 650 MHz	1.5 – 0.9 GHz	1.5 – 0.8 GHz	4.0 – 1.5 GHz
Tuning Range	29% (1.3:1)	50% (1.67:1)	61% (1.88:1)	91% (2.67:1)
FBW	5%	8%	5%	5%
$Q_u$	120 – 50	160 – 70	160 – 70	~200
IL < (dB)	3	1.7	4.5	3
RL > (dB)	9	10	10	9.5

## CHAPTER 7: FUTURE WORK

To further enhance the power handling capabilities resorting to a hard substrate based configuration would be vital. As explained in Chapter 6, the temperature rising and thermal conductivity of the materials is the limiting factor in terms of power handling capability of microfluidics based reconfigurable filters. Most reconfigurable filters are limited, in their power handling capability, by the third order intermodulation (TOI) point. Since no active devices are utilized in microfluidically based RF reconfigurable filters, there is not TOI. The materials utilized in the previous chapters present a poor temperature handling characteristic (e.g. coefficient of thermal conductivity). In Table 2 the thermal characteristics of these materials (Rogers 6010.2, BCB, and PDMS) are presented. As explained in chapter 6, the poorest thermal conductor from this materials is the carrier fluid utilized (FC-40). However, improving the thermal capacity of the material surrounding the fluid would help increase the maximum temperature of operation of the filter. Therefore, replacing the PDMS with a material presenting a higher thermal conductivity would be vital for very high power applications. Also, at high temperatures, PDMS starts absorbing liquid, which would represent a major issue due to the small volume of fluid required inside the channels. A solution to the above mentioned problems could be replacing PDMS with glass, and therefore, preliminary studies have been done in this aspect. However, the fabrication process time increase considerably due to the lengthy process of etching glass. From preliminary studies, the etching rate of glass is  $\sim 10 \mu\text{m}$  per hour. At this rate, it would take at least 25 hours to etch the desired channel. Also, most available photoresists

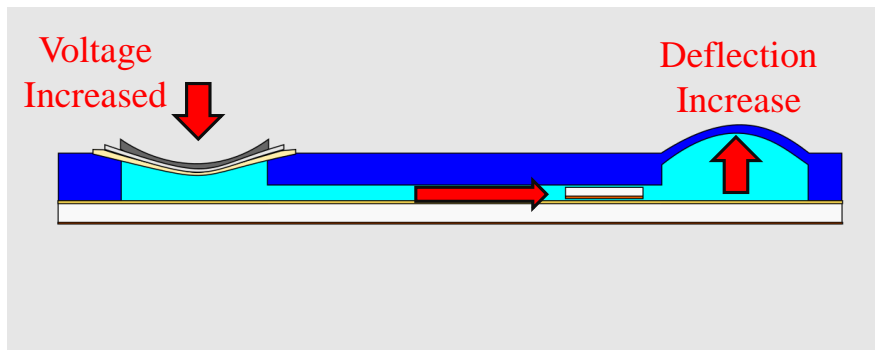
would be etched faster than the glass. One possible alternative would be using laser to etch the glass, but the expensive pricing make it a not viable solution at this point. The addition of an external heat sink could be valuable in terms of power handling capability of the filter since, once again, its main limitation is only the temperature raising of the components, and the dimensions of the filter are very small when compare to other available technologies.

Different type of resonators needs to be investigated to further expand the broad range of possibilities that microfluidics have to offer toward obtaining RF bandpass reconfigurable filters. Utilizing resonators with higher unloaded quality factor would provide a significant improvement in terms of insertion loss (lower insertion loss) and power handling capability (higher power handling), and therefore, should be investigated. Suspended line based resonators have been known for providing a high unloaded quality factor. Therefore, the transition into suspended line resonators would be vital to further decrease the insertion loss and increase the power handling capability of microfluidically reconfigurable filters.

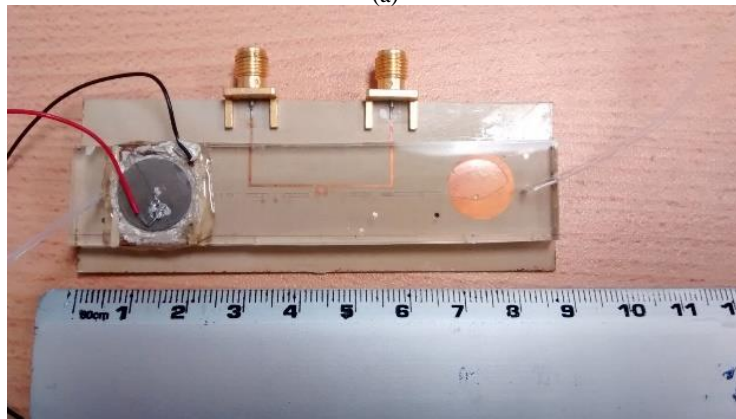
When comparing microfluidics to other available technologies, proposed reconfigurable filters lack in terms of their tuning speed. So far, the studies carried out with microfluidic reconfigurable filters presented a tuning speed of 2.12 MHz per ms, as compare to the tuning speed presented by ferroelectric varactors (for example 2 MHz per  $\mu$ s). So far, the experiments conducted on microfluidic reconfigurable devices have been done utilizing external micropumps units, and therefore, the tuning speed of the filters is directly related to the micropump capabilities in terms of flow rate. A detailed study on the micropumps could help to improve the tuning speed significantly. In addition, the viscosity of the fluid utilized to move the metallized plate inside the channel has a direct impact on the micropump functionality. So far the only fluids studied have been Teflon solution and FC-40. Different carrier fluids could be further

investigated in parallel with a variety of micropumps to determine the fastest tuning speed that can be obtained.

However, replacing the externally added micropumps with on-board actuators would be the ideal solution. One of the most popular alternatives that has been investigated so far is utilizing electrowetting as the actuation mechanism. Electrowetting consist on modifying the surface tension of dielectrics, utilizing a voltage, for the microfluidics actuation [68]. And the most common method for electrowetting have been Electrowetting on Dielectric (EWOD) [69]. However, another approach that has been investigated is resorting to pressure based actuation [70]. Therefore, another approach that is currently been investigated, by our research group, to



(a)



(b)

Figure 39: Piezo electric disk actuation proposed for future work. a) Operational principle of the actuation mechanism based on piezoelectric disk; b) Fabricated prototype of 10GHz open loop resonator loaded with a metalized plate. This picture is courtesy of Enrique Gonzales (Ph.D. student in Dr. Mumcu's research group)

replace the micropumps with in-chip actuators, and therefore, increase the tuning speed of microfluidic based reconfigurable filters, is the utilization of a piezoelectric disks to provide metallized plates backwards and forward motion capabilities. By making use of a sealed microfluidic channel, it is possible to transfer the small deflection generated by a piezo electric disk into motion. As shown in Fig. 39(a), as the voltage increases, the piezoelectric disk bends downwards and push the plate inside the channel. A second reservoir is place in the opposite end of the channel to absorb the motion (Fig. 39(a)). The proposed mechanism has been experimentally verified to provide a short moving range of 3 mm with a <10 mm in diameter piezo electric disk. Preliminary studies were carried out through a resonator at high frequencies (10 GHz) to maintain the required motion range under the 3 mm range provided by the piezo disk (Fig. 39(b)). Furthermore, the piezo electric disk could be positioned under the ground plane (below the filter area) to maintain the footprint to that of the individual reconfigurable filter. Since piezo-electric based actuation has been demonstrated to be fast, require low DC power and the displacement range required by the microfluidic based filters has been shown to be small, they present an interesting alternative for the necessary actuation mechanism.

## REFERENCES

- [1] G. M. Rebeiz, K. Entesari, I. C. Reines, S. J. Park, M. A. El-Tanani, A. Grichener, *et al.*, "Tuning in to RF MEMS," *Ieee Microwave Magazine*, vol. 10, pp. 55-72, Oct 2009.
- [2] P. Bahramzy, P. Olesen, P. Madsen, J. Bojer, S. C. Del Barrio, A. Tatomirescu, *et al.*, "A Tunable RF Front-End With Narrowband Antennas for Mobile Devices," *Ieee Transactions on Microwave Theory and Techniques*, vol. 63, pp. 3300-3310, Oct 2015.
- [3] J. Uher, and W. Hoefler, "Tunable microwave and millimeter-wave band-pass filters," *Ieee Transactions on Microwave Theory and Techniques*, vol. 39, no. 4, pp. 643-653, April 1991.
- [4] R. R. Mansour, F. X. Huang, S. Fouladi, W. D. Yan, and M. Nasr, "High-Q Tunable Filters," *Ieee Microwave Magazine*, vol. 15, pp. 70-82, Jul-Aug 2014.
- [5] G. C. Liang, D. Zhang, C. F. Shih, M. E. Johansson, and R. S. Withers, "High-power high-temperature superconducting microstrip filters for cellular base-station applications," *Ieee Transactions on Applied Superconductivity*, vol. 5, no. 2, June 1995.
- [6] S. H. Hou, J. H. Lang, A. H. Slocum, A. C. Weber, and J. R. White, "A high- $Q$  widely tunable gigahertz electromagnetic cavity resonator," *Journal of Microelectromechanical Systems*, vol. 15, no. 6, pp. 1540-1545, December 2006.
- [7] W. J. Keane, "Narrow-Band Yig Filters Aid Wide-Open Receivers," *Microwaves*, vol. 17, pp. 50-&, 1978.
- [8] L. Young, and D. Weller, "A 500-to-1000 MHz magnetically tunable band-pass filter using two YIG-disk resonators," *Ieee Transactions on Microwave Theory and Thecniques*, vol. MTT-15, no. 2, pp. 72-86, February 1967.
- [9] Y. Murakami, T. Ohgihara, and T. Okamoto, "A 0.5-4.0-GHz tunable bandpass filter using YIG film grown by LPE," *Ieee Transactions on Microwave Theory and Techniques*, vol. MTT-35, no. 12, pp. 1192-1198, December 1987.
- [10] Y. Shu, J. Navarro, and K. Chang, "Electronically switchable and tunable coplanar waveguided-slotline band-pass filter," *Ieee Transactions on Microwave Theory and Techniques*, vol. 39, no. 3, pp. 548-554, March 1991.

- [11] A. R. Brown and G. M. Rebeiz, "A varactor-tuned RF filter," *Ieee Transactions on Microwave Theory and Techniques*, vol. 48, pp. 1157-1160, Jul 2000.
- [12] C. Li *et. al.*, "A tunable high temperature superconducting bandpass filter realized using semiconductor varactors," *Ieee Transactions on Applied Superconductivity*, vol. 24, no. 5, August 2014.
- [13] J. S. Sun, N. Kaneda, Y. Baeyens, T. Itoh, and Y. K. Chen, "Multilayer Planar Tunable Filter With Very Wide Tuning Bandwidth," *Ieee Transactions on Microwave Theory and Techniques*, vol. 59, pp. 2864-2871, Nov 2011.
- [14] I. Vendik, O. Vendik, V. Pleskachev, and M. Nikol'ski, "Tunable microwave filters using ferroelectric materials," *Ieee transactions on Applied Superconductivity*, vol. 13, no. 2, pp. 716-719, June 2003.
- [15] S. Courreges, Y. Li, Z. Y. Zhao, K. Choi, A. Hunt, and J. Papapolymerou, "A Low Loss X-Band Quasi-Elliptic Ferroelectric Tunable Filter," *Ieee Microwave and Wireless Components Letters*, vol. 19, pp. 203-205, Apr 2009.
- [16] S. Courreges, Y. Li, Z. Zhao, K. Choi, A. Hunt, and J. Papapolymerou, "Two-pole X-band-tunable ferroelectric filters with tunable center frequency, fractional bandwidth, and return loss," *Ieee Transactions on Microwave Theory and Techniques*, vol. 57, no. 12, pp. 2872-2881, December 2009.
- [17] A. Abbaspour-Tamijani, L. Dussopt, and G. Rebeiz, "Miniature and tunable filters using MEMS capacitors," *Ieee Transactions on Microwave Theory and Techniques*, vol. 51, no. 7, pp. 1878-1885, July 2003.
- [18] Y. Shim, Z. Z. Wu, and M. Rais-Zadeh, "A High-Performance Continuously Tunable MEMS Bandpass Filter at 1 GHz," *Ieee Transactions on Microwave Theory and Techniques*, vol. 60, pp. 2439-2447, Aug 2012.
- [19] W. Irshad and D. Peroulis, "A 12-18 GHz electrostatically tunable liquid metal RF MEMS resonator with quality factor of 1400-1840," in *Microwave Symposium Digest (MTT), 2011 IEEE MTT-S International*, 2011, pp. 1-4.
- [20] K. Entesari and G. M. Rebeiz, "A differential 4-bit 6.5-10-GHz RF MEMS tunable filter," *Ieee Transactions on Microwave Theory and Techniques*, vol. 53, pp. 1103-1110, Mar 2005.
- [21] K. L. Chen, X. G. Liu, A. Kovacs, W. J. Chappell, and D. Peroulis, "Antibiased Electrostatic RF MEMS Varactors and Tunable Filters," *Ieee Transactions on Microwave Theory and Techniques*, vol. 58, pp. 3971-3981, Dec 2010.

- [22] X. G. Liu, L. P. B. Katehi, W. J. Chappell, and D. Peroulis, "High-Q Tunable Microwave Cavity Resonators and Filters Using SOI-Based RF MEMS Tuners," *Journal of Microelectromechanical Systems*, vol. 19, pp. 774-784, Aug 2010.
- [23] S. Fouladi, F. Huang, W. Yan, R. Mansour, "High- $Q$  narrowband tunable combline filters using MEMS capacitor banks and piezomotors," *Ieee Transactions on Microwave Theory and Techniques*, vol. 61, no. 1, pp. 393-402, January 2013.
- [24] S. Tasoglu, H. C. Tekin, F. Inci, S. Knowlton, S. Wang, F. Wang-Johanning, G. Johanning, D. Colevas, and U. Demirci, "Advance in nanotechnology and microfluidics for human papillomavirus diagnostics," *Proceedings of the Ieee*, vol. 103, no. 2, pp. 161-178, February 2015.
- [25] E. Sackmann, A. Fulton, and D. Beebe, "The present and future role of microfluidics in biomedical research," *Nature*, vol. 507, pp. 181-189, March 2014.
- [26] C. Chin, *et. al*, "Microfluidics-based diagnostics of infectious diseases in the developing world," *Nature Medicine*, vol. 17, pp. 1015-1019, August 2011.
- [27] G. Whitesides, "The origins and the future of microfluidics," *Nature*, vol. 44, pp. 368-373, July 2006.
- [28] C. Mastrangelo, M. Burns, and D. Burke, "Microfabricated devices for genetic diagnostics," *Proceedings of the Ieee*, vol. 86, no. 8, pp. 1769-1787, August 1998.
- [29] F. Su, K. Chakrabarty, and R. Fair, "Microfluidics-based biochips: technology issues, implementation platforms, and design-automation challenges," *Ieee Transactions on Computer-Aided Design of Integrated Circuits and Systems*, vol. 25, no.2, pp. 211-223, February 2006.
- [30] K. Wise, D. Anderson, J. Hetke, D. Kipke, and K. Najafi, "Wireless implantable microsystems: high-density electronic interface to the nervous system," *Proceedings of the Ieee*, vol. 92, no. 1, pp. 76-97, January 2004.
- [31] P. Paik, V. Pamula, and K. Chakrabarty, "Adaptive cooling of integrated circuits using digital microfluidics," *Ieee Transactions on Very Large Scale Integration (VLSI) Systems*, vol. 16, no. 4, pp. 432-443, April 2008.
- [32] A. Schimpf, D. Bucci, A. Magnaldo, L. Couston, and J. Broquin, "Microfluidics and integrated optics glass sensor for in-line microprobing of nuclear samples," *Ieee Transactions on Nuclear Science*, vol. 59, no. 4, pp. 1401- 1407, August 2012.
- [33] V. Jagannadh, R. Murthy, R. Srinivasan, and S. Gorthi, "Field-portable microfluidics-based imagin flow cytometer," *Journal of Lightwave Technology*, vol. 33, no. 16, pp. 3469-3474, August 2015.



- [34] M. Royal, N. Jokerst, and R. Fair, "Droplet-based sensing: optical microresonator sensor embedded in digital electrowetting microfluidics system," *Ieee Sensors Journal*, vol. 13, no. 12, pp. 4733-4742, December 2013.
- [35] H. Takao, and M. Ishida, "Microfluidic integrated circuits for signal processing using analogous relationship between pneumatic microvalve and MOSFET," *Journal of Microelectromechanical Systems*, vol. 12, no. 4, pp. 497-505, August 2003.
- [36] C. Chen, and D. Peroulis, "Liquid RF MEMS wideband reflective and absorptive switches," *Ieee Transactions on Microwave Theory and Techniques*, vol. 55, no. 12, pp. 2919-2929, December 2007.
- [37] A. Saghati, J. Batra, J. Kameoka, and K. Entesari, "Miniature and reconfigurable CPW folded slot antenna employing liquid-metal capacitive loading," *Ieee Transactions on Antennas and Propagation*, vol. 63, no. 9, pp. 3798-3807, September 2015.
- [38] D. Rodrigo, L. Jofre, and B. Centiner, "Circular beam-steering reconfigurable antenna with liquid metal parasitics," *Ieee Transactions on Antennas and Propagation*, vol. 60, no. 4, pp. 1796-1802, April 2012.
- [39] G. Huff, D. Ronaldo, P. Walters, and J. McDonald, "A frequency reconfigurable dielectric resonator antenna using colloidal dispersion," *Ieee Antennas and Wireless Propagation Letters*, vol. 9, pp. 288-290, 2010.
- [40] G. Hayes, J. So, A. Qusba, M. Dickey, and G. Lazzi, "Flexible liquid metal alloy (EGaIn) microstrip patch antenna," *Ieee Transactions on Antennas and Propagation*, vol. 60, no. 5, pp. 2151-2156, May 2012.
- [41] M. Li, B. Yu, and N. Behdad, "Liquid-tunable frequency selective surfaces," *Ieee Microwave and Wireless Components Letters*, vol. 20, no. 8, 423-425, August 2010.
- [42] M. Li, and N. Behdad, "Fluidically tunable frequency selective/phase shifting surfaces for high-power microwave applications," *Ieee Transactions on Antennas and Propagation*, vol. 60, no. 6, pp. 2748-2759, June 2012.
- [43] B. Lei, A. Zamora, T. Chun, A. Ohta, and W. Shiroma, "A wideband, pressure-driven, liquid-tunable frequency selective surface," *Ieee Microwave and Wireless Components Letters*, vol. 21, no. 9, pp. 465-467, September 2011.
- [44] A. Morishita, C. Kitamura, A. Ohta, and W. Shiroma, "A liquid-metal monopole array with tunable frequency, gain, and beam steering," *Ieee Antennas and Wireless Propagation Letters*, vol. 12, pp. 1388-1391, 2013.
- [45] W. G. Tonaki, H. Wenqi, A. T. Ohta, and W. A. Shiroma, "A reconfigurable, liquid-metal-based low-pass filter with reversible tuning," in *IEEE International Wireless Symposium (IWS)*, pp. 1-3, 2013.

- [46] M. R. Khan, G. J. Hayes, S. L. Zhang, M. D. Dickey, and G. Lazzi, "A Pressure Responsive Fluidic Microstrip Open Stub Resonator Using a Liquid Metal Alloy," *Ieee Microwave and Wireless Components Letters*, vol. 22, pp. 577-579, Nov 2012.
- [47] A. T. Ohta, G. Shuyan, L. Bao Jun, H. Wenqi, and W. A. Shiroma, "A liquid-metal tunable electromagnetic-bandgap microstrip filter," in *Wireless Information Technology and Systems (ICWITS), 2012 IEEE International Conference on*, 2012, pp. 1-4.
- [48] A. P. Saghati, J. S. Batra, J. Kameoka, and K. Entesari, "A Miniaturized Microfluidically Reconfigurable Coplanar Waveguide Bandpass Filter With Maximum Power Handling of 10 Watts," *Ieee Transactions on Microwave Theory and Techniques*, vol. 63, pp. 2515-2525, Aug 2015.
- [49] C. Koo, B. E. LeBlanc, M. Kelley, H. E. Fitzgerald, G. H. Huff, and A. Han, "Manipulating Liquid Metal Droplets in Microfluidic Channels With Minimized Skin Residues Toward Tunable RF Applications," *Journal of Microelectromechanical Systems*, vol. 24, pp. 1069-1076, Aug 2015.
- [50] T. Palomo, P. Herzig, T. M. Weller, and G. Mumcu, "Wideband Band-Stop X-Band Filter Using Electrically Small Tightly Coupled Resonators," *Ieee Microwave and Wireless Components Letters*, vol. 23, pp. 356-358, Jul 2013.
- [51] G. Mumcu, A. Dey, and T. Palomo, "Frequency-Agile Bandpass Filters Using Liquid Metal Tunable Broadside Coupled Split Ring Resonators," *Ieee Microwave and Wireless Components Letters*, vol. 23, pp. 187-189, Apr 2013.
- [52] A. P. Saghati, J. Batra, J. Kameoka, and K. Entesari, "Microfluidically-tuned miniaturized planar microwave resonators," in *Wireless and Microwave Technology Conference (WAMICON), 2014 IEEE 15th Annual*, 2014, pp. 1-3.
- [53] T. Palomo and G. Mumcu, "Highly reconfigurable bandpass filters using microfluidically controlled metallized glass plates," in *IEEE MTT-S International Microwave Symposium (IMS)*, pp. 1-3, 2014.
- [54] T. Palomo, and G. Mumcu, "Microfluidically Reconfigurable Metallized Plate Loaded Frequency-agile RF Bandpass Filters," *Ieee Transactions on Microwave Theory and Techniques*, vol. 64, no. 1, pp. 158-165, 2016.
- [55] J.-S. Hong and M. J. Lancaster, in *Microstrip Filters for RF/Microwave Applications*, ed: John Wiley & Sons, Inc., 2001.
- [56] T. Fujii, "PDMS-based microfluidic devices for biomedical applications," *Microelectronic Engineering*, vol. 61-2, pp. 907-914, Jul 2002.

- [57] M. Bahrami, M. M. Yovanovich, and J. R. Culham, "Pressure drop of fully-developed, laminar flow in microchannels of arbitrary cross-section," *Journal of Fluids Engineering*, vol. 128, pp. 1036-1044, 2006.
- [58] B. Jo, L. Van Lerberghe, K. Motsegood, and D. Beebe, "Three-dimensional micro-channel fabrication in polydimethylsiloxane (PDMS) elastomer," *Journal of Microelectromechanical Systems*, vol. 9, no. 1, pp. 76-81, March 2000.
- [59] A. A. Gheethan, M. C. Jo, R. Guldiken, and G. Mumcu, "Microfluidic Based Ka-Band Beam-Scanning Focal Plane Array," *Ieee Antennas and Wireless Propagation Letters*, vol. 12, pp. 1638-1641, 2013.
- [60] D. M. Pozar, *Microwave engineering*: John Wiley & Sons, 2009.
- [61] "Available Online <http://www.micro-components.com>"
- [62] C. Hunter, and J. Rhodes, "Electronically tunable microwave bandpass filters," *Ieee Transactions on Microwave Theory and Techniques*, vol. MTT-30, no. 9, pp. 1354-1360, September 1982.
- [63] B. Kim, and S. Yun, "Varactor-tuned combline bandpass filter using step-impedance microstrip lines," *Ieee Transactions on Microwave Theory and Techniques*, vol. 52, no.4 pp. 1279-1283, April 2004.
- [64] "Available Online <http://www.dow.com/cyclotene/>"
- [65] L. Wu, X. Zhou, W. Yin, M. Tang, and L. Zhou, "Characterization of average power handling of bandpass filters using planar half-wavelength microstrip resonators," *Ieee Microwave and Wireless Components Letters*, vol. 19, no. 11, pp. 686-688, November 2009.
- [66] A. Dey and G. Mumcu, "Microfluidically Controlled Frequency Tunable Monopole Antenna for High Power Applications," *Antennas and Wireless Propagation Letters, IEEE*, vol. PP, pp. 1-1, 2015.
- [67] "Available Online <http://www.minicircuits.com/pdfs/ZHL-16W-43+.pdf>"
- [68] J. Lee, and C. Kin, "Surface-tension-driven microactuation based on continuous electrowetting," *Journal of Microelectromechanical Systems*, vol. 9, no. 2, pp. 171-180, June 2000.
- [69] Y. Li, W. Parkes, L. Haworth, A. Ross, J. Stevenson, and A. Walton, "Room-temperature fabrication of anodic tantalum pentoxide for low-voltage electrowetting on dielectric (EWOD)," *Journal of Microelectromechanical Systems*, vol. 17, no. 6, pp. 1481-1488, December 2008.

- [70] E. Hallynck, and P. Bienstman, "Digital microfluidics with pressure-based actuation," *Ieee Photonics Technology Letters*, vol. 25, no. 17, pp. 1656-1659, September 2013.
- [71] A. Gheethan, A. Dey, and G. Mumcu, "Passive feed network design for microfluidic beam-scanning focal plane arrays and their performance evaluation," *Ieee Transactions on Antennas and Propagation*, vol. 63, no. 8, pp. 3452-3464, May 2015.
- [72] "Available Online <http://www.microchem.com/Prod-SU82000.htm>"
- [73] V. Sunkara, D. Park, H. Hwang, R. Chantiwas, S. Soper, and Y. Cho, "Simple room temperature bonding of thermoplastics and poly(dimethylsiloxane)," *Lab On a Chip*, vol. 11, pp. 962-965, 2011.
- [74] "Available Online <http://www.dow.com/cyclotene/prod/302257.htm>"

## APPENDIX A: MICROFLUIDIC CHANNEL FABRICATION

Microfluidic channel fabrication has been previously presented in [56]-[58]. The overall technique consist on fabricating a mold with the desire microchannel specification, to later pour a commercially available elastomer (Polydimethylsiloxane) in its liquid form, and cure to transition it into its solid state. After pilling of the solid elastomer, the desired microchannels will be in the bottom face. The face containing the microchannels will be sealed with a commercially available thin-film insulator to form the finalized microfluidic channel. In the following, a detailed explanation on each of the steps of the microchannel fabrication is provided.

### A.1 Microfluidic Channel Design

Initially, individual metallized plates were utilized and a meandered channel was designed to host all the plates (e.g. 2 plates were used in chapter 4). At the beginning of this dissertation, microfluidic channels were designed to have the same width as the metallized plates. However, it was quickly learned that the plate would not move inside these channels due to the high friction between the walls of the channel and the plate (e.g. channel got stuck). To overcome this issue, a detailed characterization of the channel width was performed by our group [71] by fabricating channels with widths slightly wider than the width of the metallized plates. From these studies, it was found that if the microfluidic channel was too wide, the plate could tilt inside of it causing it to get stuck and/or corrupt the performance of the filter. After fabricating channels with 100  $\mu\text{m}$ , 200  $\mu\text{m}$ , 300  $\mu\text{m}$ , 400  $\mu\text{m}$ , and 500  $\mu\text{m}$  wider than the metallized plate, it was found that, with a 100  $\mu\text{m}$  wider channel, the plate movement was smooth and repeatable.

## A.2 Micromold Fabrication

The micromold design follows conventional photolithography techniques. To start a 5 inch diameter silicon wafer is cleaned by submerging it in acetone, isopropanol, and methanol. After submerging it in methanol, it is necessary to rinse with deionized water and dry with nitrogen, quickly after it has been rinsed. To remove any water drops left on the surface, the wafer is placed in a hot plate at a high temperature ( $\sim 160^{\circ}$ ) for at least 5 min. Once the wafer is cleaned, the photo resist that will be utilized for the mold is spin coated. Originally, SU-8 2150 negative photoresist was selected as the mold material thanks to its thickness and sharp edge profile. After placing the silicon wafer in the center of the spinner, the photo resist was added starting at the center of the wafer, and progressively moving towards the edge. Adding between 3 to 4 cubic inches is enough to cover the entire wafer. The spinning recipe utilized to uniformly coat the SU-8 2150 negative resist consisted on:

A) Spreading the photoresist over the silicon wafer (Step #1):

- Spin for 10 seconds
- Rate of 500 rpm
- Acceleration rate of 100 rpm/s

B) Obtaining the desired thickness (Step #2):

- Spin for 30 seconds
- Spinning rate of 2000 rpm
- Acceleration rate of 300 rpm/s

After the spinning process is finished, a soft bake on a level hot plate at a temperature of  $\sim 100^{\circ}$  C needs to be performed for about 60 min (may require longer time). To determine that the soft baking time is satisfactory, the wafer is removed from the hot plate, cooled down to room

temperature, and replaced back on to the hot plate. In this second replacement, if wrinkles are observed at the photoresist surface, the wafer needs to be left on the hot plate; otherwise it can be utilized for the next step. In general, cool-down and heat-up process can be repeated frequently until no wrinkles are observed when the wafer is on the hot plate. Utilizing this recipe, the resultant SU-8 layer would be ~300  $\mu\text{m}$  thick. For other thicknesses, the data sheet of SU-8 2000 can be referred to [72].

After the photoresist has been coated and soft baked, it can be defined by exposing the unwanted area to UV light for a total energy of 800  $\text{mJ}/\text{cm}^2$ . Different thicknesses might require different exposure energy (refer to [72] for the specific exposure dose). A post exposure bake of 30 min at 95° C is necessary. After one minute of post exposure bake, the image of the mask should be visible on the wafer.

Later in our research, we determined that the microfluidic channel height was a crucial parameter for the performance of the filters. Therefore, a more detailed study of the reversed mold height (or microchannel depth) was performed. By resorting to a thinner, less viscous, SU-8 resist (SU-8 2075) a more detailed characterization was possible by coating the SU-8 in two layers instead of one. A first layer was coated at a low speed to obtain a thickness of ~200  $\mu\text{m}$ . On top of this layer, a second layer was coated at a high speed to obtain a thickness of ~75  $\mu\text{m}$ . The thickness of the second layer can be changed in steps as small as 5  $\mu\text{m}$ . The procedure for obtaining a 275  $\mu\text{m}$  thick channel is as follows:

#### A) Layer #1

##### 1) Spreading the photoresist on the silicon wafer (Step #1):

- Spin for 10 s
- Spinning at a rate of 500 rpm

- Acceleration of 100 rpm/s
- 2) Obtaining the desired thickness (Step #2):
- Spin for 40 s
  - Spinning at a rate of 1500 rpm
  - Acceleration of 500 rpm/s

After the first layer has been coated, wafer is soft baked on a hot plate for about 60 min. In order to determine the baking time, follow the heat-up/cool-down procedure explained above.

#### B) Layer #2

- 1) Spreading the photoresist on the silicon wafer (Step #1):
- Spin for 10 s
  - Spinning at a rate of 500 rpm
  - Acceleration of 100 rpm/s
- 2) Obtaining the desired thickness (Step #2):
- Spin for 40 s
  - Spinning at a rate of 3000 rpm
  - Acceleration of 500 rpm/s

After the second layer has been coated, a shorter bake time of 10 min at 100° C is required. However, the procedure of cooling down the wafer, and putting it back into the hot plate needs to be performed to ensure the baking process is completed.

The final step in the reverse micromold fabrication is to immerse the wafer in an SU-8 developer to remove the unwanted (unexposed) photoresist. The developing time for the specified thickness of ~300 μm was found to be 25 min. However, by using a Q-tip to peel off the unwanted (unexposed) photoresist, the process could be speed up to under 20 min. It is



recommended to always use a Q-tip to clean up the edges of the mold towards the end of the developing process.

### **A.3 Polydimethylsiloxane (PDMS) Preparation**

To continue with the microchannel fabrication, the PDMS (SYLGARD® 184 silicone elastomer kit) was mixed in a ratio of 10:1 with its curing agent. To obtain the desired 2 mm thick PDMS layer, 20 g of PDMS were mixed with 2 g of the curing agent. To remove all the trapped air bubbles, a degassed process was done. The degassed process consist on placing the mixed PDMS under vacuum and bringing it back to atmosphere pressure several times, until no bubbles are left in the mixing. The wafer, with the reverse micromold, needs to be placed inside a 5 inch diameter petri dish, and the area surrounding the molded structure needs to be delimited with aluminum foil. For larger molds, more grams of PMDS might be required. The mixed PDMS was poured carefully on top of the reversed mold to avoid the generation of new air bubbles. The petri dish was placed in the oven at 70° C for 25 min. It is also possible to cure the PDMS at room temperature, but the curing time might take up to 48 hours.

Once the PDMS have been cured, it can be peeled off from the silicon wafer and the resultant microchannel will be in the bottom surface. An X-ACTO knife can be used to remove the extra unwanted PDMS.

### **A.4 Sealing the Channel (Bonding)**

To complete the microchannel fabrication, it needs to be completely sealed with a thin-film insulator. Early experiments were carried out by sealing the microfluidic channel with readily available prepreg LCP (Rogers Corp), but later a thinner insulator Benzocyclobutene (BCB) was utilized to replace the LCP. These materials are thermoplastic and therefore a customized APTES (3-Aminopropyltriethoxysilane) based treatment that was previously used

for other thermoplastic material-PDMS bonding was utilized for the LCP/BCB-PDMS bonding process. First, the general process will be outlined, and then specific details will be given for each insulator.

The insulator substrate was treated with oxygen plasma for 30 s at a power level of ~60 W, and then merged in an aqueous solution of 2% v/v APTES for 20 min. The solution was placed on a hot plate to increase its temperature up to 80° C. Parallel to this process, the PDMS was treated with oxygen plasma at a power level of ~60 W. The activated insulator and the PDMS were kept in conformal contact inside the oven at a temperature of 70° C for 10 min. It is possible to seal the bond at room temperature, but high temperatures can help to strengthen it. A more detailed explanation of this procedure can be found in [73].

LCP is a commercially available substrate with predefined thickness (Ultralam 3880 ( $\epsilon_r = 2.4$ ,  $\tan\delta = 0.0025$ )). The prepreg form of LCP helps to obtain stronger bonds due to the smooth surface. The thickness of the BCB (Cyclotene 3022-57, Dow Chemical Company) can be customized through spin coating procedures. For this, BCB is spin coated over the desired substrate (e.g. Rogers 6010.2). To obtain the required 6  $\mu\text{m}$  layer of BCB, the recipe utilized was:

Step 1 (Spreading the BCB):

- Spin for 7 s
- Spinning rate of 500 rpm
- Acceleration rate of 200 rpm/s

Step 2 (Obtaining the desired thickness)

- Spin for 40 s
- Spinning rate of 4000 rpm

- Acceleration rate of 1000 rpm/s

The input and output microstrip lines of the circuit should be covered with a high temperature resistant tape to be able to make electrical connection to them afterwards and to avoid an extra etching step at the end of the fabrication procedure. After spinning the BCB, it is necessary to bake it for a period of 60 s at a temperature that can range from 80° C to 150° C. After baking, the thermal curing process requires a ramping temperature increase from 100° C to 250° C for a period of 3 hours. For more detail on BCB processing and thicknesses, manufacturer supplied data sheet can be seen [74]. Once the BCB is cured (completely polymerized), the bonding procedures explained above can be followed.


It is important to remember to open the inlet and outlet holes in the PDMS, and manually insert the selectively metallized plate inside the microchannel prior to the bonding.


#### **A.5 Selectively Metallized Plate Fabrication**

Different substrates were originally tested to fabricate the selectively metallized plate. Since the selected fluid was Teflon solution from DuPont (400S2-100-1), which consists of 1% Teflon powder dissolved in 3M FC-40 solution, with a density of 1.855 g/cm<sup>3</sup>, the selectively metallized plate was preferably fabricated in a substrate with a density value close to 1.855 g/cm<sup>3</sup>. Studies were carried out with silicon (2.33 g/cm<sup>3</sup>) and quartz (2.65 g/cm<sup>3</sup>) with little successful movement due to their high density difference. Therefore, substrates such as PMMA (1.18 g/cm<sup>3</sup>) and Rogers 5880LZ (1.4 g/cm<sup>3</sup>) were investigated. Initial filter prototypes were fabricated using PMMA, however, this required an extra step of metallization, which led us to select 254 μm thick Rogers 5880LZ readily available with a 17 μm thick metallized layer. Resorting to conventional photolithography techniques, the unwanted metal was removed.

## APPENDIX B: COPYRIGHT PERMISSIONS

Below is permission for the use of the images in Figure 1

Home Create Account Help Live Chat



**IEEE**  
Requesting permission to reuse content from an IEEE publication

**Title:** Electronically switchable and tunable coplanar waveguide-slotline band-pass filters

**Author:** Y. H. Shu; J. A. Navarro; K. Chang

**Publication:** Microwave Theory and Techniques, IEEE Transactions on

**Publisher:** IEEE

**Date:** Mar 1991

Copyright © 1991, IEEE

LOGIN

If you're a copyright.com user, you can login to RightsLink using your copyright.com credentials. Already a RightsLink user or want to [learn more?](#)

### Thesis / Dissertation Reuse

**The IEEE does not require individuals working on a thesis to obtain a formal reuse license, however, you may print out this statement to be used as a permission grant:**

*Requirements to be followed when using any portion (e.g., figure, graph, table, or textual material) of an IEEE copyrighted paper in a thesis:*

- 1) In the case of textual material (e.g., using short quotes or referring to the work within these papers) users must give full credit to the original source (author, paper, publication) followed by the IEEE copyright line © 2011 IEEE.
- 2) In the case of illustrations or tabular material, we require that the copyright line © [Year of original publication] IEEE appear prominently with each reprinted figure and/or table.
- 3) If a substantial portion of the original paper is to be used, and if you are not the senior author, also obtain the senior author's approval.

*Requirements to be followed when using an entire IEEE copyrighted paper in a thesis:*

- 1) The following IEEE copyright/ credit notice should be placed prominently in the references: © [year of original publication] IEEE. Reprinted, with permission, from [author names, paper title, IEEE publication title, and month/year of publication]
- 2) Only the accepted version of an IEEE copyrighted paper can be used when posting the paper or your thesis on-line.
- 3) In placing the thesis on the author's university website, please display the following message in a prominent place on the website: In reference to IEEE copyrighted material which is used with permission in this thesis, the IEEE does not endorse any of [university/educational entity's name goes here]'s products or services. Internal or personal use of this material is permitted. If interested in reprinting/republishing IEEE copyrighted material for advertising or promotional purposes or for creating new collective works for resale or redistribution, please go to [http://www.ieee.org/publications\\_standards/publications/rights/rights\\_link.html](http://www.ieee.org/publications_standards/publications/rights/rights_link.html) to learn how to obtain a License from RightsLink.

If applicable, University Microfilms and/or ProQuest Library, or the Archives of Canada may supply single copies of the dissertation.

BACK

CLOSE WINDOW

Copyright © 2016 Copyright Clearance Center, Inc. All Rights Reserved. [Privacy statement](#). [Terms and Conditions](#).  
Comments? We would like to hear from you. E-mail us at [customercare@copyright.com](mailto:customercare@copyright.com)

Below is permission for the use of images in Figure 2



RightsLink®

Home

Create Account

Help



**Title:** A Low Loss X-Band Quasi-Elliptic Ferroelectric Tunable Filter  
**Author:** S. Courreges; Y. Li; Z. Zhao; K. Choi; A. Hunt; J. Papapolymerou  
**Publication:** IEEE Microwave and Wireless Components Letters  
**Publisher:** IEEE  
**Date:** April 2009  
Copyright © 2009, IEEE

LOGIN

If you're a [copyright.com](#) user, you can login to RightsLink using your [copyright.com](#) credentials. Already a [RightsLink](#) user or want to [learn more?](#)

### Thesis / Dissertation Reuse

**The IEEE does not require individuals working on a thesis to obtain a formal reuse license, however, you may print out this statement to be used as a permission grant:**

*Requirements to be followed when using any portion (e.g., figure, graph, table, or textual material) of an IEEE copyrighted paper in a thesis:*

- 1) In the case of textual material (e.g., using short quotes or referring to the work within these papers) users must give full credit to the original source (author, paper, publication) followed by the IEEE copyright line © 2011 IEEE.
- 2) In the case of illustrations or tabular material, we require that the copyright line © [Year of original publication] IEEE appear prominently with each reprinted figure and/or table.
- 3) If a substantial portion of the original paper is to be used, and if you are not the senior author, also obtain the senior author's approval.

*Requirements to be followed when using an entire IEEE copyrighted paper in a thesis:*

- 1) The following IEEE copyright/ credit notice should be placed prominently in the references: © [year of original publication] IEEE. Reprinted, with permission, from [author names, paper title, IEEE publication title, and month/year of publication]
- 2) Only the accepted version of an IEEE copyrighted paper can be used when posting the paper or your thesis on-line.
- 3) In placing the thesis on the author's university website, please display the following message in a prominent place on the website: In reference to IEEE copyrighted material which is used with permission in this thesis, the IEEE does not endorse any of [university/educational entity's name goes here]'s products or services. Internal or personal use of this material is permitted. If interested in reprinting/republishing IEEE copyrighted material for advertising or promotional purposes or for creating new collective works for resale or redistribution, please go to [http://www.ieee.org/publications\\_standards/publications/rights/rights\\_link.html](http://www.ieee.org/publications_standards/publications/rights/rights_link.html) to learn how to obtain a License from RightsLink.

If applicable, University Microfilms and/or ProQuest Library, or the Archives of Canada may supply single copies of the dissertation.

BACK

CLOSE WINDOW

Copyright © 2016 [Copyright Clearance Center, Inc.](#) All Rights Reserved. [Privacy statement.](#) [Terms and Conditions.](#)

Comments? We would like to hear from you. E-mail us at [customer@copyright.com](mailto:customer@copyright.com)

Below is permission for the use of images in figure 3.



RightsLink®

Home

Create Account

Help



**Title:** Miniature and tunable filters using MEMS capacitors  
**Author:** A. Abbaspour-Tamijani; L. Dussopt; G. M. Rebeiz  
**Publication:** Microwave Theory and Techniques, IEEE Transactions on  
**Publisher:** IEEE  
**Date:** July 2003  
Copyright © 2003, IEEE

LOGIN  
If you're a [copyright.com user](#), you can login to RightsLink using your [copyright.com credentials](#). Already a [RightsLink user](#) or want to [learn more?](#)

### Thesis / Dissertation Reuse

**The IEEE does not require individuals working on a thesis to obtain a formal reuse license, however, you may print out this statement to be used as a permission grant:**

*Requirements to be followed when using any portion (e.g., figure, graph, table, or textual material) of an IEEE copyrighted paper in a thesis:*

- 1) In the case of textual material (e.g., using short quotes or referring to the work within these papers) users must give full credit to the original source (author, paper, publication) followed by the IEEE copyright line © 2011 IEEE.
- 2) In the case of illustrations or tabular material, we require that the copyright line © [Year of original publication] IEEE appear prominently with each reprinted figure and/or table.
- 3) If a substantial portion of the original paper is to be used, and if you are not the senior author, also obtain the senior author's approval.

*Requirements to be followed when using an entire IEEE copyrighted paper in a thesis:*

- 1) The following IEEE copyright/ credit notice should be placed prominently in the references: © [year of original publication] IEEE. Reprinted, with permission, from [author names, paper title, IEEE publication title, and month/year of publication]
- 2) Only the accepted version of an IEEE copyrighted paper can be used when posting the paper or your thesis on-line.
- 3) In placing the thesis on the author's university website, please display the following message in a prominent place on the website: In reference to IEEE copyrighted material which is used with permission in this thesis, the IEEE does not endorse any of [university/educational entity's name goes here]'s products or services. Internal or personal use of this material is permitted. If interested in reprinting/republishing IEEE copyrighted material for advertising or promotional purposes or for creating new collective works for resale or redistribution, please go to [http://www.ieee.org/publications\\_standards/publications/rights/rights\\_link.html](http://www.ieee.org/publications_standards/publications/rights/rights_link.html) to learn how to obtain a License from RightsLink.

If applicable, University Microfilms and/or ProQuest Library, or the Archives of Canada may supply single copies of the dissertation.

BACK

CLOSE WINDOW

Copyright © 2016 Copyright Clearance Center, Inc. All Rights Reserved. [Privacy statement](#). [Terms and Conditions](#).  
Comments? We would like to hear from you. E-mail us at [customercare@copyright.com](mailto:customercare@copyright.com)

Below is permission for the use of images in figure 4.



RightsLink®

Home

Create Account

Help



**Title:** A differential 4-bit 6.5-10-GHz RF MEMS tunable filter  
**Author:** K. Entesari; G. M. Rebeiz  
**Publication:** Microwave Theory and Techniques, IEEE Transactions on  
**Publisher:** IEEE  
**Date:** March 2005  
Copyright © 2005, IEEE

LOGIN

If you're a [copyright.com user](#), you can login to RightsLink using your [copyright.com](#) credentials. Already a [RightsLink user](#) or want to [learn more?](#)

### Thesis / Dissertation Reuse

**The IEEE does not require individuals working on a thesis to obtain a formal reuse license, however, you may print out this statement to be used as a permission grant:**

*Requirements to be followed when using any portion (e.g., figure, graph, table, or textual material) of an IEEE copyrighted paper in a thesis:*

- 1) In the case of textual material (e.g., using short quotes or referring to the work within these papers) users must give full credit to the original source (author, paper, publication) followed by the IEEE copyright line © 2011 IEEE.
- 2) In the case of illustrations or tabular material, we require that the copyright line © [Year of original publication] IEEE appear prominently with each reprinted figure and/or table.
- 3) If a substantial portion of the original paper is to be used, and if you are not the senior author, also obtain the senior author's approval.

*Requirements to be followed when using an entire IEEE copyrighted paper in a thesis:*

- 1) The following IEEE copyright/ credit notice should be placed prominently in the references: © [year of original publication] IEEE. Reprinted, with permission, from [author names, paper title, IEEE publication title, and month/year of publication]
- 2) Only the accepted version of an IEEE copyrighted paper can be used when posting the paper or your thesis on-line.
- 3) In placing the thesis on the author's university website, please display the following message in a prominent place on the website: In reference to IEEE copyrighted material which is used with permission in this thesis, the IEEE does not endorse any of [university/educational entity's name goes here]'s products or services. Internal or personal use of this material is permitted. If interested in reprinting/republishing IEEE copyrighted material for advertising or promotional purposes or for creating new collective works for resale or redistribution, please go to [http://www.ieee.org/publications\\_standards/publications/rights/rights\\_link.html](http://www.ieee.org/publications_standards/publications/rights/rights_link.html) to learn how to obtain a License from RightsLink.

If applicable, University Microfilms and/or ProQuest Library, or the Archives of Canada may supply single copies of the dissertation.

BACK

CLOSE WINDOW

Copyright © 2016 [Copyright Clearance Center, Inc.](#) All Rights Reserved. [Privacy statement](#). [Terms and Conditions](#).

Comments? We would like to hear from you. E-mail us at [customercare@copyright.com](mailto:customercare@copyright.com)

Below is permission for the use of images in figure 5.



RightsLink®

Home

Create Account

Help



**Title:** High- Tunable Microwave Cavity Resonators and Filters Using SOI-Based RF MEMS Tuners  
**Author:** X. Liu; L. P. B. Katehi; W. J. Chappell; D. Peroulis  
**Publication:** Microelectromechanical Systems, IEEE/ASME Journal of  
**Publisher:** IEEE  
**Date:** Aug. 2010  
Copyright © 2010, IEEE

LOGIN  
If you're a **copyright.com** user, you can login to RightsLink using your copyright.com credentials. Already a **RightsLink** user or want to [learn more?](#)

### Thesis / Dissertation Reuse

**The IEEE does not require individuals working on a thesis to obtain a formal reuse license, however, you may print out this statement to be used as a permission grant:**

*Requirements to be followed when using any portion (e.g., figure, graph, table, or textual material) of an IEEE copyrighted paper in a thesis:*

- 1) In the case of textual material (e.g., using short quotes or referring to the work within these papers) users must give full credit to the original source (author, paper, publication) followed by the IEEE copyright line © 2011 IEEE.
- 2) In the case of illustrations or tabular material, we require that the copyright line © [Year of original publication] IEEE appear prominently with each reprinted figure and/or table.
- 3) If a substantial portion of the original paper is to be used, and if you are not the senior author, also obtain the senior author's approval.

*Requirements to be followed when using an entire IEEE copyrighted paper in a thesis:*

- 1) The following IEEE copyright/ credit notice should be placed prominently in the references: © [year of original publication] IEEE. Reprinted, with permission, from [author names, paper title, IEEE publication title, and month/year of publication]
- 2) Only the accepted version of an IEEE copyrighted paper can be used when posting the paper or your thesis on-line.
- 3) In placing the thesis on the author's university website, please display the following message in a prominent place on the website: In reference to IEEE copyrighted material which is used with permission in this thesis, the IEEE does not endorse any of [university/educational entity's name goes here]'s products or services. Internal or personal use of this material is permitted. If interested in reprinting/republishing IEEE copyrighted material for advertising or promotional purposes or for creating new collective works for resale or redistribution, please go to [http://www.ieee.org/publications\\_standards/publications/rights/rights\\_link.html](http://www.ieee.org/publications_standards/publications/rights/rights_link.html) to learn how to obtain a License from RightsLink.

If applicable, University Microfilms and/or ProQuest Library, or the Archives of Canada may supply single copies of the dissertation.

BACK

CLOSE WINDOW

Copyright © 2016 [Copyright Clearance Center, Inc.](#) All Rights Reserved. [Privacy statement](#). [Terms and Conditions](#).

Comments? We would like to hear from you. E-mail us at [customercare@copyright.com](mailto:customercare@copyright.com)



Below are permissions for the use of images in figure 6.



RightsLink®

Home

Create Account

Help



**Title:** Miniature and Reconfigurable CPW Folded Slot Antennas Employing Liquid-Metal Capacitive Loading  
**Author:** A. Pourghorban Saghati; J. Singh Batra; J. Kameoka; K. Entesari  
**Publication:** Antennas and Propagation, IEEE Transactions on  
**Publisher:** IEEE  
**Date:** Sept. 2015  
Copyright © 2015, IEEE

LOGIN

If you're a **copyright.com** user, you can login to RightsLink using your copyright.com credentials. Already a **RightsLink** user or want to [learn more?](#)

### Thesis / Dissertation Reuse

**The IEEE does not require individuals working on a thesis to obtain a formal reuse license, however, you may print out this statement to be used as a permission grant:**

*Requirements to be followed when using any portion (e.g., figure, graph, table, or textual material) of an IEEE copyrighted paper in a thesis:*

- 1) In the case of textual material (e.g., using short quotes or referring to the work within these papers) users must give full credit to the original source (author, paper, publication) followed by the IEEE copyright line © 2011 IEEE.
- 2) In the case of illustrations or tabular material, we require that the copyright line © [Year of original publication] IEEE appear prominently with each reprinted figure and/or table.
- 3) If a substantial portion of the original paper is to be used, and if you are not the senior author, also obtain the senior author's approval.

*Requirements to be followed when using an entire IEEE copyrighted paper in a thesis:*

- 1) The following IEEE copyright/ credit notice should be placed prominently in the references: © [year of original publication] IEEE. Reprinted, with permission, from [author names, paper title, IEEE publication title, and month/year of publication]
- 2) Only the accepted version of an IEEE copyrighted paper can be used when posting the paper or your thesis on-line.
- 3) In placing the thesis on the author's university website, please display the following message in a prominent place on the website: In reference to IEEE copyrighted material which is used with permission in this thesis, the IEEE does not endorse any of [university/educational entity's name goes here]'s products or services. Internal or personal use of this material is permitted. If interested in reprinting/republishing IEEE copyrighted material for advertising or promotional purposes or for creating new collective works for resale or redistribution, please go to [http://www.ieee.org/publications\\_standards/publications/rights/rights\\_link.html](http://www.ieee.org/publications_standards/publications/rights/rights_link.html) to learn how to obtain a License from RightsLink.

If applicable, University Microfilms and/or ProQuest Library, or the Archives of Canada may supply single copies of the dissertation.

BACK

CLOSE WINDOW

Copyright © 2016 Copyright Clearance Center, Inc. All Rights Reserved. [Privacy statement](#). [Terms and Conditions](#).

Comments? We would like to hear from you. E-mail us at [customercare@copyright.com](mailto:customercare@copyright.com)



**Title:** Fluidically Tunable Frequency Selective/Phase Shifting Surfaces for High-Power Microwave Applications  
**Author:** M. Li; N. Behdad  
**Publication:** Antennas and Propagation, IEEE Transactions on  
**Publisher:** IEEE  
**Date:** June 2012  
Copyright © 2012, IEEE

LOGIN

If you're a [copyright.com](#) user, you can login to RightsLink using your [copyright.com](#) credentials. Already a [RightsLink](#) user or want to [learn more?](#)

### Thesis / Dissertation Reuse

**The IEEE does not require individuals working on a thesis to obtain a formal reuse license, however, you may print out this statement to be used as a permission grant:**

*Requirements to be followed when using any portion (e.g., figure, graph, table, or textual material) of an IEEE copyrighted paper in a thesis:*

- 1) In the case of textual material (e.g., using short quotes or referring to the work within these papers) users must give full credit to the original source (author, paper, publication) followed by the IEEE copyright line © 2011 IEEE.
- 2) In the case of illustrations or tabular material, we require that the copyright line © [Year of original publication] IEEE appear prominently with each reprinted figure and/or table.
- 3) If a substantial portion of the original paper is to be used, and if you are not the senior author, also obtain the senior author's approval.

*Requirements to be followed when using an entire IEEE copyrighted paper in a thesis:*

- 1) The following IEEE copyright/ credit notice should be placed prominently in the references: © [year of original publication] IEEE. Reprinted, with permission, from [author names, paper title, IEEE publication title, and month/year of publication]
- 2) Only the accepted version of an IEEE copyrighted paper can be used when posting the paper or your thesis on-line.
- 3) In placing the thesis on the author's university website, please display the following message in a prominent place on the website: In reference to IEEE copyrighted material which is used with permission in this thesis, the IEEE does not endorse any of [university/educational entity's name goes here]'s products or services. Internal or personal use of this material is permitted. If interested in reprinting/republishing IEEE copyrighted material for advertising or promotional purposes or for creating new collective works for resale or redistribution, please go to [http://www.ieee.org/publications\\_standards/publications/rights/rights\\_link.html](http://www.ieee.org/publications_standards/publications/rights/rights_link.html) to learn how to obtain a License from RightsLink.

If applicable, University Microfilms and/or ProQuest Library, or the Archives of Canada may supply single copies of the dissertation.

BACK

CLOSE WINDOW

Copyright © 2016 [Copyright Clearance Center, Inc.](#) All Rights Reserved. [Privacy statement.](#) [Terms and Conditions.](#)

Comments? We would like to hear from you. E-mail us at [customer@copyright.com](mailto:customer@copyright.com)



**Title:** A Liquid-Metal Monopole Array With Tunable Frequency, Gain, and Beam Steering

**Author:** A. M. Morishita; C. K. Y. Kitamura; A. T. Ohta; W. A. Shiroma

**Publication:** IEEE Antennas and Wireless Propagation Letters

**Publisher:** IEEE

**Date:** 2013

Copyright © 2013, IEEE

LOGIN

If you're a [copyright.com](#) user, you can login to RightsLink using your [copyright.com](#) credentials. Already a [RightsLink](#) user or want to [learn more?](#)

### Thesis / Dissertation Reuse

**The IEEE does not require individuals working on a thesis to obtain a formal reuse license, however, you may print out this statement to be used as a permission grant:**

*Requirements to be followed when using any portion (e.g., figure, graph, table, or textual material) of an IEEE copyrighted paper in a thesis:*

- 1) In the case of textual material (e.g., using short quotes or referring to the work within these papers) users must give full credit to the original source (author, paper, publication) followed by the IEEE copyright line © 2011 IEEE.
- 2) In the case of illustrations or tabular material, we require that the copyright line © [Year of original publication] IEEE appear prominently with each reprinted figure and/or table.
- 3) If a substantial portion of the original paper is to be used, and if you are not the senior author, also obtain the senior author's approval.

*Requirements to be followed when using an entire IEEE copyrighted paper in a thesis:*

- 1) The following IEEE copyright/ credit notice should be placed prominently in the references: © [year of original publication] IEEE. Reprinted, with permission, from [author names, paper title, IEEE publication title, and month/year of publication]
- 2) Only the accepted version of an IEEE copyrighted paper can be used when posting the paper or your thesis on-line.
- 3) In placing the thesis on the author's university website, please display the following message in a prominent place on the website: In reference to IEEE copyrighted material which is used with permission in this thesis, the IEEE does not endorse any of [university/educational entity's name goes here]'s products or services. Internal or personal use of this material is permitted. If interested in reprinting/republishing IEEE copyrighted material for advertising or promotional purposes or for creating new collective works for resale or redistribution, please go to [http://www.ieee.org/publications\\_standards/publications/rights/rights\\_link.html](http://www.ieee.org/publications_standards/publications/rights/rights_link.html) to learn how to obtain a License from RightsLink.

If applicable, University Microfilms and/or ProQuest Library, or the Archives of Canada may supply single copies of the dissertation.

BACK

CLOSE WINDOW

Copyright © 2016 [Copyright Clearance Center, Inc.](#) All Rights Reserved. [Privacy statement.](#) [Terms and Conditions.](#)

Comments? We would like to hear from you. E-mail us at [customer@copyright.com](mailto:customer@copyright.com)

Below is permission for the use of images in figure 7



RightsLink®

Home

Create Account

Help



**Title:** A Pressure Responsive Fluidic Microstrip Open Stub Resonator Using a Liquid Metal Alloy  
**Author:** M. R. Khan; G. J. Hayes; S. Zhang; M. D. Dickey; G. Lazzi  
**Publication:** IEEE Microwave and Wireless Components Letters  
**Publisher:** IEEE  
**Date:** Nov. 2012  
Copyright © 2012, IEEE

LOGIN

If you're a **copyright.com** user, you can login to RightsLink using your copyright.com credentials. Already a **RightsLink** user or want to [learn more?](#)

### Thesis / Dissertation Reuse

**The IEEE does not require individuals working on a thesis to obtain a formal reuse license, however, you may print out this statement to be used as a permission grant:**

*Requirements to be followed when using any portion (e.g., figure, graph, table, or textual material) of an IEEE copyrighted paper in a thesis:*

- 1) In the case of textual material (e.g., using short quotes or referring to the work within these papers) users must give full credit to the original source (author, paper, publication) followed by the IEEE copyright line © 2011 IEEE.
- 2) In the case of illustrations or tabular material, we require that the copyright line © [Year of original publication] IEEE appear prominently with each reprinted figure and/or table.
- 3) If a substantial portion of the original paper is to be used, and if you are not the senior author, also obtain the senior author's approval.

*Requirements to be followed when using an entire IEEE copyrighted paper in a thesis:*

- 1) The following IEEE copyright/ credit notice should be placed prominently in the references: © [year of original publication] IEEE. Reprinted, with permission, from [author names, paper title, IEEE publication title, and month/year of publication]
- 2) Only the accepted version of an IEEE copyrighted paper can be used when posting the paper or your thesis on-line.
- 3) In placing the thesis on the author's university website, please display the following message in a prominent place on the website: In reference to IEEE copyrighted material which is used with permission in this thesis, the IEEE does not endorse any of [university/educational entity's name goes here]'s products or services. Internal or personal use of this material is permitted. If interested in reprinting/republishing IEEE copyrighted material for advertising or promotional purposes or for creating new collective works for resale or redistribution, please go to [http://www.ieee.org/publications\\_standards/publications/rights/rights\\_link.html](http://www.ieee.org/publications_standards/publications/rights/rights_link.html) to learn how to obtain a License from RightsLink.

If applicable, University Microfilms and/or ProQuest Library, or the Archives of Canada may supply single copies of the dissertation.

BACK

CLOSE WINDOW

Copyright © 2016 Copyright Clearance Center, Inc. All Rights Reserved. [Privacy statement](#). [Terms and Conditions](#).

Comments? We would like to hear from you. E-mail us at [customercare@copyright.com](mailto:customercare@copyright.com)

Below is permission for the use of images in figure 8.



RightsLink®

Home

Create Account

Help



**Title:** A liquid-metal tunable electromagnetic-bandgap microstrip filter  
**Conference Proceedings:** Wireless Information Technology and Systems (ICWITS), 2012 IEEE International Conference on  
**Author:** A. T. Ohta; S. Guo; B. J. Lei; W. Hu; W. A. Shiroma  
**Publisher:** IEEE  
**Date:** 11-16 Nov. 2012  
Copyright © 2012, IEEE

**LOGIN**  
If you're a **copyright.com** user, you can login to RightsLink using your copyright.com credentials. Already a **RightsLink** user or want to [learn more?](#)

### Thesis / Dissertation Reuse

**The IEEE does not require individuals working on a thesis to obtain a formal reuse license, however, you may print out this statement to be used as a permission grant:**

*Requirements to be followed when using any portion (e.g., figure, graph, table, or textual material) of an IEEE copyrighted paper in a thesis:*

- 1) In the case of textual material (e.g., using short quotes or referring to the work within these papers) users must give full credit to the original source (author, paper, publication) followed by the IEEE copyright line © 2011 IEEE.
- 2) In the case of illustrations or tabular material, we require that the copyright line © [Year of original publication] IEEE appear prominently with each reprinted figure and/or table.
- 3) If a substantial portion of the original paper is to be used, and if you are not the senior author, also obtain the senior author's approval.

*Requirements to be followed when using an entire IEEE copyrighted paper in a thesis:*

- 1) The following IEEE copyright/ credit notice should be placed prominently in the references: © [year of original publication] IEEE. Reprinted, with permission, from [author names, paper title, IEEE publication title, and month/year of publication]
- 2) Only the accepted version of an IEEE copyrighted paper can be used when posting the paper or your thesis on-line.
- 3) In placing the thesis on the author's university website, please display the following message in a prominent place on the website: In reference to IEEE copyrighted material which is used with permission in this thesis, the IEEE does not endorse any of [university/educational entity's name goes here]'s products or services. Internal or personal use of this material is permitted. If interested in reprinting/republishing IEEE copyrighted material for advertising or promotional purposes or for creating new collective works for resale or redistribution, please go to [http://www.ieee.org/publications\\_standards/publications/rights/rights\\_link.html](http://www.ieee.org/publications_standards/publications/rights/rights_link.html) to learn how to obtain a License from RightsLink.

If applicable, University Microfilms and/or ProQuest Library, or the Archives of Canada may supply single copies of the dissertation.

BACK

CLOSE WINDOW

Copyright © 2016 Copyright Clearance Center, Inc. All Rights Reserved. [Privacy statement](#), [Terms and Conditions](#).

Comments? We would like to hear from you. E-mail us at [customercare@copyright.com](mailto:customercare@copyright.com)

Below is permission for the use of images in figure 9.




# RightsLink®

[Home](#)

[Create Account](#)

[Help](#)

 [Live Chat](#)



**IEEE**  
Requesting permission to reuse content from an IEEE publication

**Title:** A Miniaturized Microfluidically Reconfigurable Coplanar Waveguide Bandpass Filter With Maximum Power Handling of 10 Watts

**Author:** A. Pourghorban Saghati; J. S. Batra; J. Kameoka; K. Entesari

**Publication:** Microwave Theory and Techniques, IEEE Transactions on

**Publisher:** IEEE

**Date:** Aug. 2015

Copyright © 2015, IEEE

[LOGIN](#)

**If you're a [copyright.com](#) user**, you can login to RightsLink using your [copyright.com](#) credentials. Already a **RightsLink user** or want to [learn more?](#)

### Thesis / Dissertation Reuse

**The IEEE does not require individuals working on a thesis to obtain a formal reuse license, however, you may print out this statement to be used as a permission grant:**

*Requirements to be followed when using any portion (e.g., figure, graph, table, or textual material) of an IEEE copyrighted paper in a thesis:*

- 1) In the case of textual material (e.g., using short quotes or referring to the work within these papers) users must give full credit to the original source (author, paper, publication) followed by the IEEE copyright line © 2011 IEEE.
- 2) In the case of illustrations or tabular material, we require that the copyright line © [Year of original publication] IEEE appear prominently with each reprinted figure and/or table.
- 3) If a substantial portion of the original paper is to be used, and if you are not the senior author, also obtain the senior author's approval.

*Requirements to be followed when using an entire IEEE copyrighted paper in a thesis:*

- 1) The following IEEE copyright/ credit notice should be placed prominently in the references: © [year of original publication] IEEE. Reprinted, with permission, from [author names, paper title, IEEE publication title, and month/year of publication]
- 2) Only the accepted version of an IEEE copyrighted paper can be used when posting the paper or your thesis on-line.
- 3) In placing the thesis on the author's university website, please display the following message in a prominent place on the website: In reference to IEEE copyrighted material which is used with permission in this thesis, the IEEE does not endorse any of [university/educational entity's name goes here]'s products or services. Internal or personal use of this material is permitted. If interested in reprinting/republishing IEEE copyrighted material for advertising or promotional purposes or for creating new collective works for resale or redistribution, please go to [http://www.ieee.org/publications\\_standards/publications/rights/rights\\_link.html](http://www.ieee.org/publications_standards/publications/rights/rights_link.html) to learn how to obtain a License from RightsLink.

If applicable, University Microfilms and/or ProQuest Library, or the Archives of Canada may supply single copies of the dissertation.


[BACK](#)

[CLOSE WINDOW](#)

Copyright © 2016 [Copyright Clearance Center, Inc.](#) All Rights Reserved. [Privacy statement](#). [Terms and Conditions](#).  
Comments? We would like to hear from you. E-mail us at [customercare@copyright.com](mailto:customercare@copyright.com)

Below is permission for the use of material in Chapter 2.

Home Create Account Help Live Chat



Requesting permission to reuse content from an IEEE publication

**Title:** Wideband Band-Stop X-Band Filter Using Electrically Small Tightly Coupled Resonators

**Author:** Timothy Palomo; Paul Herzig; Thomas M. Weller; Gokhan Mumcu

**Publication:** IEEE Microwave and Wireless Components Letters

**Publisher:** IEEE

**Date:** July 2013

Copyright © 2013, IEEE

LOGIN

If you're a [copyright.com](#) user, you can login to RightsLink using your copyright.com credentials. Already a [RightsLink](#) user or want to [learn more?](#)

### Thesis / Dissertation Reuse

**The IEEE does not require individuals working on a thesis to obtain a formal reuse license, however, you may print out this statement to be used as a permission grant:**

*Requirements to be followed when using any portion (e.g., figure, graph, table, or textual material) of an IEEE copyrighted paper in a thesis:*

- 1) In the case of textual material (e.g., using short quotes or referring to the work within these papers) users must give full credit to the original source (author, paper, publication) followed by the IEEE copyright line © 2011 IEEE.
- 2) In the case of illustrations or tabular material, we require that the copyright line © [Year of original publication] IEEE appear prominently with each reprinted figure and/or table.
- 3) If a substantial portion of the original paper is to be used, and if you are not the senior author, also obtain the senior author's approval.

*Requirements to be followed when using an entire IEEE copyrighted paper in a thesis:*

- 1) The following IEEE copyright/ credit notice should be placed prominently in the references: © [year of original publication] IEEE. Reprinted, with permission, from [author names, paper title, IEEE publication title, and month/year of publication]
- 2) Only the accepted version of an IEEE copyrighted paper can be used when posting the paper or your thesis on-line.
- 3) In placing the thesis on the author's university website, please display the following message in a prominent place on the website: In reference to IEEE copyrighted material which is used with permission in this thesis, the IEEE does not endorse any of [university/educational entity's name goes here]'s products or services. Internal or personal use of this material is permitted. If interested in reprinting/republishing IEEE copyrighted material for advertising or promotional purposes or for creating new collective works for resale or redistribution, please go to [http://www.ieee.org/publications\\_standards/publications/rights/rights\\_link.html](http://www.ieee.org/publications_standards/publications/rights/rights_link.html) to learn how to obtain a License from RightsLink.

If applicable, University Microfilms and/or ProQuest Library, or the Archives of Canada may supply single copies of the dissertation.

BACK

CLOSE WINDOW

Copyright © 2016 [Copyright Clearance Center, Inc.](#) All Rights Reserved. [Privacy statement.](#) [Terms and Conditions.](#)  
Comments? We would like to hear from you. E-mail us at [customercare@copyright.com](mailto:customercare@copyright.com)

Below is permission for the use of material in Chapter 3.



RightsLink®

Home

Create Account

Help



**Title:** Frequency-Agile Bandpass Filters Using Liquid Metal Tunable Broadside Coupled Split Ring Resonators  
**Author:** Gokhan Mumcu; Abhishek Dey; Timothy Palomo  
**Publication:** IEEE Microwave and Wireless Components Letters

**Publisher:** IEEE  
**Date:** April 2013  
Copyright © 2013, IEEE

LOGIN

If you're a [copyright.com](#) user, you can login to RightsLink using your [copyright.com](#) credentials. Already a [RightsLink](#) user or want to [learn more?](#)

### Thesis / Dissertation Reuse

**The IEEE does not require individuals working on a thesis to obtain a formal reuse license, however, you may print out this statement to be used as a permission grant:**

*Requirements to be followed when using any portion (e.g., figure, graph, table, or textual material) of an IEEE copyrighted paper in a thesis:*

- 1) In the case of textual material (e.g., using short quotes or referring to the work within these papers) users must give full credit to the original source (author, paper, publication) followed by the IEEE copyright line © 2011 IEEE.
- 2) In the case of illustrations or tabular material, we require that the copyright line © [Year of original publication] IEEE appear prominently with each reprinted figure and/or table.
- 3) If a substantial portion of the original paper is to be used, and if you are not the senior author, also obtain the senior author's approval.

*Requirements to be followed when using an entire IEEE copyrighted paper in a thesis:*

- 1) The following IEEE copyright/ credit notice should be placed prominently in the references: © [year of original publication] IEEE. Reprinted, with permission, from [author names, paper title, IEEE publication title, and month/year of publication]
- 2) Only the accepted version of an IEEE copyrighted paper can be used when posting the paper or your thesis on-line.
- 3) In placing the thesis on the author's university website, please display the following message in a prominent place on the website: In reference to IEEE copyrighted material which is used with permission in this thesis, the IEEE does not endorse any of [university/educational entity's name goes here]'s products or services. Internal or personal use of this material is permitted. If interested in reprinting/republishing IEEE copyrighted material for advertising or promotional purposes or for creating new collective works for resale or redistribution, please go to [http://www.ieee.org/publications\\_standards/publications/rights/rights\\_link.html](http://www.ieee.org/publications_standards/publications/rights/rights_link.html) to learn how to obtain a License from RightsLink.

If applicable, University Microfilms and/or ProQuest Library, or the Archives of Canada may supply single copies of the dissertation.

BACK

CLOSE WINDOW

Copyright © 2016 [Copyright Clearance Center, Inc.](#) All Rights Reserved. [Privacy statement](#). [Terms and Conditions](#).

Comments? We would like to hear from you. E-mail us at [customercare@copyright.com](mailto:customercare@copyright.com)



Below is permission for the use of material in Chapter 4.

 **Copyright Clearance Center** **RightsLink®** [Home](#) [Create Account](#) [Help](#) [Live Chat](#)

 **IEEE**  
Requesting permission to reuse content from an IEEE publication

**Title:** Highly reconfigurable bandpass filters using microfluidically controlled metallized glass plates

**Conference Proceedings:** Microwave Symposium (IMS), 2014 IEEE MTT-S International

**Author:** Timothy Palomo; Gokhan Mumcu

**Publisher:** IEEE

**Date:** 1-6 June 2014

Copyright © 2014, IEEE

[LOGIN](#)

If you're a copyright.com user, you can login to RightsLink using your copyright.com credentials. Already a RightsLink user or want to [learn more?](#)

### Thesis / Dissertation Reuse

**The IEEE does not require individuals working on a thesis to obtain a formal reuse license, however, you may print out this statement to be used as a permission grant:**

*Requirements to be followed when using any portion (e.g., figure, graph, table, or textual material) of an IEEE copyrighted paper in a thesis:*

- 1) In the case of textual material (e.g., using short quotes or referring to the work within these papers) users must give full credit to the original source (author, paper, publication) followed by the IEEE copyright line © 2011 IEEE.
- 2) In the case of illustrations or tabular material, we require that the copyright line © [Year of original publication] IEEE appear prominently with each reprinted figure and/or table.
- 3) If a substantial portion of the original paper is to be used, and if you are not the senior author, also obtain the senior author's approval.

*Requirements to be followed when using an entire IEEE copyrighted paper in a thesis:*

- 1) The following IEEE copyright/ credit notice should be placed prominently in the references: © [year of original publication] IEEE. Reprinted, with permission, from [author names, paper title, IEEE publication title, and month/year of publication]
- 2) Only the accepted version of an IEEE copyrighted paper can be used when posting the paper or your thesis on-line.
- 3) In placing the thesis on the author's university website, please display the following message in a prominent place on the website: In reference to IEEE copyrighted material which is used with permission in this thesis, the IEEE does not endorse any of [university/educational entity's name goes here]'s products or services. Internal or personal use of this material is permitted. If interested in reprinting/republishing IEEE copyrighted material for advertising or promotional purposes or for creating new collective works for resale or redistribution, please go to [http://www.ieee.org/publications\\_standards/publications/rights/rights\\_link.html](http://www.ieee.org/publications_standards/publications/rights/rights_link.html) to learn how to obtain a License from RightsLink.

If applicable, University Microfilms and/or ProQuest Library, or the Archives of Canada may supply single copies of the dissertation.

[BACK](#)

[CLOSE WINDOW](#)

Copyright © 2016 Copyright Clearance Center, Inc. All Rights Reserved. [Privacy statement](#). [Terms and Conditions](#).

Comments? We would like to hear from you. E-mail us at [customercare@copyright.com](mailto:customercare@copyright.com)

Below is permission for the use of material in Chapter 5.

 **Copyright Clearance Center**  [Home](#) [Create Account](#) [Help](#)  [Live Chat](#)

 **IEEE**  
Requesting permission to reuse content from an IEEE publication

**Title:** Microfluidically Reconfigurable Metallized Plate Loaded Frequency-Agile RF Bandpass Filters  
**Author:** Timothy Palomo; Gokhan Mumcu  
**Publication:** Microwave Theory and Techniques, IEEE Transactions on  
**Publisher:** IEEE  
**Date:** Jan. 2016  
Copyright © 2016, IEEE

[LOGIN](#)  
If you're a [copyright.com](#) user, you can login to RightsLink using your [copyright.com](#) credentials. Already a [RightsLink](#) user or want to [learn more?](#)

### Thesis / Dissertation Reuse

**The IEEE does not require individuals working on a thesis to obtain a formal reuse license, however, you may print out this statement to be used as a permission grant:**

*Requirements to be followed when using any portion (e.g., figure, graph, table, or textual material) of an IEEE copyrighted paper in a thesis:*

- 1) In the case of textual material (e.g., using short quotes or referring to the work within these papers) users must give full credit to the original source (author, paper, publication) followed by the IEEE copyright line © 2011 IEEE.
- 2) In the case of illustrations or tabular material, we require that the copyright line © [Year of original publication] IEEE appear prominently with each reprinted figure and/or table.
- 3) If a substantial portion of the original paper is to be used, and if you are not the senior author, also obtain the senior author's approval.

*Requirements to be followed when using an entire IEEE copyrighted paper in a thesis:*

- 1) The following IEEE copyright/ credit notice should be placed prominently in the references: © [year of original publication] IEEE. Reprinted, with permission, from [author names, paper title, IEEE publication title, and month/year of publication]
- 2) Only the accepted version of an IEEE copyrighted paper can be used when posting the paper or your thesis on-line.
- 3) In placing the thesis on the author's university website, please display the following message in a prominent place on the website: In reference to IEEE copyrighted material which is used with permission in this thesis, the IEEE does not endorse any of [university/educational entity's name goes here]'s products or services. Internal or personal use of this material is permitted. If interested in reprinting/republishing IEEE copyrighted material for advertising or promotional purposes or for creating new collective works for resale or redistribution, please go to [http://www.ieee.org/publications\\_standards/publications/rights/rights\\_link.html](http://www.ieee.org/publications_standards/publications/rights/rights_link.html) to learn how to obtain a License from RightsLink.

If applicable, University Microfilms and/or ProQuest Library, or the Archives of Canada may supply single copies of the dissertation.

[BACK](#)

[CLOSE WINDOW](#)

Copyright © 2016 [Copyright Clearance Center, Inc.](#) All Rights Reserved. [Privacy statement](#). [Terms and Conditions](#).  
Comments? We would like to hear from you. E-mail us at [customercare@copyright.com](mailto:customercare@copyright.com)

## **ABOUT THE AUTHOR**

Timothy Palomo was born in Maracay, Venezuela, on October 5th, 1990. He received the B.S. and M.S. degrees in electrical engineering from University of South Florida, Florida, United States, in 2011 and 2013, respectively.

He is currently a Ph.D. candidate at the University of South Florida with expected graduation date May 2016. He has been a Research Assistant of the Center for Wireless and Microwave Information Systems (WAMI) at the University of South Florida since 2011, and his research has been focused on the development of highly reconfigurable RF filters through microfluidic techniques. From May 2015 to December 2016, he has been a Design Engineer Intern with Qorvo.

Mr. Palomo graduated from high school in 2007 as the best of his class. He was the outstanding student of the USF's electrical engineering department in 2011. He received the best poster award in the USF research day competitions three straight years and was awarded conference travel grants. Mr. Palomo also played tennis at the professional level in Venezuela and was awarded a full scholarship by West Virginia University to pursue his career.